FUNDAMENTAL RESEARCH

ON

A UNIQUE ROTARY MACHINE

By

Lixin Peng, B.Eng., M. Eng.

A Thesis

Submitted to the School of Graduate Studies

in Partial Fulfilment of the Requirements

for the Degree of

Doctor of Philosophy

McMaster University

May 1994

FUNDAMENTAL RESEARCH ON A UNIQUE

ROTARY MACHINE

DOCTOR OF PHILOSOPHY (1994) McMASTER UNIVERSITY

(Mechanical Engineering) Hamilton, Ontario

TITLE: Fundamental research on a unique rotary machine

AUTHOR: Lixin Peng B.Eng. (Hunan University)

M.Eng. (Hunan University)

SUPERVISOR: Dr. G.F. Round

NUMBER OF PAGES: xiv, 156

ABSTRACT

A unique rotary machine, which can be modified to function as an air motor, a hydraulic pump or a rotary combustion engine, has been developed. This thesis is concerned with both theoretical modelling of the engine aspects of the machine and the testing of a model and prototype. The machine is a simple rotational machine with an internal parallel axis arrangement. It is unique in the sense that there are two rotors turning in the same direction on their own stationary centres of gravity and working with the fluid around a full 360^0 degree path.

Using CAD/CAM techniques a model of the air motor and a prototype hydraulic pump were built and tested. Both of them have demonstrated very good performance features.

The engine described in this work is a true rotary engine with a unique semi-internal/external combustion system. It has a large power/weight ratio with a unique eight power strokes per revolution feature. Its multi fuel capability is a special contribution to the development of internal combustion engines where and when it is necessary to use alternative fuels.

A three zone turbulence eddy entrance thermodynamic model has been developed to predict the performance of the engine and optimize some of the structural and operational parameters. The results of the theoretical analysis indicate that this engine

has excellent features which are improvements over those of the reciprocating engines as well as the Wankel rotary engine.

ACKNOWLEDGEMENTS

The author wishes to express his sincere appreciation to his supervisor Dr. G.F. Round for his enthusiastic interest, constructive advice and continual encouragement throughout this work.

The author would like to thank Dr. B. Latto, Professor W.R. Newcombe and Dr. R.L. Judd, members of the Ph.D. supervisory committee for their valuable suggestions and recommendations.

The author would particularly like to acknowledge Mr. Bill Valavaara of Valavaara Technologies Ltd. for his continual interest and support of this work.

The construction of the physical model and other experimental facilities would not be possible without the support and assistance of the mechanical workshop technicians, in particular, Dave Schick and Ron Lodewyks.

Financial support for this work from NSERC is acknowledged.

Finally, the author expresses his sincere thanks to his wife Jing Chao for her continued patience, encouragement and support.

TABLE OF CONTENTS

ABSTRACT iii

ACKNOWLEDGEMENTS v

NOMENCLATURE x

CHAPTER 1 INTRODUCTION 1

CHAPTER 2 LITERATURE REVIEW 5

2.1 Rotary Machine Patents 5

2.2 Development of the Wankel Engine 13

2.3 Theoretical Models for Combustion Engines 17

2.3.1 Zero-Dimensional Model 20

2.3.2 Quasi-Dimensional Models 27

CHAPTER 3 GENERAL DESCRIPTION OF THE RVP ROTARY MACHINE 32

3.1 Introduction 32

3.2 Curve Fitting and Rotor Design 34

3.3 RVP Rotary Engine -- an Application of the RVP Rotary Machine 35

CHAPTER 4 INVESTIGATION OF AIR MOTOR AND HYDRAULIC PUMP VARIANTS 39

4.1 Introduction 39

4.2 Air Motor as a Physical Model to Verify Principles 40

4.3 Prototype Hydraulic Pump for Industrial Applications 43

4.3.1 Prototype Hydraulic Pump 43

4.3.2 Prototype Performance 45

4.3.3 Performance Analysis and its Comparison With Other Commercial Hydraulic Pumps 50

CHAPTER 5 ROTARY ENGINE -- CHAMBER FLOW SIMULATION 54

5.1 Introduction 54

5.2 Mass Flow From Pre-Chamber to the Power Chamber 57

5.3 Velocity Profile Along the Wall of the Power Chamber 61

5.3.1 Assumptions 61

5.3.2 Governing Equations 63

5.3.3 Initial and Boundary Conditions 68

5.3.4 Finite Difference Solutions 71

CHAPTER 6 ROTARY ENGINE -- THERMODYNAMIC MODEL 79

6.1 Introduction 79

6.2 Three Zone Combustion Submodel 80

6.2.1 Three Zone Assumptions 80

6.2.2 Combustion Submodel With a Turbulence Eddy Entrainment Model 84

6.3 Other Thermodynamic Submodels 88

6.3.1 Gas Property Submodel 88

6.3.2 Heat Transfer Submodel 94

6.4 Thermodynamic Model Analysis 94

CHAPTER 7 ROTARY ENGINE -- PERFORMANCE PREDICTION AND PARAMETER OPTIMIZATION 97

7.1 Introduction 97

7.2 Engine Performance Prediction and Comparison With Other Commercial Engines 98

7.2.1 Calculation of Power Generated by Thrust Gases 98

7.2.2 Predicted Performance of RVP Rotary Engine 107

7.2.3 Engine Parameter Optimization Through Theoretical Model Analysis 116

7.3 Performance Comparison With Other Commercial Engines 120

CHAPTER 8 SUMMARY AND FUTURE WORK 123

8.1 Summary of the Work 123

8.2 Recommendation for Future Work 126

REFERENCES 126

APPENDIX A	Opening Area of the Passage Between Two Chambers A(t)	132
APPENDIX B	Elliptical Coordinate Transformations	134
APPENDIX C	Boundary Coordinates of the Flowing Domain	136
APPENDIX D	Calculated Results of Mass Flow	139
APPENDIX E	Calculated Results of Velocity Profile	140
APPENDIX F	Calculated Results of Power Generated by the Thrust Gas	147
APPENDIX G	Turbulence Eddy Structure and Derivation of the Formula to Calculate Characteristic Time τ_b	148
APPENDIX H	Derivation of the Formula to Calculate Internal Energies	152

NOMENCLATURE

a	reaction order with respect to fuel, efficiency parameter in Weibe function
a_0	semi major length of the ellipse that is equivalent to the power chamber
A	area of wall exposed to gases, cross section area of passage, a special constant
A_f	area of flame front
A_p	area of piston top
b	reaction order with respect to oxygen
b_0	semi minor length of the ellipse that is equivalent to the power chamber
C_m	average piston speed
C_p	specific heat at constant pressure
C, C_x, C_L, C_d, C_u	constants relative to some parts of engine structure
d, D	diameter of cylinder
DPV	displacement per unit volume of the pump
e	eccentricity
e_b, e_u	internal energy of burnt gases and of unburnt gases
E, e	total internal energy of the gases
E_a	activation energy
E_v	volumetric efficiency

F	force generated by gases
f	body force
f_c	number of moles of fuel required to burn one mole of air completely
g	gravity force
g_e	gas consumption rate
h	heat transfer coefficient, metric coefficient for elliptical coordinates
h_i	chamber hight at ignition
h_s	hight of suction lift of the pump
H_u	lower heating value of fuel
IEC	internal combustion engine
k	ratio of specific heats
K_T	turbulence factor
L_i	integral scale
M,m	mass of gases, form factor in Wiebe function
m	number of hydrogen atoms in hydrocarbon fuel
M_b, M_u	mass or molecular weight of burnt gases and of unburnt gases
M_f, m_f	mass of fuel input into each power chamber for one cycle
M_R, M_p	molecular weight of general gas and of combustion products
M_o, m_o	total mass of gases and liquid fuel
N	engine speed
n	number of carbon molecule in hydrocarbon fuel

n_u, n_b	number of moles of unburnt and burnt gases
p	pressure
P_o	pressure history without combustion
P_s	suction pressure at inlet port of the pump
q	velocity vector
Q	heat released due to combustion, volumetric flow rate
Q_w	heat transferred to the wall
R	gas constant
R_o	universal gas constant, radial distance
R_e	Reynolds number
S_l, S_T	laminar and turbulence flame speed
S_p	piston speed
t	time count by seconds
T, T_w	temperature of gas and of wall
TM, T_{av}	average temperature inside combustion chamber
U	velocity of rotors at the edge point, extra number of monatomic molecules due to dissociation of diatomic molecules
U_j	injection jet velocity
U'_i	turbulence intensity
V	volume
v, v_b, v_u	specific volume of gases, of burnt gases and of unburnt gases

V, V_e	velocity variable and relative velocity
VA	average velocity
V_2	gas velocity from pre combustion chamber to expansion chamber
V_s	swept volume of combustion chamber
W	output power
W_J	width in normal direction of the cross section of the injection flow along the wall
X	mass fraction of burnt fuel $X = M_b / M_f$
Y	extra number of diatomic molecules due to dissociation of triatomic molecules
Y_F, Y_{O2}	mole fraction of fuel molecules and of oxygen in unburned mixtures
Z	suction distance of the pump at operation
α_p, α_ρ	relaxation factor for pressure and density calculations
θ	crank angle counted from some reference, say TDC
θ_0, $\Delta\theta$	angle at which spark ignites and burning duration
γ	ratio of specific heats
ρ, ρ_b, ρ_u	densities of general gases, of burnt gases and of unburnt gases
ρ_{ui}	density of unburnt gases at injection
η, ζ	variables of elliptical coordinates
η	amount of combustion residuals from last cycle by percentage
μ	fluid dynamic viscosity, molecular ratio of hydrogen to carbon in the fuel

ν	fluid kinetic viscosity
τ_b	characteristic burning time
ϕ	equivalence ratio of fuel/air
ω	angular speed
Δm	mass of gases transferred from precombustion chamber to power chamber

CHAPTER 1

INTRODUCTION

The notion of the conversion of fluid energy directly into rotational mechanical energy or vice versa without any reciprocating parts has always been appealing to engineers. The benefits are immediately obvious; the end use is almost always rotational, so that theoretically high efficiencies are possible because of lower mechanical losses.

James Watt for example, experimented with rotary designs for steam engines in the 1770's in England. Since then, many patents for rotary machines have been filed.

Felix Wankel in cooperation with NSU (Germany) manufactured a rotary engine and successfully installed it in a commercial car for the first time in 1964. The rotary engine has no reciprocating piston and valvetrain - which are sources of vibration and limitation of high engine speeds. The rotary engine usually has more power strokes per revolution than a reciprocating piston engine. Hence, the inherent features of a rotary engine are less vibration, compactness, lightweight and high performance.

However, the Wankel engine has inherent problems which affect reliability, efficiency and emissions. It may not be the best engine to demonstrate all of the merits of a rotary engine.

Rotary pumps are rotary machines designed to convert mechanical power to fluid

energy. Gear pumps and vane pumps are the main examples of rotary pumps presently being widely used in industry. Only a small angular portion of gear rotors in gear pumps are able to do useful work - this means an inefficient device. In vane pumps, working pressure may largely be limited by the rigidity of the sliding vanes.

A unique rotary machine is proposed in this work. Two rotors with a set of intricate meshing surfaces, rotate in the same direction to obtain compression or expansion chambers.

During the course of these investigations, an air motor made of aluminum and lucite was operated successfully using compressed air as a physical model, which verified the design principles. A prototype hydraulic pump has also been constructed and tested to demonstrate its potential for industrial applications. As the ultimate objective of the study, a unique rotary engine is proposed. Fundamental theoretical research has been done on the engine.

This engine has a pure rotary mechanical structure and semi-internal/external combustion system. The rotors move in a purely rotational manner around their own fixed centres. It is naturally free from mechanical vibration, bumping forces and noise. The fuel will be burnt continuously in a precombustion chamber, which is externally attached to the main body of the engine, and then introduced periodically into the power chambers. It is a unique thermodynamic system, from which the engine could be easily adapted to various kinds of alternative energy sources; high efficiency and good emission control are expected to be achieved. The mechanism has been demonstrated in a CAD

software by animation. A physical working model has been operated successfully.

In order to understand and optimize the performance of an engine, intensive theoretical research has been conducted. A three zone turbulence eddy entrainment thermodynamic model has been constructed to analyze such a new engine. The performance of the engine can be predicted and major control parameters analyzed to optimize the performance with the theoretical model.

The original contributions of this work include:

i) establishment of a curve fitting method to complete the mechanical design of the meshing rotors

ii) development of a unique hydraulic pump and a fuel flexible combustion engine

iii) construction of a unique thermodynamic model to analyze the engine with a combination of internal and external combustion systems

The major emphasis in this thesis is the development, from concept to model and prototype, of a unique rotary machine and the theoretical thermodynamic analysis of the engine aspect of the machine.

The first part (Chapter 2) will be a literature review of some typical rotary machine patents, development of the typical rotary engine, Wankel Engine and theoretical modelling of combustion in the engine. The second part (Chapter 3 and Chapter 4) will be the general description of the rotary machine and two versions of the machine namely the air motor and hydraulic pump. The third part includes three chapters (chapter 5 through chapter 7) to demonstrate the theoretical work on the rotary engine. Chapter

eight will conclude this work and make recommendations for future work. Most of the detailed derivation of equations and calculation results are placed in Appendices.

CHAPTER 2

LITERATURE REVIEW

Rotary machines have been widely used as pumps, fans, compressors and heat engines. The variety of rotary machine arrangements seems to be almost infinite. Vastly different basic configurations are possible, of which, each individual type may be executed in many and greatly differing versions. There are hundreds of rotary machine patents being filed every year, some of which could be traced back to eighteenth century.

Felix Wankel made a comprehensive survey of rotary machines in 1965 in his book 'Rotary Piston Machines'. This book included so many examples and illustrations that it remained for decades the best known technical review in this field.

It is not intended to make a comprehensive coverage of all rotary machine in this review. A brief classification of the rotary machines will be given in the first part. It will then be followed by a brief review of the development of the Wankel engine, the most successful rotary engine to date and the literature dealing with thermodynamic modelling of engines.

2.1 Rotary Machine Patents

The term 'machine' used in this work refers to dynamic machines which are used to transform a given form of energy from some working media, gas or liquid, into a

more useful form such that work can be done by the shaft of the machine on the environment. The term also applies for machines where environment activates the shaft and work is done on the working media. The former is a motor/engine and the latter is a pump. It is a mechanism which contains a working chamber, surrounded by solid walls for the accommodation of the working media. The chamber volume is varied by the relative movement of at least one part of the chamber wall with respect to the rest while maintaining efficient sealing contact. Dynamic machines may be divided into two major groups according to the behaviour of the centre of gravity (c.g.) of the power output/input member and the method of chamber volume variation. That is, machines with reciprocating motion and those with unidirectional motion. Reciprocating (piston) machine, in which the c.g. of the power transmitting part (piston) moves to and fro in a straight line belongs to the first category. Rotary machines of which the c.g. of the power component (rotor) moves in one direction along a circular or differently shaped closed path belongs to the second category. One or more rotor(s) are usually included in the rotary machines, which are constructed with teeth or lobes. The term 'teeth' or 'lobes' are rather broadly used in this sense and may signify corners, projections, scallops, involutes and other gear tooth shapes.

Rotary machines may be divided into three distinct groups according to the mode of motion imparted to the centres of gravity of the moving parts: single rotation machines (SIM), planetary rotation machines (PLM) and rotating piston machines (ROM). For a single rotation machine, all the moving parts rotate at uniform angular velocities about

their own stationary centre of gravity. These machines may be completely balanced, hence there are no dynamic loads on the bearings. Consequently, they are eminently suitable for the highest rotational speeds.

All moving parts of planetary machines rotate at constant angular velocities in addition to which at least one of the moving members performs a constant planetary rotation - the centre of gravity moves in some way besides turning. Although the orbiting parts may be completely balanced, the force due to their moving masses must affect the loads imposed on at least one bearing.

When any of the moving parts rotates at variable angular velocity, displaying characteristics similar either to the single rotation machine or planetary rotation machine, it belongs to the rotating piston machine group. This type of machine will be found suitable only for low to medium speeds, which will not be discussed in this work.

Besides the rotational mode of the rotors it is necessary to further distinguish rotary machines by the relative positions of their axes of rotation, either in parallel axes or inclined axes. Furthermore, parallel axes may be arranged externally in the same way as the axes of two external teeth spur gears or internally as those of an external spur gear meshing with the internal teeth of a ring gear.

Figure 2.1 shows examples of single rotation machines with parallel axes being arranged either internally or externally. Both the outer piece and inner piece rotate around their own centre of gravities to compensate for the eccentricity between them in the internal arrangement. It is notable from the diagrams that most of the machines in

these designs do not have sealing components. The external arrangement machines are mainly for pumps or compressors and the internal ones for engines. Figure 2.2 shows examples of planetary machines, most of which have internal parallel arrangements. In each design, at least one of the pieces is stationary and the rotor turns inside it in an internal arrangements or beside it as in external arrangement. It is the planetary movement of the rotor that compensates for the eccentricity. Sealing components are necessary in the internal case because of the high relative speeds between the running rotor and stationary housing.

For example, comparing the Fixen design in Figure 2.1 with Herrmann and Wankel design in Figure 2.2 we can see that a planetary rotation machine could be modified to a single rotation machine by just having the outer housing turn with the inner

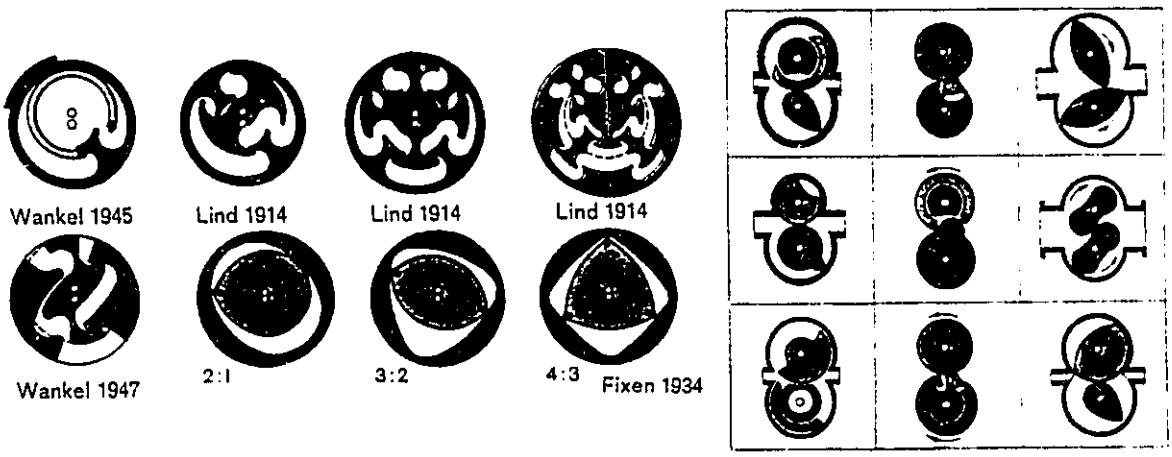

(a) Internal parallel axes (b) External parallel axes

Figure 2.1 Single rotation machines

rotor.

Some rotary machine designs with rolling-piston rotor or reciprocating engagement that may belong to one of three above discussed category are shown in Figure 2.3. Rotary machines with reciprocating engagement were widely used as steam engines in the early days.

During the survey, it was interesting to find that a group of rotary machines are related in terms of rotor shape and operation no matter when their patents were filed. This group of patented machines are shown in Figure 2.4. In the diagram, the figures with a solid dot in one of the two centre points represent the planetary machines and those with two hollow circles the simple rotation machines. It seems that these are the precursor for Felix Wankel's engine, which is today's only successfully commercially

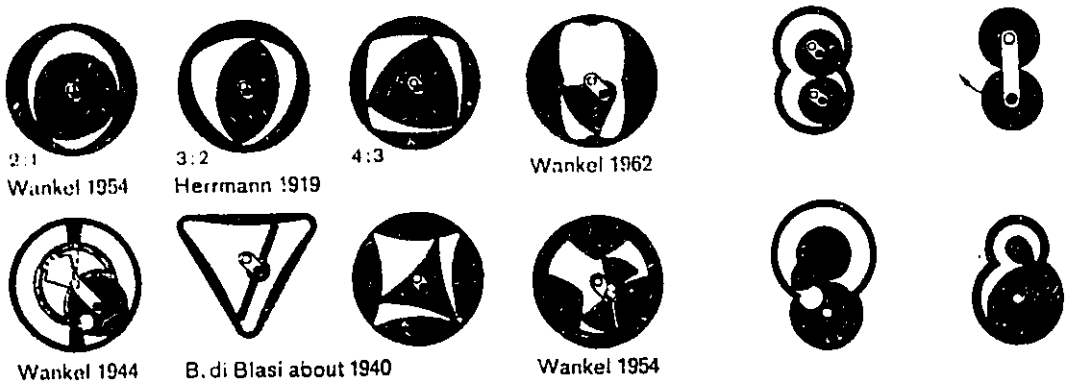

(a) Internal parallel axes (b) External parallel axes

Figure 2.2 Planetary rotation machines

operating rotary engine. Earlier designs (Galloway and Sauveur) are simple rotation machines without sealing components. It is hard to tell if the lobes of Galloway's design could engage with the outer rotor all around the path at that time, even though we can now mathematically prove its possibility for that simple circular lobe case. However, it is fairly sure that Sauveur's design will not perform that kind of engagement even with today's CAD techniques. Later, sealing components were employed in similar designs. Most of these later designs belong to planetary rotary machine types which have unbalanced mechanical forces. de Lavaud's design is a simple rotary machine. The eccentricity that will determine the flow capacity is restricted by the performance of the

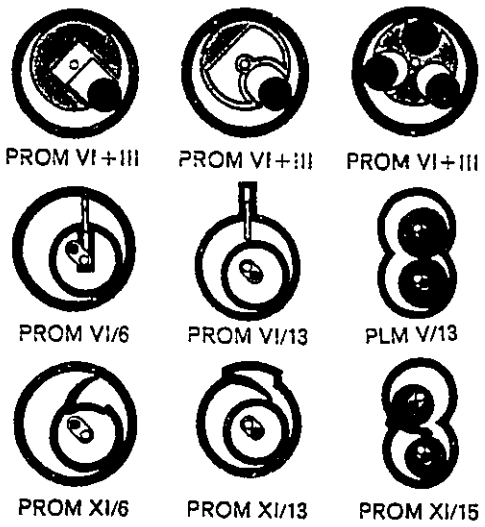

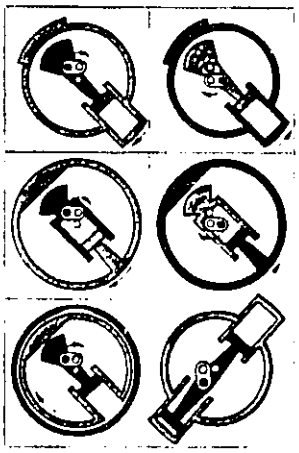

(a) with rolling-piston rotor (b) with reciprocating engagement

Figure 2.3 Some typical designs of rotary machines

sealing component. Also it seems that high pressure is not preferred inside the chambers otherwise a deformation of the sealing component may result.

Among the rotary machine patents, rotary engines is the largest group. By 1910 more than 2,000 patents were filed world-wide on the concept of a rotary engine (Jackson, 1992). Some interesting engine patents will be introduced in the following while the most important rotary engine -- the Wankel rotary engine is described in the next section.

Figure 2.5 shows an example of a simple rotation engine with an external parallel axis arrangement. Gas exchange is controlled by a sliding cylinder between the two rotors. Apparently it will have a small power/weight ratio resulting from the external arrangement. Figure 2.6 shows an example of a planetary rotational engine with rolling

Figure 2.4 An interesting group of rotary machines

piston rotors. Those cylinders move in a planetary motion so that the volume of the chambers varies while the main rotor rotates around its own stationary centre of gravity.

A rotary engine with vane engagement is shown in Figure 2.7. Four rigid vanes are controlled by a set of Sun-planet gears and a four bar mechanism crank to form the properly timed volume variable working chambers. With a rotary engine, it is relatively easy to construct a stationary position of the energy receiver. A heat exchanger, for example, could be used as a kind of that energy receiver. Therefore, alternative energy sources to liquid fuels, such as solar energy, nuclear energy and so on may be used. In the device shown in Figure 2.8 (Gudzenko, 1982) the working medium is sealed inside the power system and oscillates between the power device and heat exchanger to convert

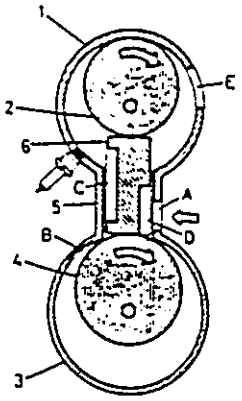

(American Pat 3364906)

Figure 2.5 A simple rotational engine with external parallel axes

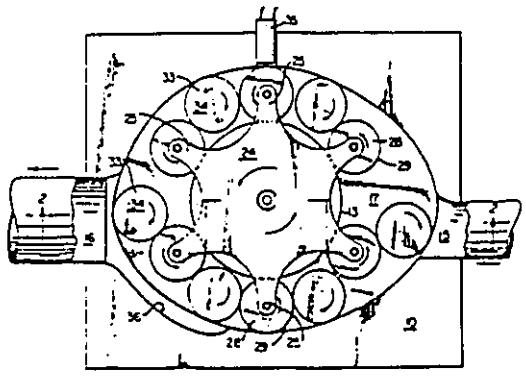

(American Pat 3641985)

Figure 2.6 A planetary rotational engine with rolling piston rotors

heat energy to mechanical energy. Laser energy in this case is delivered through a window to heat the working medium and drive the rotor.

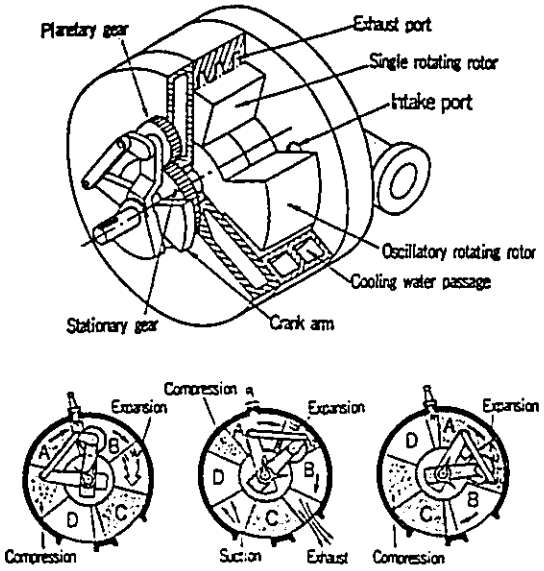

Figure 2.7 Rotary engine with vane engagement (Kauertz's rotary engine)

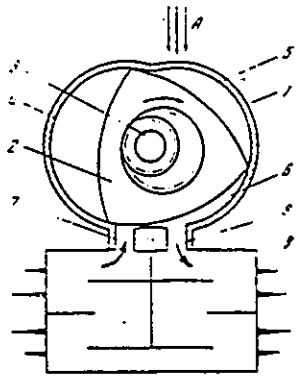

Figure 2.8 A Rotary engine using laser energy

2.2 Development of the Wankel Engine

The Wankel engine, in the forms of either the initial design (Yamomoto, 1981), stratified charge or supercharge (Tashima, 1991 and Mount, 1987), with water or air cooling (Adam, 1980) are finding more and more applications for auto, marine craft and motorcycles (Jones, 1985, Mount, 1987 and Garside, 1982).

The basic structure of the Wankel type rotary engine is shown in Figure 2.9 (Yamamoto, 1981). The inner surface of the rotor housing is cocoon shaped, and the

rotor performs a rotating motion inside the housing. By arranging side housings on both sides of the rotor housing, three working chambers are formed.

To control the motion of the rotor, a rotor gear and a stationary gear is fitted to the rotor and side housing with a gear ratio of 3:2. As shown in Figure 2.10, by having the rotor gear rotate while being meshed with the stationary gear, the apex of the rotor will rotate by drawing a epitrochoid which is the basic curve of the rotor housing. It belongs to the planetary rotational machine category.

Figure 2.11 is a cross section of a typical Wankel rotary engine, which is now being built by Toyo Kogyo (Mazda) company.

Felix Wankel first manufactured the mechanism in the form of rotary compressor in 1951 and successfully developed a rotary engine in 1954 with the cooperation of NSU.

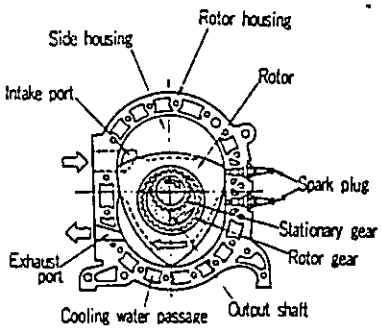

Figure 2.9 Basic structure of the Wankel rotary engine

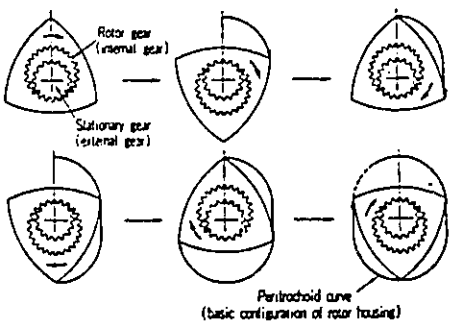

Figure 2.10 Generation of epitrochoid curve

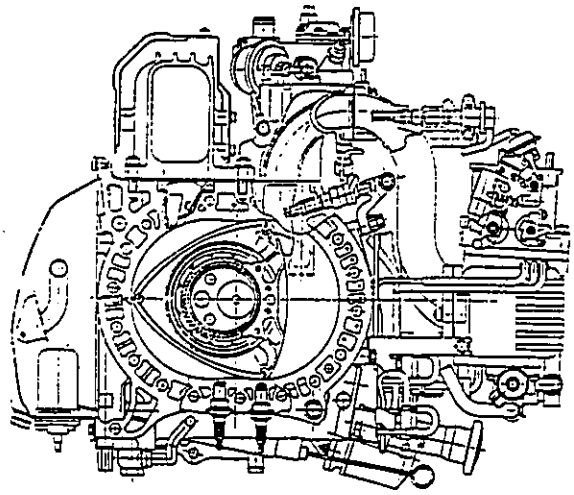

Figure 2.11 Cross section of a typical Wankel engine

In 1959, the NSU-Wankel rotary engine successfully completed a durability test and in 1964 NSU installed a 497.5 cc*1 rotary engine in its 'Spider' sports car. This became the first rotary engine powered car in the market.

Toyo Kogyo company in Japan introduced the Wankel engine in its 'cosmo sports' car in 1967 and started its mass production for the Mazda Rx-7 sports car from 1970. It has powered three generations of Rx-7 and won innumerable races. In a comparison test of sports cars in 1992, RX-7 won the silver medal for its performance (Bedard, 1992). Due mainly to its unique engine, it was the lightest (about 280 kg or less) and least expensive car among the competitors. Its 1993 model (Figure 2.12) is powered by a twin-turbocharged two rotor Wankel rotary engine, which produces 255 horsepower

with its 1.3 litre displacement. Another generation of Wankel engines is projected to burn hydrogen and it is presently being fleet-tested (Lachapelle, 1992). The Wankel engine has been described as being "ideally suited for hydrogen use" because its separation of the intake and combustion chamber to eliminate the problems of preignition and backfiring.

The Wankel rotary engine is the only successful rotary engine in the commercial market so far. It is however, not the best one to demonstrate all the benefits of the rotary engine because of the following:

a) It is a planetary rotational machine, which has unbalanced forces so that high speed is still restricted.

b) High relative speeds exist at the tips of the rotor against the housing which results

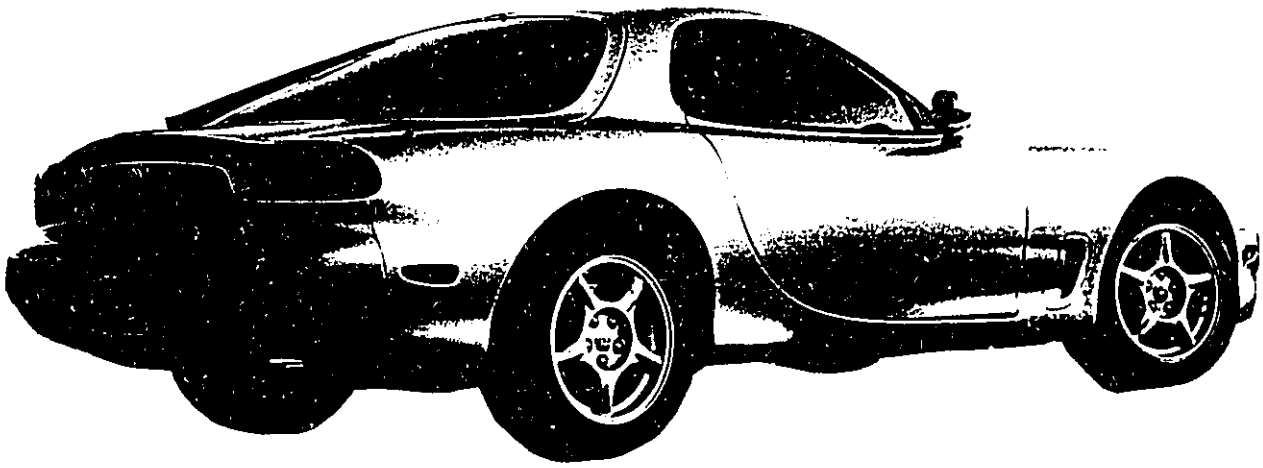

Figure 2.12 1993 model of Mazda Rx-7

in wear/friction and leakage problems.

c) The long and narrow shape of combustion chamber results in a large surface to volume ratio and long flame travel path which causes problems of heat loss, HC emissions and detonation.

2.3 Theoretical Models for Combustion Engines

In the past two decades there has been a substantial increase in thermodynamic modelling activities to improve the design and operation of internal combustion engines (ICE) to meet increasing stringent emission and economic requirements. The majority of these models are prediction models with the following purposes:

i) To predict behaviour over a wide range of design and operating variables and to optimize design and control parameters before major hardware being built.

ii) To develop a more complete understanding of the physical system inside the engines.

The development of experimental technologies plays an important role in modelling studies. It provides a tool which enables us to get a better understanding of the phenomena and to verify the results of the models. HIGH-SPEED PHOTOGRAPHY METHODS have been used to observe flame propagation behaviour for a long time (Nishida, 1986). The results afforded much qualitative knowledge for understanding the process but little quantitative information is available. PRESSURE TRANSDUCERS are

reliably used in practice but the mass burning rate is difficult to measure, since an accurate evaluation of transient heat loss is not possible (Borman, 1987). HOT WIRE ANEMOMETRY has been used to measure gas velocity and turbulence characteristics in cylinders (Dent, 1975 and Lancaster, 1976). The measurement is limited to a few local points and the probe is likely to interfere with the flow and may be easily destroyed by a hostile environment. LASER DOPPLER ANEMOMETERS have been used successfully to measure gas flow and turbulence without combustion (Rask, 1979, Zimmerman, 1983 and Chouinard, 1990). However, as soon as combustion starts, problems such as seeding the flow and optical access will be the big obstacle to accurate measurement (Lancaster, 1976 and Craig, 1988). HOLOGRAPH INTERFEROMETRY has been recently used for combustion measurement, but few publications are available (Craig, 1988).

A "thermodynamic model" refers to the numerical simulation of the process inside the cylinder of an engine. A model may concentrate on some specific problem(s) in reasonable detail according to the purpose and available cost. There are two kinds of models:

(a) Multidimensional Models and

(b) Phenomenological Models

Multidimensional models (such as those by Steinthorsson, 1988, Grasso, 1987 and Zellat, 1990) calculate the time and space dependent patterns of gas flow, heat transfer and combustion in the cylinder by numerically solving the governing partial differential

conservation equations, such as the mass, energy, momentum equations. Depending on what kind of predictions and how detailed the information requirements are for a particular purpose of investigation. All or some of those equations are incorporated in a one, two or three dimensional computational grid using a finite difference or finite element method. Thus, a one, two or three dimensional model may presented. This approach is capable of basically predicting local and instantaneous gas flow, temperature and species concentration. It promises universal applicability to a particular type of combustion system and will give information which may be difficult to obtain by direct measurements. It is, however, still in a development stage (Borman, 1987 and Kazuo, 1992). There are some arguments about the adequacy of turbulence models, boundary and initial conditions, and numerical errors with grid spacing. There are also some ambiguous phenomena which are difficult to model and need to be investigated by experimental analysis. For example, only very simple reaction-rate modelling is possible and a full turbulence model has not yet been established in present multi-dimensional models.

Phenomenological models (such as that by Blumverg, 1979), on the other hand, attempt to describe complex engine behaviour in terms of separate, physically based submodels, such as a mass burning submodel, a heat transfer submodel and a gas property submodel. Typically, the first law of thermodynamics and the perfect gas law are involved in the submodels and explicit spatial variables are not available. For some phenomena which may not be quantitatively definable, such as the turbulent flame

propagation and heat transfer coefficient, a empirical or semi-empirical method is adopted. With a successful phenomenological model, one can predict the performance of a engine and obtain such quantities as power output, fuel consumption, total heat loss or NO_x and HC emissions, as a function of design and control parameters such as spark or injection timing, intake system, speed, fuel air ratio and EGR (Exhaust Gas Recycled) ratio. These design and control parameters can be optimized through the model to obtain a good performance prediction of the engine.

A phenomenological model will be established in this work to predict the performance of the engine investigated in this work for evaluation and improvement. Therefore, a relatively detailed review will only be given to this kind of model. It is classified as a zero-dimensional model and a quasi-dimensional model in the following discussion.

2.3.1 Zero-Dimensional Model

The following assumptions are commonly used in the zero-dimensional model:

i) Time is the only independent variable for all the thermodynamic parameters such as temperature, pressure, and gas composition of the gases in the cylinder

ii) All gases in the cylinder, burned and unburned, are in thermal and chemical equilibrium and satisfy the perfect gas law

iii) Combustible mixture is 'changed' to combustion products and hence heat is released in an assumed fashion with time - called mass burning rate, and this

occurs irrespective of location

iv) Heat losses from the wall of the chamber are by forced convection due to the difference of time dependent bulk gas temperature and constant wall temperature.

The First Law of Thermodynamics

$$\frac{dQ(\theta)}{d\theta} = \frac{dE(\theta)}{d\theta} + \frac{dQ_w(\theta)}{d\theta} + P\frac{dV(\theta)}{d\theta} \qquad (2-1)$$

and Perfect Gas Law

$$pV = MRT \qquad (2-2)$$

are the only governing equations.

In the model, pressure **p** and temperature **T** are the unknown variables to be predicted from equations (2-1) and (2-2). $V(\theta)$ is determined by the engine design. A heat release submodel, heat transfer submodel and gas property submodel are established to calculate $Q(\theta)$, $Q_w(\theta)$ and $E(\theta)$ respectively.

(a) Heat Release Submodel

Heat released at some instant $Q(\theta)$ is calculated as

$$Q(\theta) = H_u * M_f * X(\theta) \qquad (2-3)$$

For premixed engine models, the mass burned fraction $\mathbf{X}(\theta)$ is related experimentally with the ignition time θ_0 and burning duration $\Delta\theta$ in some fashion. For these, the Wiebe function and Cousin burning law (Heywood, 1988) are widely used. Some engine dependent parameters are used in these functions. They are useful for extrapolation from conditions for which experimental data are available.

Taking the **Wiebe function** for example, it uses an efficiency parameter a $(3<a<10)$ and a form factor **m** $(1<m<3)$ to fit the experimental data:

$$X(\theta) = 1 - \exp(-a(\frac{\theta-\theta_0}{\Delta\theta})^{m+1}) \qquad (2-4)$$

It was obtained by J.J. Wiebe in 1960 and is still widely used in the performance prediction of both SI engines (Heywood, 1979) and Wankel engines (Roberts, 1986).

(b) Heat Transfer Submodel

Heat loss of the engine is commonly calculated as a forced convection loss

$$Q_w(\theta) = A(\theta)h(\theta)[T(\theta)-T_w] \qquad (2-5)$$

where wall area exposed to the gas $\mathbf{A}(\theta)$ is determined by the geometry and piston movement. Gas temperature $\mathbf{T}(\theta)$ will be obtained by an iterative method. $\mathbf{T_w}$ is usually assumed to be a constant - this is in accord with experimental results. Heat transfer coefficient $\mathbf{h}(\theta)$ is a complex function of gas properties, flow field and boundary layer. It can only be determined empirically from experimental results. There is a large body of research literature on heat transfer coefficient for ICE. A few important steps in the development can be described briefly as follows:

Nusselt (1923) found by trial the following formula using a spherical bomb:

$$h = 0.99\sqrt[3]{P^2T} \qquad (2-6)$$

Later, to allow for the influence of piston motion in the engine, Nusselt added the additional factor of average piston speed $\mathbf{C_m}$ to obtain the well-known formula

$$h = 0.99(1+1.24Cm)\sqrt[3]{P^2T} \qquad (2-7)$$

Eichelberg (1939) followed Nusselt's work and considered the influence of radiation in a lumped form by increasing the power of **T** and decreasing the power of **P** by empirical means to obtain:

$$h = 2.1\sqrt[3]{Cm}\sqrt{PT} \qquad (2-8)$$

Annand (1963) extended the radiation term, considered the gas flow pattern inside the cylinder and proposed a more applicable formula.

$$h=0.49(\frac{k}{d})R_e^{0.7}+0.91[\frac{(\frac{T}{100})^4-(\frac{T_w}{100})^4}{T-T_w}] \qquad (2-9)$$

Woschni (1967) concentrated his experimental research on the effects of combustion on the heat transfer in the engine, pointing out that combustion process accelerates the gas movement inside the cylinder, thus accelerating forced convection heat transfer. The results of his experiments also showed that gas and flame radiation is insignificant in heat transfer for homogenous mixture combustion. The empirical formula developed 25 years ago is still a widely used practical tool in the prediction of heat transfer for conventional SI engines (Gatowski, 1984 and Tabaczynski, 1980), stratified charge SI engine (Hires, 1976), Wankel engine (Danieli, 1974 and Dimpefeld, 1987) and diesel engines (Lakshminarayanan, 1986 and Pinchon, 1985):

$$h=110d^{-0.2}P^{0.8}T^{-0.53}[C_1C_m+C_2\frac{V_ST_1}{P_1V_1}(P-P_0)]^{0.8} \qquad (2-10)$$

where, C_1 and C_2 are empirical parameters determined by the specific engine design. P_1,T_1 and V_1 are associated with a known state of the gas, say inlet closure.

To use Woshni's formula for a Wankel engine, some characteristic parameters have to be redefined according to geometric changes of the engine. G.A. Danieli (1974) checked experimentally the constants in the formula and redefined the characteristic velocity as V = r ω/3 (r = generating radius, ω = crankshaft angular velocity) and characteristic diameter as hydraulic diameter of flow passage. P. Dimpelfeld (1987) simplified the procedure by using a rotor width and rotor apex velocity as the characteristic length and velocity respectively.

(c) Gas Property Submodel

It is a common assumption in gas property submodels (Lavoie, 1970, Blizard, 1974 and Tabaczynski, 1977) that the volume of the reaction zone is negligible and that the gas within a cylinder consists of a burned fraction at thermodynamic equilibrium plus an unburned fraction frozen at its original composition. Together with the assumption of uniform pressure in the cylinder, the equations for conservation of volume and energy are

$$\frac{V}{M} = \int_0^X v_b dx + \int_X^1 v_u dx \qquad (2 - 11)$$

$$\frac{E}{M} = \int_0^X e_b dx + \int_X^1 e_u dx \qquad (2-12)$$

There are three different techniques in the literature for dealing with gas property evaluation: fitting data, combining curve fitting with some approximations to thermodynamic equilibrium calculations and basic theoretical analysis.

J.A. Roberts (1986) used a straight line to fit the data of the ratio of specific heats γ with temperature, which is believed to be the most important thermodynamic property used in the calculating heat release rates for engines:

$$\gamma(T) = 1.427 - 8.87(10)^{-5}T(K) \qquad (2-13)$$

Blizard and Keck (1974) used the data from Taylor and Taylor (1966) and JANAF (1960) tables for fitting curves to set up a program to calculate internal energy, specific heat and its ratio γ for burned and unburned gases as the function of temperature, equivalence ratio and recycled fraction. In the program, only seven thermodynamically important species are considered: C_nH_m, N_2, O_2, H_2O, CO_2, CO and H_2.

Martin and Heywood (1977) developed a program theoretically to calculate molecular weight M, density ρ, and enthalpy h for combustion products as the function of temperature, equivalence ratio and the molecular dissociation.

2.3.2 Quasi-Dimensional Models

To obtain more information about combustion characteristics quasi-dimensional models modify the zero-dimensional models by substituting heat release submodels with flame propagation submodels. The submodels of heat transfer and gas property are retained and are the same as in the zero-dimensional models.

In a typical quasi-dimensional model, a spherical flame front moving outward from the spark plug divides the cylinder volume into two zones: unburned zone and burned zone. The flame front characterized by turbulence and the techniques of how to deal with the turbulent flame propagation determine the features of a specific model. The common assumptions for these models are:

i) uniform pressure distribution across the whole region

ii) uniform distributions of all thermodynamic parameters, such as temperature, gas composition etc, within each zone

iii) the volume of the reaction (burning) zone is negligible and the gas within a cylinder consists of a burned fraction at thermodynamic equilibrium plus an unburned fraction frozen at its original composition.

There are two basic approaches for the modelling of the combustion process.

(a) Flame Propagation model

In this model, the flame front is assumed to be wrinkled due to turbulent reflection upon a moving front with laminar burning velocity. The effect of turbulence

on the flame propagation is empirically lumped in some engine structure and/or operating condition dependent constants.

The flame propagates according to following burning rate, with **X** be defined as the mass fraction of burnt fuel:

$$\frac{dX}{dt} = \frac{dm_b}{dt}/m_0 = \rho_u A_f S_T / m_0 \qquad (2 - 14)$$

Lucas (1973) related the turbulence flame speed S_T to laminar flame speed S_l by the expression

$$S_T = K_T S_l \qquad (2 - 15)$$

where, K_T is a constant depending on engine speed **N**: $K_T = 1 + 0.002 * N$

The laminar flame speed S_l can be calculated with Bantiggelen's formula (1957).

Samaga (1975) accounted for the expansion effect of the burning gases by introducing a flame transportation coefficient C_T:

$$S_T = C_T \sqrt{S_l^2 + C_1 R_e^{C_2}} \qquad (2 - 16)$$

where C_T is calculated from the pressure-burned volume history, C_1 and C_2 are the constants depending only on engine's geometry and **Re** is a Reynolds parameter given by $R_e = U_j D\rho/T_{av.}^{0.67}$ (U_j = induction jet velocity, D = cylinder bore diameter).

(b) Eddy Entrainment Model

The second approach attempts to simulate the turbulent engine combustion process based on fundamental physical parameters such as the turbulent eddy structure, turbulent intensity and laminar flame speed. The so-called "Eddy Entrainment Model" is a notable example of this approach. As an extension of the ideas of Damkohler (1940) and Shchelin (1943) to the SI engine, Blizard and Keck (1974) set up this model. Later, Tabaczynski and Fergusion (1977) and Hires, Tabaczynski and Norak (1978) extended the model successfully by postulating a detailed turbulent eddy structure and eddy burn-up model and related the parameters of that structure to those of the geometry and control of the engine. Later, some major modification and wide applications were made to the SI engine (MeCuiston, 1977, Hires, 1978 and Groff, 1987), Wankel engine (Danieli, 1978) and alternative fuelled SI engine (Rao, 1983).

The following assumptions are adopted in the combustion model:

(a) A flame front with finite thickness propagates through the combustion chamber containing homogeneously distributed eddies. This flame front divides the volume into two zones, namely, burned and unburned zones.

(b) No heat is transferred through the flame front. Unburned gas is compressed isentropically before being burned.

(c) At spark ignition, the turbulence integral scale L_i and turbulent intensity U'_i are proportional to the chamber height h_i and the piston speed S_p respectively. i.e.

$$L_i = C_L h_i$$

$$U'_i = C_u S_p$$

(d) After the beginning of measurable heat release, taken as 1% mass fraction burned, the turbulence intensity and integral scale of the unburned gas are governed by the conservation of angular momentum of the individual eddies. That is

$$L = L_i (\rho_{ui} / \rho_u)^{1/3}$$

$$U' = U'_i (\rho_u / \rho_{ui})^{1/3}$$

The eddy entrainment model can be used to calculate the burning rate as a function of certain design and operating parameters of engine (Hires etc, 1978):

$$\frac{dx}{dt} = C_x \left(\frac{A_f}{A_b}\right)\left(\frac{\rho_{ui}}{\rho_u}\right)^{-10/9}\left(\frac{h_i}{S_p S_l}\right)^{-2/3} \nu^{-1/3} \qquad (2 - 17)$$

where

$$C_x = \frac{C_L}{1.8(15/A)^{1/3}(C_l/C_u)^{2/3}} \qquad (2-18)$$

is a constant dependent only on engine geometry and independent of engine operating conditions. **A** is a constant of order of one, which comes from the derivation of Taylor microscale in isotropic turbulence (Tennekes, 1972).

CHAPTER 3

GENERAL DESCRIPTION OF THE ROTARY MACHINE

3.1 Introduction

The rotary machine being developed in this work, which will be referred to as the RVP rotary machine because of patent designation, is a single rotational machine with internal parallel axes arrangement. It comprises two rotors, an outer rotor and an inner rotor, both rotating at constant angular speed about their own stationary centres of gravity. The outer rotor is mounted on an outer rotor bearing rotating on the outer rotor axis and the inner rotor on the inner rotor axis. These two parallel axes are offset from

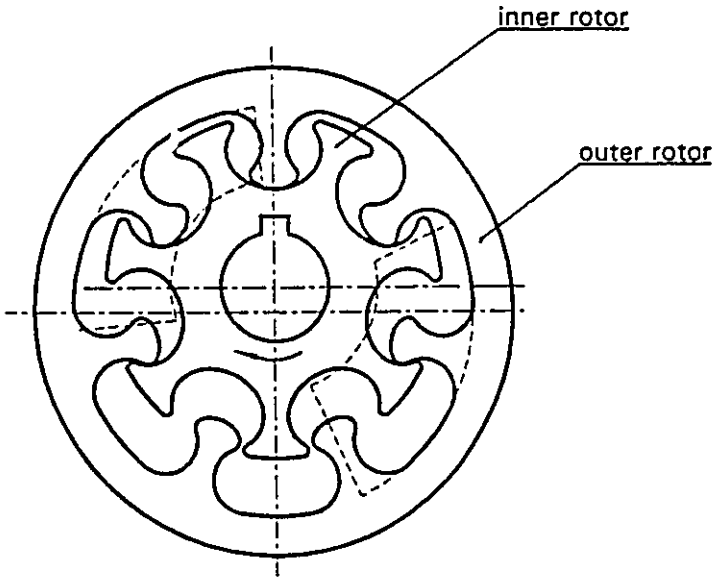

Figure 3.1 Rotors design for RVP rotary machine

each other by a distance - the eccentricity (refer to figure 3.1 for the mechanical design of the rotors).

An array of lobes projecting radially inward from the body of the outer rotor defines an array of peripheral recesses. The inner rotor has arms projecting from its body contacting a point on the boundary of the outer recess and completing an enclosed chamber. N number of lobes will define N number of chambers within the annular space of the inner and outer rotors. Because of the eccentricity between these two rotors, the chambers formed below the centre of outer rotor will bigger than those above if the eccentricity is positive. Therefore, while the two meshing rotors rotate together in the same direction, the chambers will contract on one side and expand on the other side. This is essential for this machine to perform energy conversion.

The structure is similar to that of the internal gear arrangement. However, it is unlike an internal gear arrangement which only has a small portion of gears (about 1/3 of the total) meshed while working, the rotors in the RVP rotary machine are meshed almost entirely around 360 degrees (refer to Chapter 4 for details). As a dynamic machine, either a pump to convert mechanical power to fluid energy or a motor to convert fluid energy to mechanical power, this feature means a great improvement in efficiency.

The question of how the curves forming the lobes on the outer rotor and the arms on the offset inner rotor mesh together throughout a rotation is the first fundamental problem that has to be solved in this work.

3.2 Curve fitting and rotors design

The first problem is to generate a proper curve enabling the arm (or lobe) to mesh with a given lobe (or arm) at a fixed eccentricity throughout 360 degrees. For the engine design, the lobes must be shaped to meet the aerodynamic requirement of the injection (refer to later sections for details) so that maximum momentum exchange could be obtained. Considering other geometrical limitations, the asymmetrical lobes, and hence asymmetrical rotors are designed for the engine. In the case of pump, the fluid dynamic requirement during the induction will no longer be that important. For the purpose of simplicity, symmetrical rotors are designed.

The shape of lobes on the outer rotor were designed first to meet the fluid dynamic requirements and the arms on the inner rotor were designed to mesh the lobes. A curve fitting method was created by computer to generate the curve point-by-point.

Equations were set up describing the geometrical contour of the curve of an arm relative to the curve of a lobe. In these equations, some of the variables depend on the curve of the lobe and the relative position of the two curves. Because of this, some numerical method had to be devised to solve the equations by computer. The result of the solution was a series of coordinates to describe the curve. This computer output could be used to generate the curve by CAD techniques. The closer the coordinate points spatially placed, the more accurate curve could be obtained.

The following parameters are the primary variables that should be determined

before a meshing curve can be created during rotor design:

a) Diameters of both two rotors, which are determined by the required fluid flow capacity and material strengths.

b) Number of lobes/arms, which is determined by size of the machine, characteristic requirements of the operation and material strength.

c) Eccentricity, which is determined by the function of the machine, the geometrical compression ratio and fluid flow capacity.

d) Input and output ports shape and position, which are dependent on the function of the machine and the characteristics of the fluid.

These parameters are not independent of each other. They are usually determined by a trial and error method using CAD techniques during the initial design stage.

3.3 RVP rotary engine - an application of the RVP rotary machine

Applications of the RVP rotary machine may be in the following two fields: a pump or a power motor. A prototype hydraulic pump and a concept design of a rotary engine have been investigated in this work. As an introduction, the rotary engine will be described in this section as an example of the application of the RVP rotary machine.

The advantages of a rotary engine are well known: simple structure, high power/weight ratio, high speed capability and smooth operation. Based on the fundamental design of the RVP rotary machine, adding a pre-combustion chamber

externally to the machine, a new rotary engine (RVP-ROE) has been proposed.

Figure 3.2 shows a prototype RVP rotary engine design. Two rotors with 8 mushroom shaped lobes/arms each turn in the same direction. The mashing lobes/arms create chambers of expanding and contracting volume, and in doing so, the engine undergoes intake, compression. expansion and exhaust strokes as a conventional four-cycle engine does. A rich mixture burns continuously in the precombustion chamber. As the rotors turn, burning gases are injected into the power chambers through the injection port periodically when slots in the outer rotor are aligned. During the process of injection, the hot burning gases mix with fresh air charged through the intake port to complete their combustion at a lean mixture level in the power chambers. In the power chambers the gases expand and do work on the rotor system until an appropriate chamber is connected to the exhaust port and then they exhaust to the atmosphere. There are eight power strokes per revolution of the

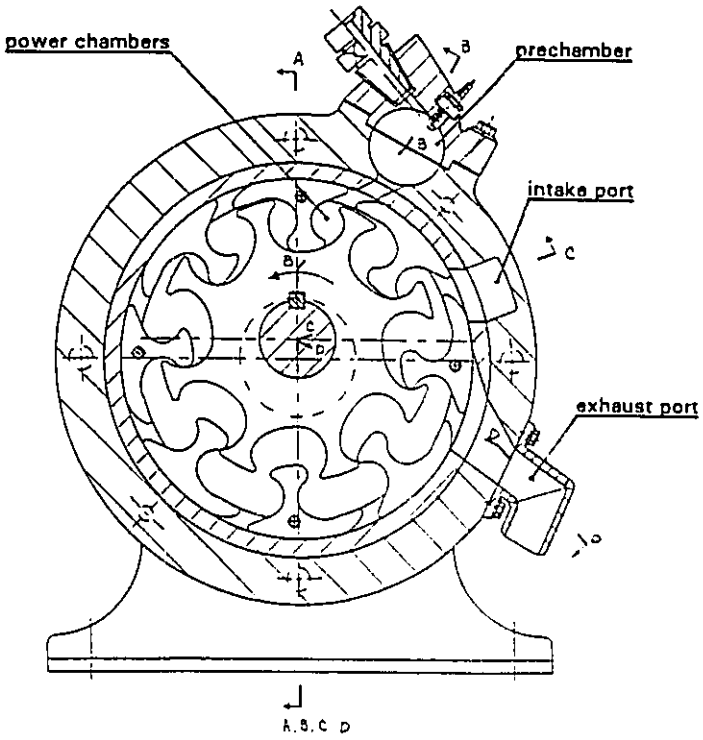

Figure 3.2 Prototype of RVP rotary engine

shaft.

Beside the common advantages a rotary engine may have, the RVP rotary engine also has the following special features:

a) Fuel flexible feature. Because the precombustion process takes place continuously outside the expansion chambers, the engine is readily suitable for any gaseous fuels, such as natural gas, propane and hydrogen. For example, a typical problem of power drop because of lower charge due to the low density of these gaseous fuels will be automatically eliminated because of the external precombustion system. By sealing a working medium inside the system and using some kind of energy exchange system, even nuclear or solar energy may possibly be adapted.

b) Smooth and quiet operation. Because of its purely rotational structure, the engine will be naturally free from mechanical vibration and bumping and thus will operate quietly. Additionally, the feature of multi power strokes per revolution (eight power strokes/revolution in this design) will result in very smooth torque output characteristics.

c) Good performance for efficiency and emission. It is easy to organize a stratified charge combustion: lean mixture burns in the power chamber while rich mixture burns in the precombustion chamber. With a compact combustion chamber compared with that of Wankel engine, a good performance of the engine both in terms of efficiency and emission is expected.

d) Low friction/wear. The two rotors rotate together in the same direction. The relative velocity at the contact surfaces between them will be very low which will contribute much to the solution of sealing, friction and wear problems.

It has been confirmed by the literature survey that the RVP rotary engine is a unique engine design.

CHAPTER 4

INVESTIGATION OF AIR MOTOR AND HYDRAULIC PUMP VARIANTS

4.1 Introduction

The RVP rotary engine has many potential advantages because of the features described in Chapter 3. It is an engine that may be easily manufactured, work efficiently, cleanly and smoothly and will certainly be competitive in the market. Most importantly, the feature of multi-fuel capability will help solve the pressing problems of energy resource deficiency and environmental protection. To verify the principles of the mechanism of the RVP rotary machine as well as the engine, a physical model was built and operated. It was done by substituting for precombustion chamber a compressed air supply. It basically works as an air motor. The model was built with CAD/CAM techniques and showed an excellent performance on the test bench.

Once the principles had been established by the model, a prototype hydraulic pump was built and tested. The pump again demonstrated good performance of the machine. It has a larger pumping ability per unit bulk volume than that of conventional rotary pumps. The service life can also be expected to be longer. It is also a unique pump design.

In this Chapter, a brief description of the physical model, acting as an air motor,

will be given: the design, manufacture and test results of the prototype hydraulic pump will then be presented.

4.2 Air Motor as a Physical Model to Verify Principles

An air motor was built as a physical model to verify the principles of the RVP rotary machine. The model was made of aluminum and lucite (Figure 4.1). Lucite was chosen so that the curve fitting situation and the dynamic meshing of the rotors with rotation could be observed. The details of the air motor is shown in Figure 4.1. It is

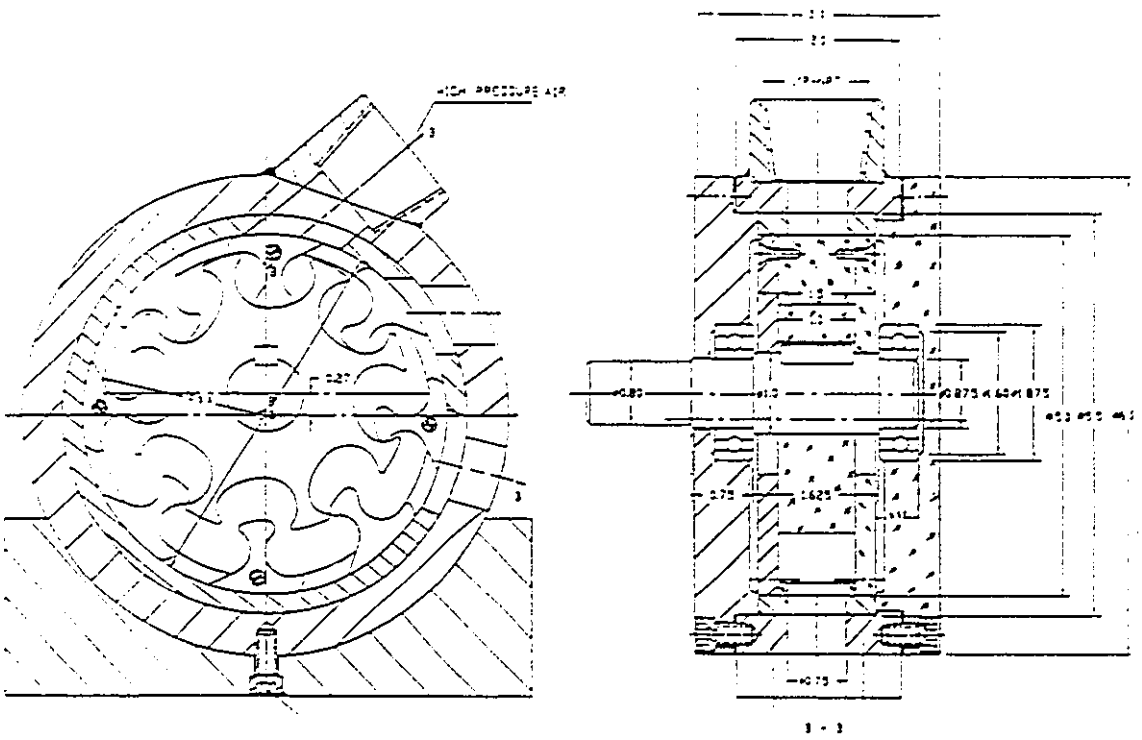

Figure 4.1 Construction of an Air Motor as a Physical Model

basically a modification of the rotary engine design using a compressed air supply instead of a combustion chamber. The modes of operation is as follows. Compressed air (about 50 psig for the tests) thrusts into chambers through the inlet port and expands as the rotors rotate until the exhaust port is aligned with the corresponding chamber. Both the thrust force and expansion of the air result in output power to drive the output shaft and do useful mechanical work. There are three cycles during the process: intake, expansion and exhaust. Thus compared with the process a typical four cycle combustion engine may have, it lacks a compression cycle.

From the mechanical point of view, a major difference between the air motor and the rotary engine is the pressure/temperature levels. The rotary engine will undergo a high pressure and high temperature process with combustion and rapid expansion while the air motor only experiences a process of low pressure variation in a low and constant temperature environment. The air motor is essentially a simplification of the engine and is an adequate physical model of the engine design. The model was operated using compressed air on a test bench. It performed well and demonstrated the successful mechanism of the RVP rotary machine and the principles of the RVP rotary engine.

The design and manufacturing process of the model will prove to be very useful to the RVP rotary engine or other RVP machines. CAD/CAM techniques were extensively used in the process.

The lobes of outer rotor must be designed to have a good aerodynamic shape to obtain maximum momentum transformation of the thrust gas. The curves of the arms

of the inner rotor were generated through computer software to fit the lobes using the method described in Chapter 3. Both the lobes and arms are asymmetrical. The design parameters such as the diameters of the rotors, the number of cavities and the eccentricity were optimized through an AutoCAD package. The intent was to achieve a maximum eccentricity to obtain a large expansion ratio and flow capacity for a given size. The design results were put into another CAD software package -- I-DEAS to verify the mechanism of the machine. The rotors were constructed by the solid model technique in the computer to have a close observation and analysis of the meshing situation. The finite element function of the software allowed the mechanical strength of the critical parts to be checked. An animation function allowed 'running' the motor on the screen dynamically to complete the computer aided design process.

For manufacture of the rotors, the drawing data file was transferred to a CAM software called SmartCAM. All the necessary information such as cutter selection and technique procedures of the cutting were fixed in the software. This file was then converted to CNC code and sent to a NC milling machine to cut the rotors.

The success of the physical model of air motor demonstrated that the rotary machine had no mechanical problem and could achieve good sealing between the chambers. It also showed that the machine, as a motor, could function well to convert hydraulic power to mechanical power through the processes of thrust, expansion and exhaust.

Following the successful completion of this work another variant of the rotary

machine in the form of hydraulic pump was investigated. A prototype pump was designed, built and tested.

4.3 Prototype Hydraulic Pump for Industrial Applications

4.3.1 Prototype hydraulic pump

Figure 4.2 shows a prototype RVP hydraulic pump. Two rotors mesh together to form a series of chambers with contraction on one side and expansion in the other side. In the case of the hydraulic pump, there was no aerodynamic requirement for the designing of the lobes. Therefore they were designed as a simple symmetrical mushroom shape; the meshing arms were also symmetrical about any radial axis. Inlet and outlet ports were reversed compared with those of motor to perform reverse work, i.e. convert mechanical power to hydraulic energy.

As the rotors turned in a clockwise direction (refer to Figure 4.2), the volume of the chambers defined by two adjacent sealing points increased at the suction (inlet) port. It caused a local vacuum to suck in fluid. When the same chambers moved to the pressure (outlet) port region the volume was reduced and forced the fluid out through the pressure port. Therefore a continuous flow was produced.

The following are pump requirements:

i) a large flow capacity. A large swept volume per revolution and a high speed capability.

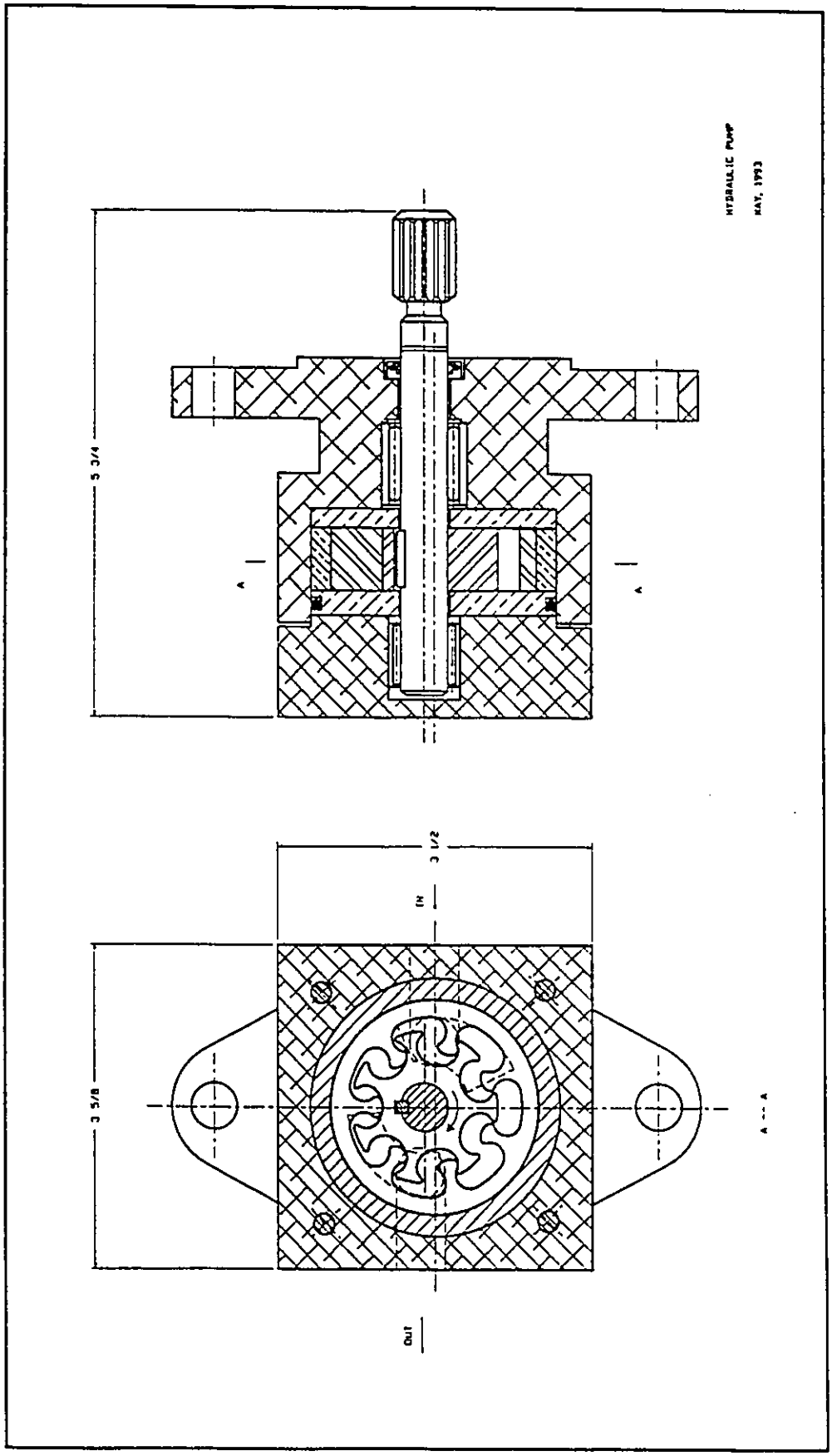

Figure 4.2 Prototype Hydraulic Pump

ii) ability to overcome high output pressure. Good and reliable sealing against high pressure between the inlet and the outlet regions is required.

iii) avoidance of cavitation or vibration. No expansion or contraction is permitted beyond the port regions because of the incompressible nature of the fluid.

iv) smooth operation. A multi output pulse will result in a smooth operation of the pump and output lines.

The RVP rotary pump is inherently an excellent design to achieve the above requirements. The prototype built in this work demonstrated these features. In order to optimize performance, it was sought in the design to have a maximum value of eccentricity and maximum number of chambers per revolution within a physically limited size and material strength. A computer program was generated to solve for the curve describing the arms of the inner rotor in a point-by-point manner to mesh the given symmetrical lobes of the outer rotor. Using CAD/CAM techniques, the two rotors were rotated graphically and displayed to check the mechanical performance. The inlet and outlet ports design was also evaluated by a CAD software to have a proper shape and position in order to have a largest possible flow capacity and avoid cavitation. After completing the design stages, the drawing data files of both rotors were converted to CNC codes through a CAM software and the rotors were cut by a NC milling machine.

The prototype pump pumped fluid as soon as it was assembled and tested. After some minor mechanical changes it demonstrated good performance.

4.3.2 Performance Test and Results

Figure 4.3 shows the test rig for performance testing of the prototype hydraulic pump. The pump has driven by a DC motor, the speed of which could be controlled and measured. A tank of SAE 10 oil with kinematic viscosity ν = 40 cSt (about 180 SSU) at the testing temperature served as the working fluid. Valves placed in series were used to control operating conditions: valve #1 for controlling inlet vacuum (detected by manometer), valve #2 for controlling back pressure (measured by pressure gauge) and valves #3 and #4 for controlling the outflow directions.

Figure 4.4 shows the results of capacity and volumetric efficiency measurements. At zero back pressure and high speed, a high volumetric efficiency was obtained (Figure 4.4 - a). From the trend of the curve it may be seen that the value would be higher at

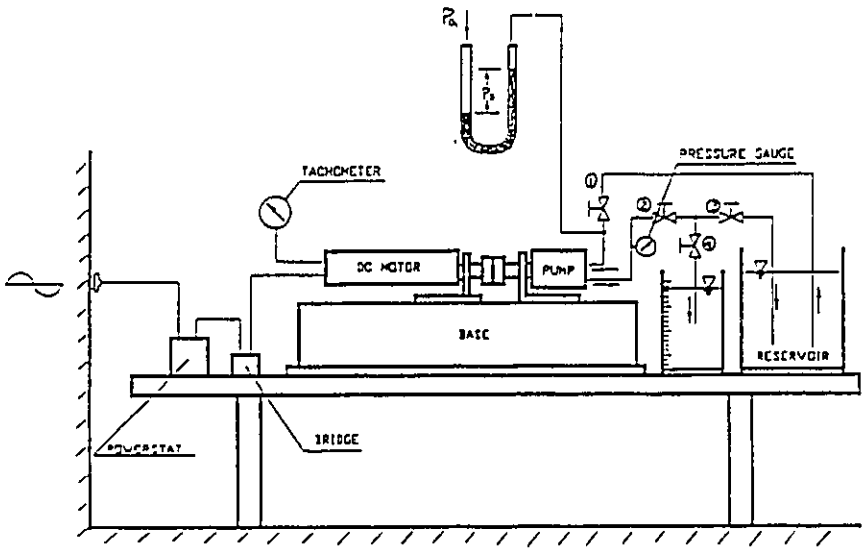

Figure 4.3 Test Rig for the RVP Pump

higher speed. At speeds higher than 1500 rpm, the pump worked smoothly. However, at these speeds the coupling caused some problems.

Figure (4.4-b) shows the capacity and volumetric efficiency as a function of back pressure. The curves are fairly flat compared with those of conventional rotary pumps. That means internal leakage is small at high pressure. At the pressures higher than 1000 kPa, the pump still performed well; no external leakage or vibration was noticed.

In order to examine the suction ability of the pump, Figure 4.5 is plotted based on the test data. During the test, instead of lowering suction level, a gate valve was placed in the suction pipe (Valve #1 in Figure 4.3). By controlling the pressure drop, the required vacuum at the suction port could be obtained. It was assumed that the first air bubble in the delivery side was a sign of cavitation. The maximum suction vacuum is shown on Figure (4.5 - a). Based on the vacuum and velocity at the suction port the maximum suction lift in meters of oil was calculated and plotted on Figure (4.5 - b). It was found that the pump had an extremely large suction ability without cavitation.

Equations used for the test analysis are as follows:

Capacity:

$$Q\,(l/\mathrm{min}) = \frac{Volume(l)}{Time(s)\ /60\ (s/\mathrm{min})}$$

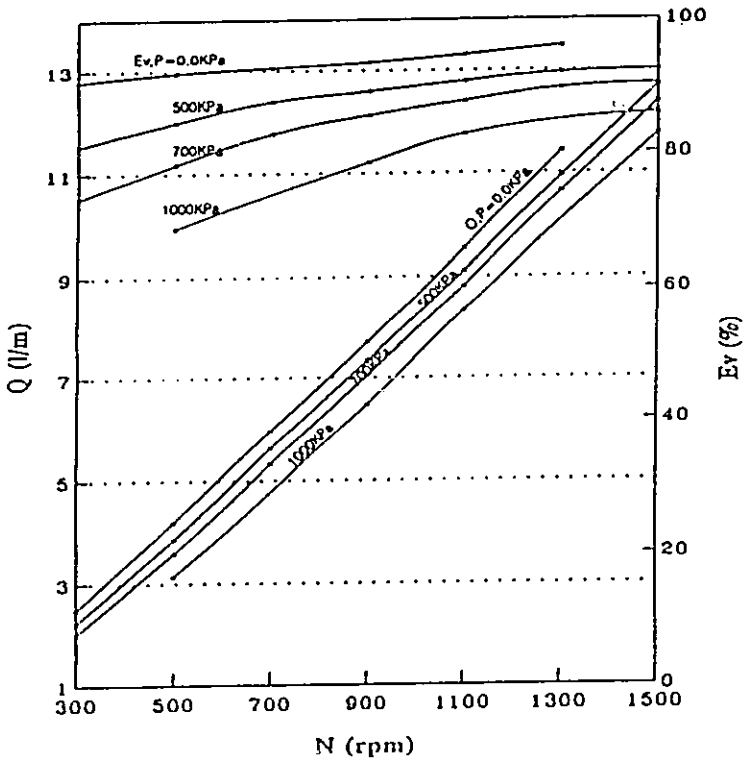

(a) Capacity and Efficiency vs Speed

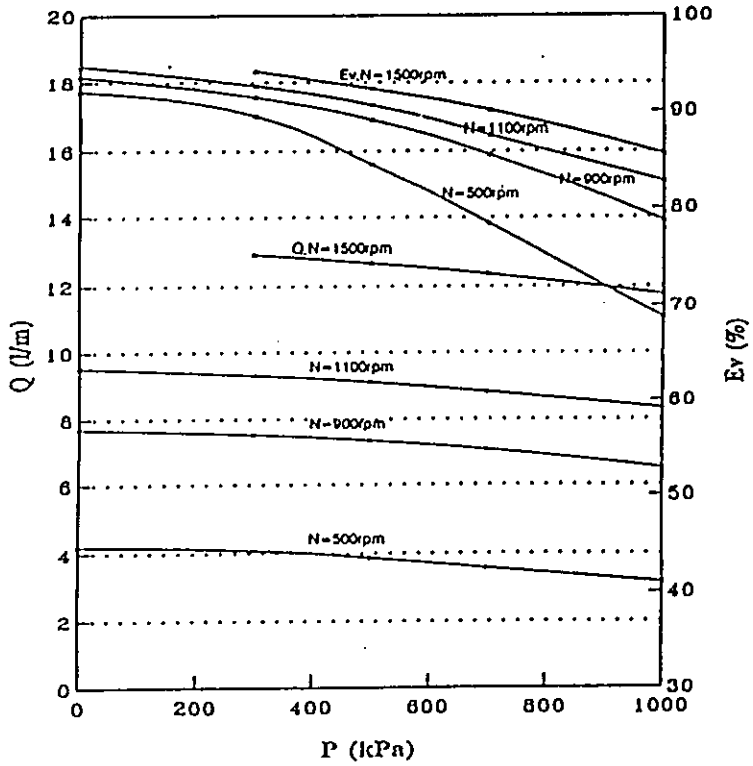

(b) Capacity and Efficiency vs Pressure

Figure 4.4 Results of Performance Test for the RVP Pump

Liquid: SAE 10 oil at 28 C (40 cSt)

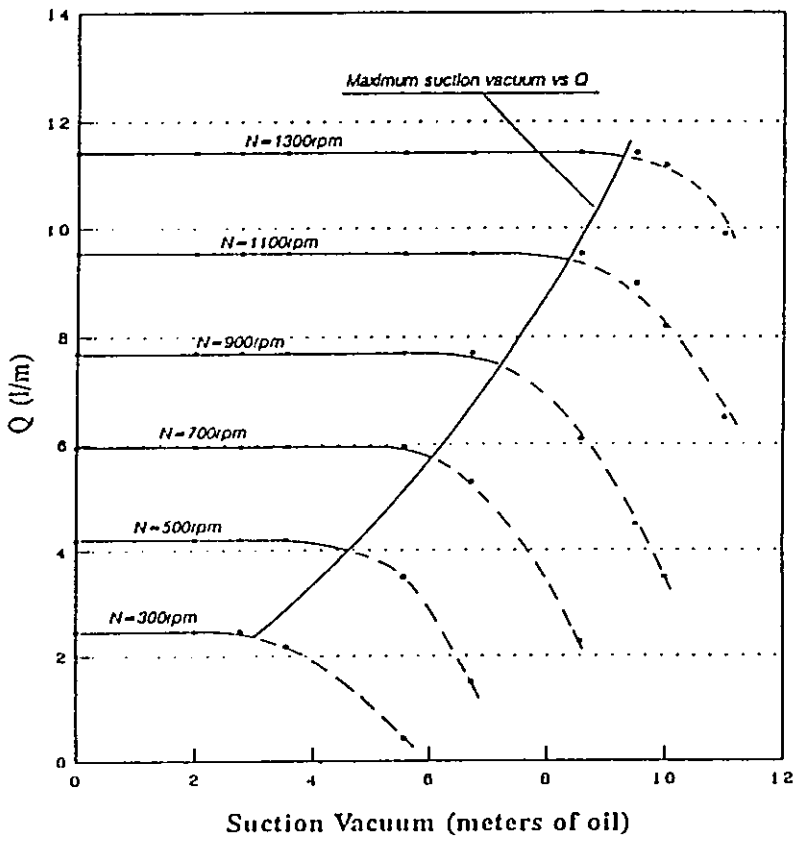

(a) Maximum Suction Vacuum Without Cavitation

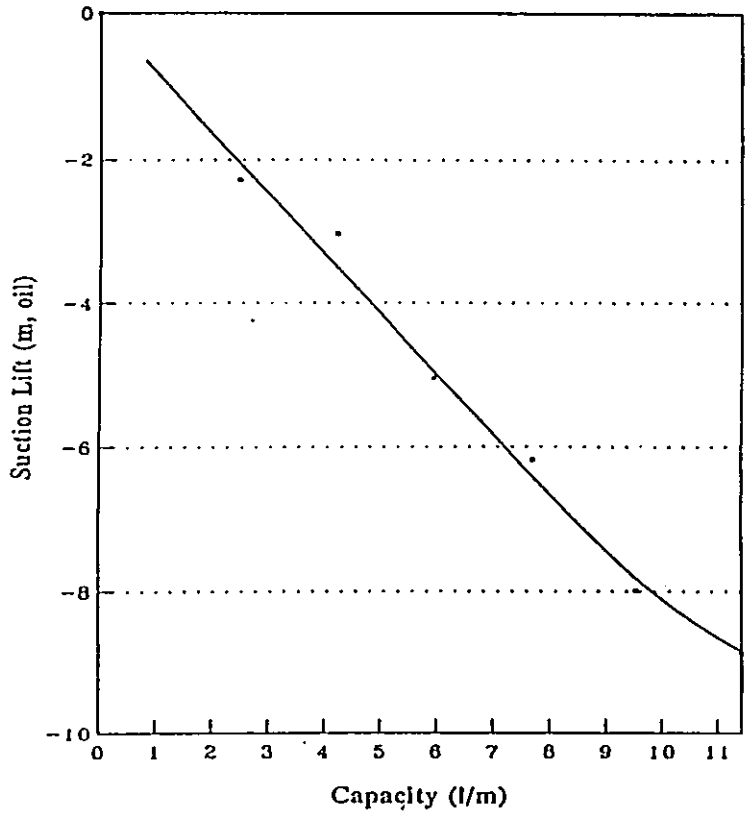

(b) Maximum Suction Lift

Figure 4.5 Results of Test for Suction Ability

Liquid: SAE 10 oil at 28 C (40 cSt)

Volumetric Efficiency:

$$E_v(\%) = \frac{Capacity(l/\min) * 1000(cc/l)}{Displacement(cc/rev.) * Speed(rpm)}$$

Suction Lift:

$$h_s = P_s + Z + \frac{V^2}{2g} \quad (meters, oil\ pumped)$$

4.3.3 Performance analysis and comparison with some commercial hydraulic pumps

The RVP pump is a rotary pump and has apparent advantages over conventional rotary pumps such as gear pumps and vane pumps. The RVP pump has a similar structure as an internal gear pump. However, while only about one third of the range of the rotors in an internal gear pump is effective from the viewpoint of compressing fluid, the RVP pump works over the full range of rotation with fluid (refer to figure 4.6). The result of this special structure is a large capacity per unit bulk volume and a smooth and quiet operation. Compared with vane pumps, there is no high speed impaction movement in the RVP pump. Two rotors in the RVP pump rotate in the same direction and thus the relative speed between the contact surfaces is very small. This will certainly extend the service life of the pump. Better sealing is expected than that of gear pumps as well as a better volumetric efficiency.

Some commercial gear and vane pumps (labelled pump 'B', 'C' and 'D') are given in Table 4.1 to compare their performances with those of the RVP pump (pump A). In order to compare the capacity at the same base of pump size, a dimensionless

parameter DPV factor is defined as the displacement over bulk volume (outline size) of the pump. i.e.

$$DPV = \frac{Displacement(l/rev)}{Bulk\ volume(l)}$$

A pump that has a bigger DPV factor will have a bigger displacement at the same size. From Table 4.1, we can see that RVP pump has the biggest DPV factor. The larger working range (refer to figure 4.6) is the key reason for this.

The volumetric efficiencies of these pumps are plotted against the dimensionless parameter $P/\mu N$ in figure 4.7 to compare with that of the RVP pump (represented by the solid curve). The RVP pump has obviously a larger volumetric efficiency than gear pumps (pump B and C). The vane pump (pump D) has a larger volumetric efficiency. However, its ability to stand high pressure is highly limited -- it works only in the range of $P/\mu N < 2.0$. Besides, the RVP pump has a much higher DPV factor than the vane pump (about 40% higher) . It is thus could be concluded that the RVP pump has a big flow capacity per unit volume and can overcome high working pressure.

TABLE 4.1 COMPARISON OF RVP PUMP PERFORMANCE WITH COMMERCIAL GEAR AND VANE PUMPS

	Pump A	Pump B	Pump C	Pump D
Pump type	RVP pump	Internal gear pump	External gear pump	Vane pump
Dimensions (W*H*L, mm)	92*89*146	89*88*129	81*68*189	125*123*119
Bulk volume (l)	1.196	1.010	1.041	1.830
Displacement (l/rev.)	9.15E-3	6.79E-3	6.72E-3	8.19E-3
Capacity at 1200rpm	10.50	7.95	7.90	9.63
DPV factor	7.65E-3	6.72E-3	6.46E-3	4.48E-3

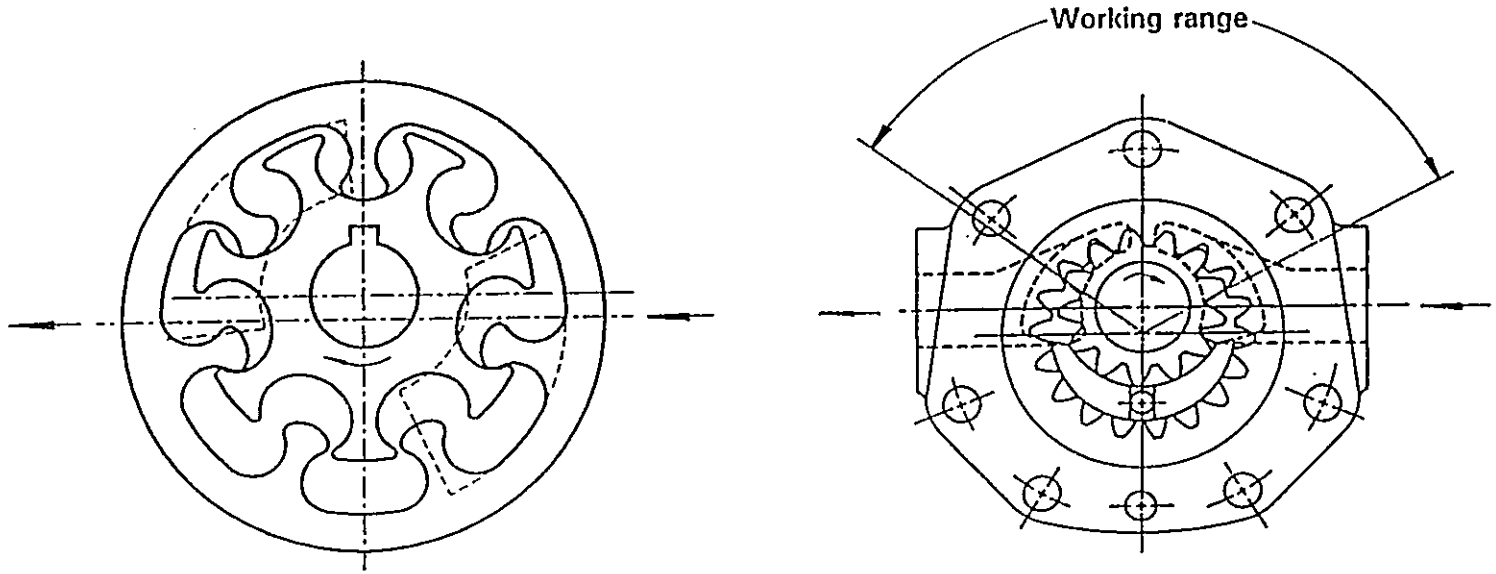

(a) The RVP Pump

(b) Internal Gear Pump

Figure 4.6 Comparison of the RVP Pump with Internal Gear Pump

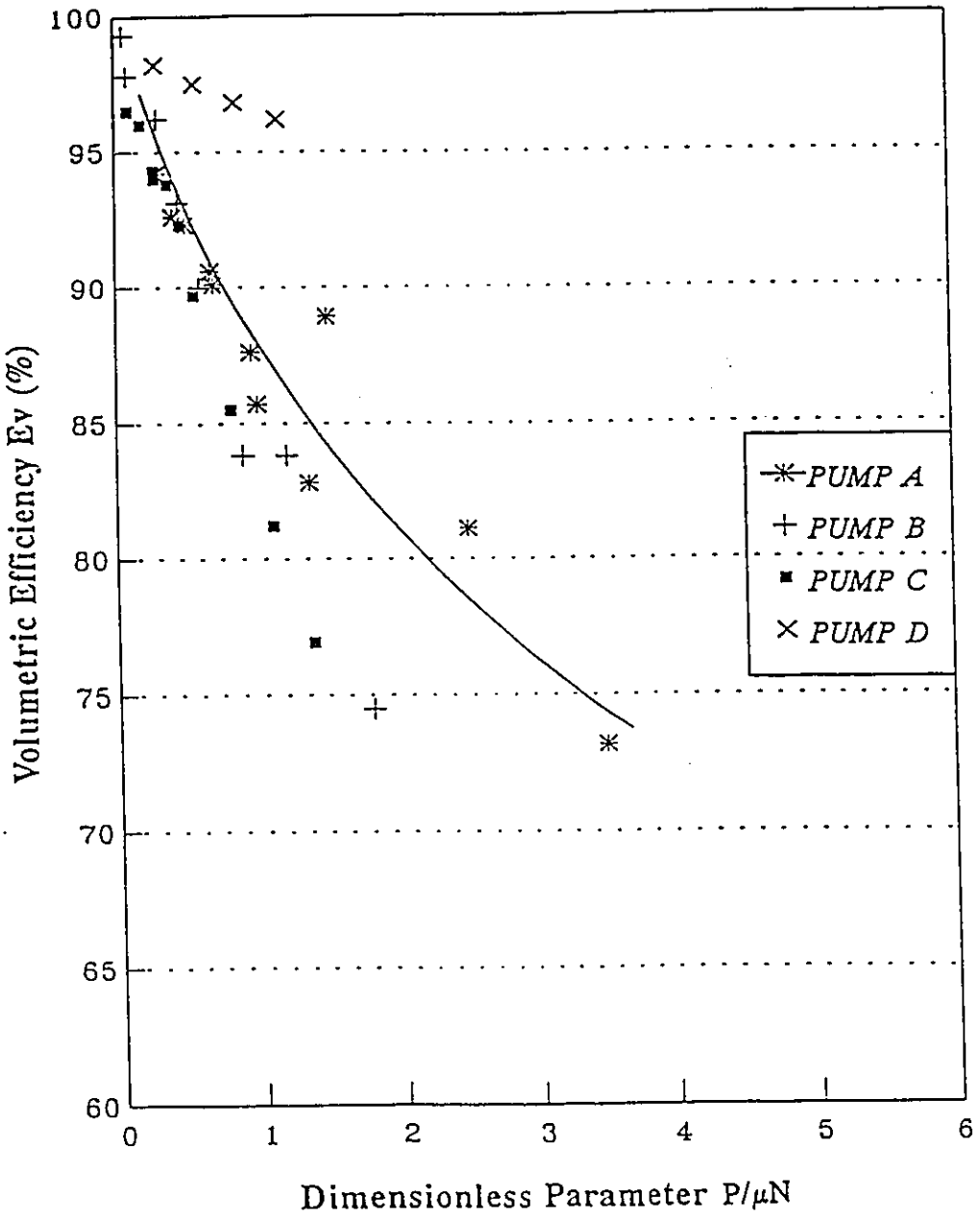

Figure 4.7 Comparison of Volumetric Efficiency of the RVP Pump with Other Rotary Pumps (parameters of pump A,B,C,D are listed on the table 4.1, the solid curve is plotted to fit the dots representing RVP pump)

CHAPTER 5

ROTARY ENGINE -- CHAMBER FLOW SIMULATION

5.1 INTRODUCTION

The RVP rotary engine has a great potential for multi-fuel capability, high power/weight ratio and smooth operation. Its physical model, an air motor, performed well to verify the principles. Before a hardware prototype engine is built, intensive theoretical research must be conducted. This research includes a chamber flow simulation to investigate the flow phenomenon in the power chamber and a thermodynamic mathematical model to predict the performance and optimize some structure and operation parameters of the engine. The chamber flow simulation will be described in this chapter.

Figure 5.1 shows the gas flow phenomenon in the combustion chambers of the RVP rotary engine. There are two kinds of combustion chamber in this engine -- a pre-combustion chamber structured externally to the main body of engine and eight power chambers defined by two rotors.

A mass flow of air/fuel mixture is induced to the pre-combustion chamber to facilitate continuous combustion. Meanwhile, the burning hot mixture of semi-burnt gases thrusts into each power chamber through the injection port periodically when the

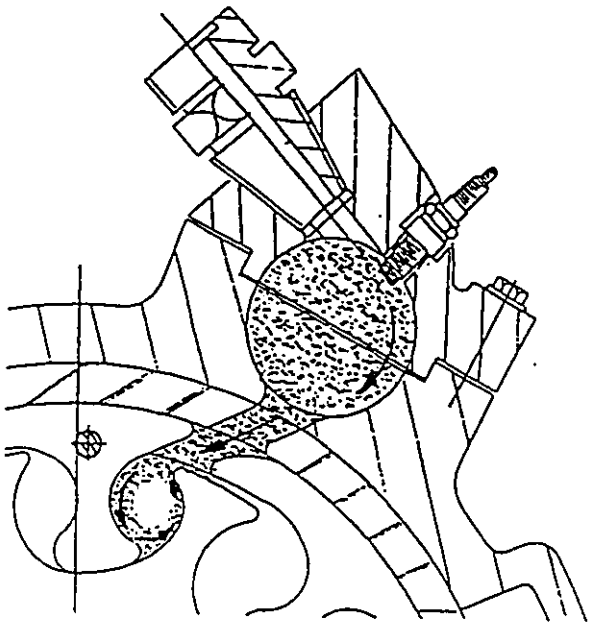

Figure 5.1 Flow Phenomenon in RVP Rotary Engine

slots in the outer rotor are aligned to it.

At some working conditions of the engine, such as load and speed, a type of dynamic equilibrium may exist in the pre-combustion chamber. This occurs when the mass which enters the chamber equals the mass leaving the chamber and the energy of entering mass plus the energy released from combustion equals the energy carried by the mass exiting from the chambers plus the losses through heat transfer. At this point, the temperature and pressure inside the chamber will be at some constant value and the mass flow through the chamber will be at steady state. Apparently, there will be a small fluctuation of the state due to the periodical injection and combustion fluctuations. Also, any changes in the working conditions of the engine will disturb this equilibrium.

The chambers defined by the lobes and arms of the two rotors are irregularly shaped. Both the shape and volume change while the two rotors rotate. It was found through a computer analysis that when the chamber is near its injection timing the volume is close to its minimum value (equivalent to 'topper centre TC' in a piston engine) and stays almost constant. From the display it may be assumed that its shape at this moment is very close to a standard ellipse (refer to Figure 5.1) with major axis along a radial axis of the inner rotor.

When the hot burning gases are injected into the power chamber, the smooth streamline shape of the lobes will guide the gases thrust along the wall until all the momentum and kinetic energy contained in the gases is transferred to pressure energy. Chemical reactions never stop during the injection and in the power chamber. Due to mass accumulation and energy release through further combustion, the pressure will increase rapidly inside the power chamber. The injection process continues until either the pressure inside the power chamber reaches the same value of that in the pre-combustion chamber or the injection port is closed due to the rotation of the rotors.

This is a very complicated flow phenomenon. A set of assumptions are adapted to simplify the problem in this work in order to perform a possible flow simulation along the wall of the power chamber. The remainder of this chapter deals with the following problems under specific working conditions of the engine:

i) mass flow rate from the pre-combustion chamber to the power chamber

ii) velocity profile along the wall of the power chamber in the major flow period

5.2 Mass flow from pre-chamber to the power chamber

In the engine there will be continuous combustion inside a chamber after initial ignition by a spark plug in the pre-combustion chamber. As there will be an essential balance between the combustible mixture supplied to the pre-combustion chamber and the mass delivered to the power chambers, a constant pressure in the pre-combustion chamber will presumably be approached. This pressure can be controlled according to the power and/or speed of the engine.

The following assumptions are made in the calculation of the mass flow rate (figure 5.2):

a) In the pre-combustion chamber all thermodynamic parameters, such as pressure, temperature and density, are in an equilibrium state at any time and kept constant during the whole process.

b) Both the mass flow process between the two chambers and the compression process in the power chamber are isentropic.

c) All the gases involved in the process satisfy the ideal gas equation.

d) Instantaneous gas density in the power chambers is spatially

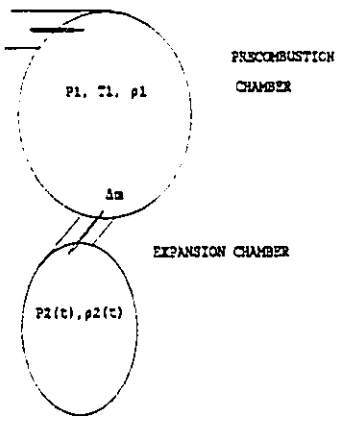

Figure 5.2 Mass flow between two chambers

uniform.

e) The power chamber has constant volume during the flow interval.

The instantaneous mass flow rate to the power chamber from the pre-combustion chamber is

$$\dot{m}(t) = A(t) * \rho_2(t) * V_2(t) \qquad (5-1)$$

In this equation the velocity for an isentropic flow is:

$$V_2(t) = \sqrt{\frac{2k}{k-1} * R * T_1 [1 - (\frac{P_2(t)}{P_1})^{\frac{k-1}{k}}]} \qquad (5-2)$$

where, all the parameters with sub '1' refer to those in the pre-combustion chamber, which are constant values. And those script with subscript '2' refer to the parameters at the other end of passage, which are functions of time. From assumption d) we know

$$\rho_2(t) = \frac{m_2(t)}{\overline{V}} = \frac{m_2^0(t) + \Delta m(t)}{\overline{V}} = \rho_2^0(t) + \frac{\Delta m(t)}{\overline{V}} \qquad (5-3)$$

where $\rho^{o}(t)$ is the instantaneous density at the previous step and $\Delta m(t) = \Delta t * \dot{m}(t)$ refers to the mass increase in the current time step.

With the isentropic assumption

$$P_2(t) = P_2^0(t) * [\frac{\rho_2(t)}{\rho_2^0(t)}]^k \qquad (5-4)$$

and the perfect gas assumption

$$P_2(t) = \rho_2(t) * R * T_2(t) \qquad (5-5)$$

we have a system of five equations (equ. (5 - 1) to equ. (5 - 5)) with five unknowns:

$$P_2(t),\ T_2(t),\ \rho_2(t),\ \Delta m(t) \text{ and } V_2(t)$$

Figure 5.3 outlines the calculation procedure for solving the equations during which an iterative technique has been used.

Considering the design parameters (refer to Appendix A for the definition of the parameters used) to be

$\theta_1 = 10^0$, $\theta_2 = 12^0$, N = 5,000 rpm, A_0 = 0.871E-3m^2, A_p = 0.581E-3 m^2

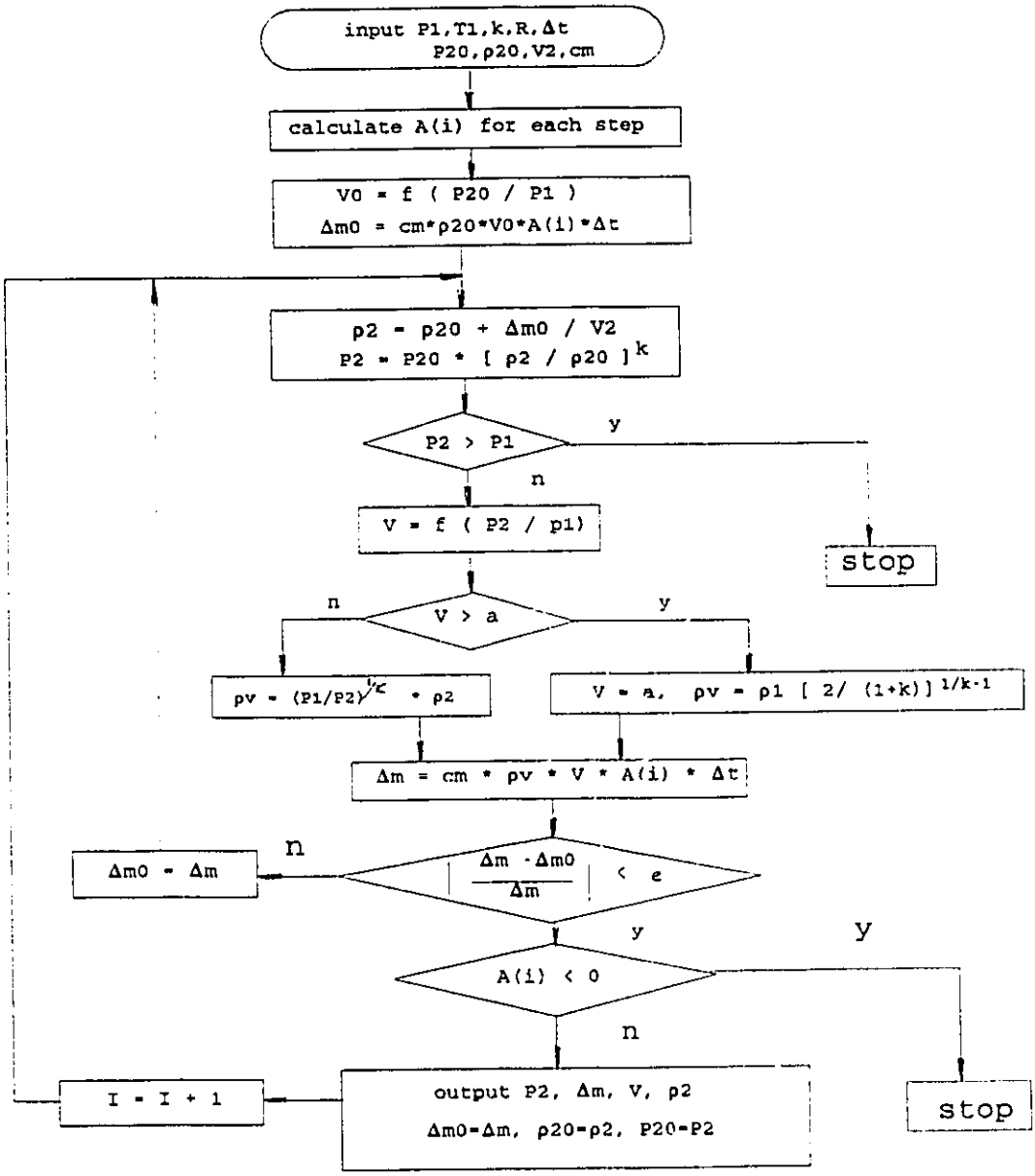

Figure 5.3 Flow Chart for Calculation of Mass Flow Rate

the area of the passage **A(t)** can be calculated according to Appendix A:

$$A'(t) = \begin{cases} 2.614*t & 0 \le t \le 0.333ms \\ 0.871E-3 & 0.333ms < t < 0.40ms \\ 1.916E-3-2.614*t & t \ge 0.4ms \end{cases} \qquad (5-6)$$

and

$$A(t) = \min\ (\ A'(t),\ \ 0.581e-3\ ) \qquad (5-7)$$

5.3 Velocity profile along the wall of the power chamber

As soon as the burning gas thrusts into the power chamber, it will flow along the wall obeying the momentum conservation law. The gas will accumulate inside the chamber until the pressure difference between the two chambers and thus the velocity becomes zero. This is an unsteady, compressible, multidimensional problem with a complex boundary. Assumptions have to be made to achieve a possible solution.

5.3.1 Assumptions

a) The shape of the chamber is approximated by an ellipse with the major axis

radially oriented with the radial axis of the inner rotor

b) The volume of the chamber will not change during the period of injection

c) The flow will only be along the tangential direction of the wall and be kept at a constant cross-sectional area for the whole flow process

d) The flow right adjacent to the wall side satisfies the nonslip condition (V = 0.0) and that adjacent to the gas side satisfies the free slip condition (no frictions)

e) The flow process is an isentropic process

f) The flow will not be significant after the front of the flow reaches the end of the physical domain

It is not feasible to discuss the errors of the calculation resulting from the above assumptions quantitatively. However we can discuss them in a qualitative way.

Assumption a): this is made due to the fact that the shape of the currently designed power chamber is very close to the shape of an ellipse

$$\frac{X^2}{a^2} + \frac{Y^2}{b^2} = 1 \qquad (5-8)$$

with $a = 0.0131$ m, $b = 0.0106$ m

Assumption b): injection period falls close to the upper dead centre. The volume change will not exceed 3% at this period.

Assumption c): the velocity vector could be resolved to be two components: tangential and normal components. The tangential component is induced by the injection

and the normal component is induced by diffusion if no impact occurs during the injection. Compared with the high injection velocity, the diffusion component is relatively small enough to be ignored and the cross-sectional area will be defined by the area of the port which has been assumed to be constant during the injection period.

Assumption d): nonslip assumption is commonly used in the viscous fluid against a solid boundary. However, it seems better to assume a free slip condition on the gas side because of the low viscosity of the gas.

Assumption e): the whole process takes place in a very small time interval, approximately 0.5 micro seconds, during which time there is negligible heat transfer.

Assumption f): at the time when the gases reach the boundary to complete a closed gas ring, combustion will dominate in the chamber. At this time the flow will no longer be significant and will not be calculated.

5.3.2 Governing Equations

Momentum equation

$$\frac{\partial q}{\partial t}+(q.\nabla)q = f-\frac{\nabla p}{\rho}+\frac{\mu}{3\rho}\nabla(\nabla q)+\frac{\mu}{\rho}\nabla^2 q \qquad (5-8)$$

where, **q** is the velocity vector, **f** the body force, **P** the pressure, ρ the density and μ the viscosity.

Continuity equation

$$\frac{\partial q}{\partial t} + \nabla(\rho q) = 0 \qquad (5-9)$$

For an unsteady compressible problem, density is a function of time and position.

Energy equation

From the isentropic assumption we have

$$\frac{D}{Dt}\left(\frac{P}{\rho^{\gamma}}\right) = 0 \qquad (5 - 10)$$

where γ is the ratio of specific heats, which is assumed to be 1.4 for air.

According to assumption b) and Appendix B, the gas will flow only along the η direction in elliptical coordinates (refer to figure 5.4). We can thus further assume:

$$V_{\xi} = 0, \quad \frac{\partial^k V_{\xi}}{\partial \xi^k} = 0, \quad \frac{\partial^k V_{\xi}}{\partial \eta^k} = 0$$

With these assumptions we can derive the Governing Equations in the η direction for elliptical coordinates (refer to Appendix B and Round and Garg, 1986):

In equation (5 - 8)

$$\left.\frac{\partial q}{\partial t}\right|_{\eta} = \frac{\partial V_{\eta}}{\partial t} \qquad (a)$$

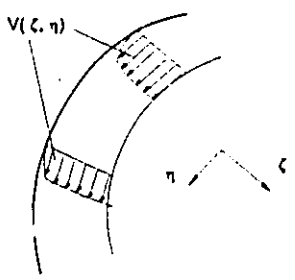

Figure 5.4 Flow in Elliptical Coordinate

$$(q.\nabla)\,q\Big|_{\eta} = \frac{1}{h}[(V_{\xi}\frac{\partial V_{\xi}}{\partial \eta}+V_{\eta}\frac{\partial V_{\eta}}{\partial \eta})+\frac{V_{\xi}}{h}(\frac{\partial(hV_{\eta})}{\partial \xi}-\frac{\partial(hV_{\xi})}{\partial \eta})] = \frac{V_{\eta}}{h}\frac{\partial V_{\eta}}{\partial \eta} \qquad (b)$$

where h is a metric coefficient and is defined as $h = c\sqrt{\sinh^2\zeta + \sin^2\eta}$

$$\frac{\nabla P}{\rho}\Big|_{\eta} = \frac{1}{\rho h}\frac{\partial P}{\partial \eta} \qquad (c)$$

$$\nabla(\nabla.q)\Big|_{\eta} = \frac{1}{h}[\frac{\partial}{\partial \eta}(\nabla.q)] = \frac{1}{h}[\frac{\partial}{\partial \eta}(\frac{1}{h^2}\frac{\partial(hV_{\eta})}{\partial \eta}+\frac{1}{h^2}\frac{\partial(hV_{\xi})}{\partial \xi})]$$

$$=\frac{1}{h}[\frac{\partial}{\partial \eta}(\frac{1}{h^3}V_{\eta}c^2\sin\eta\cos\eta+\frac{1}{h}\frac{\partial V_{\eta}}{\partial \eta})]$$

$$=\frac{1}{h}[\frac{\partial}{\partial \eta}(\frac{V_{\eta}}{h^3}c^2\frac{1}{2}\sin(2\eta)+\frac{1}{h}\frac{\partial V_{\eta}}{\partial \eta})]$$

$$=\frac{1}{h}[\frac{\frac{\partial V_{\eta}}{\partial \eta}c^2\frac{1}{2}\sin(2\eta)+c^2V_{\eta}\cos(2\eta))h^3-3h^2\frac{c^2}{h}\sin\eta\cos\eta V_{\eta}\; c^2\frac{1}{2}\sin(2\eta)}{h^6} \qquad (d)$$

$$-\frac{1}{h^2}\frac{c^2\sin\eta\cos\eta}{h}\frac{\partial V_{\eta}}{\partial \eta}+\frac{1}{h}\frac{\partial^2 V_{\eta}}{\partial \eta^2}]$$

$$=\frac{c^2}{h^6}[\frac{1}{2}\sin2\eta h^2\frac{\partial V_{\eta}}{\partial \eta}+\cos(2\eta)h^2V_{\eta}-3(c\frac{1}{2}\sin2\eta)^2V_{\eta}-(\frac{h^2}{2}\sin2\eta\frac{\partial V_{\eta}}{\partial \eta}+\frac{h^4}{c^2}\frac{\partial^2 V_{\eta}}{\partial \eta^2})]$$

$$=\frac{1}{h^2}\frac{\partial^2 V_{\eta}}{\partial \eta^2}+\frac{c^2}{h^6}(\cos(2\eta)h^2-3\sin^2\eta\cos^2\eta c^2)V_{\eta}$$

$$\nabla^2 q|_\eta = \frac{1}{h}\left[\frac{\partial}{\partial \eta}(\nabla q)\right] + \frac{1}{h}\left[\frac{\partial}{\partial \xi}\left(\frac{1}{h^2}\left(\frac{\partial(hV_\eta)}{\partial \xi} - \frac{\partial(hV_\xi)}{\partial \eta}\right)\right)\right] \qquad \text{(e)'}$$

$$\frac{1}{h}\frac{\partial}{\partial \xi}\left(\frac{1}{h^2}\frac{\partial(hV_\eta)}{\partial \xi}\right) - \frac{1}{h}\frac{\partial}{\partial \xi}\left[\left(\frac{V_\eta}{h^3}c^2\cosh\xi\sinh\xi + \frac{1}{h}\frac{\partial V_\eta}{\partial \xi}\right)\right]$$

$$-\frac{1}{h}\left[\frac{\partial V_\eta}{\partial \xi}c^2\cosh\xi\sinh\xi + V_\eta c^2\cosh 2\xi\right)h^3 - 3h^2\frac{c^2}{h}\cosh\xi\sinh\xi V_\eta c^2\cosh\xi\sinh\xi\Big]\frac{1}{h^6}$$

$$+\frac{1}{h}\left[-\frac{1}{h^2}\frac{c^2}{h}\cosh\xi\sinh\xi\frac{\partial V\eta}{\partial \xi} + \frac{1}{h}\frac{\partial^2 V_\eta}{\partial \xi^2}\right]$$

$$-\frac{1}{h}\left[\frac{c^2\sinh 2\xi}{2h^3}\frac{\partial V_\eta}{\partial \xi} + \frac{c^2\cosh 2\xi}{h^3}V_\eta - \frac{3c^4\sinh^2 2\xi}{4h^5}V_\eta - \frac{c^2\sinh 2\xi}{4h^3}\frac{\partial V_\eta}{\partial \xi} + \frac{1}{h}\frac{\partial^2 V_\eta}{\partial \xi^2}\right]$$

$$-\frac{1}{h^2}\frac{\partial^2 V_\eta}{\partial \xi^2} + \frac{c^2}{h^6}\left[\cosh(2\xi)h^2 - 3c^2\cosh^2\xi\sinh^2\xi\right]V_\eta$$

Therefore

$$\nabla^2 q|_\eta = \frac{1}{h^2}\frac{\partial^2 V_\eta}{\partial \eta^2} + \frac{1}{h^2}\frac{\partial^2 V_\eta}{\partial \xi^2} + \frac{c^2}{h^6}\left[\cos(2\eta)h^2 - 3c^2\sin^2\eta\cos^2\eta + h^2\cosh(2\xi) - 3c^2\cosh^2\xi\sinh^2\xi\right]V_\eta \qquad \text{(e)}$$

Substituting equation (a)-(e) into equation (5-8) and assuming body force f = 0 we have

$$\frac{\partial V_\eta}{\partial t} + \frac{V_\eta}{h}\frac{\partial V_\eta}{\partial \eta} - \frac{4}{3}\frac{\nu}{h^2}\frac{\partial^2 V_\eta}{\partial \eta^2} - \frac{\nu}{h^2}\frac{\partial^2 V_\eta}{\partial \xi^2} + \frac{\nu c^2}{3h^6}\left[-4\cos(2\eta)h^2 + 3(c\sin(2\eta))^2\right.$$

$$\left.-3h^2\cosh(2\xi) + (3c\cosh\xi\sinh\xi)^2\right] * V_\eta + \frac{1}{h\rho}\frac{\partial P}{\partial \eta} = 0$$

To have a simpler form, the following parameters can be used in above equation

$$A = \frac{4\nu}{3}\frac{1}{h^2}, \qquad B = \frac{\nu}{h^2}, \qquad C = \frac{\nu c^2}{3h^6}$$

$$D = -4\cos(2\eta)h^2+3(c\sin(2\eta))^2-3h^2\cosh(2\xi)+(3c\cosh\xi\sinh\xi)^2$$

$$x = \eta, \qquad y = \xi, \qquad V = V_\eta$$

The **momentum equation** in the η direction of the elliptical coordinates can thus be written as

$$\frac{\partial V}{\partial t}+\frac{V}{h}\frac{\partial V}{\partial x}-A\frac{\partial^2 V}{\partial x^2}-B\frac{\partial^2 V}{\partial y^2}+(C*D)*V+\frac{1}{h\rho}\frac{\partial P}{\partial x} = 0 \qquad (5-8A)$$

By the same token, the **continuity equation** (5 - 9) can be written as

$$\frac{\partial \rho}{\partial t}+\frac{V}{h}\frac{\partial \rho}{\partial x}+E*V*\rho+\frac{\rho}{h}\frac{\partial V}{\partial x} = 0 \qquad (5-9A)$$

where

$$E = \frac{c^2}{h^3}\sin(x)\cos(x)$$

and the **energy equation** (5 - 10) can be written:

$$\left(\frac{\partial P}{\partial t}+\frac{V}{h}\frac{\partial P}{\partial x}\right) - \frac{\gamma P}{\rho}\left(\frac{\partial \rho}{\partial t}+\frac{V}{h}\frac{\partial \rho}{\partial x}\right) = 0 \qquad (5 - 10\ A)$$

5.3.3 Initial and Boundary Conditions

Initial conditions

The flow is static inside the chamber before the thrust process starts. i.e.

$$V(x, y, t) = 0 \qquad when\ t \le 0 \qquad (5 - 11)$$

Because of the initial compression the values of pressure and density are slightly higher than ambient values. The spatially constant values are assumed as

$$P(x, t \le 0) = 1.5E5\ Pa \qquad (5 - 12)$$

$$\rho(x, t \le 0) = 1.57\ kg/m^3 \qquad (5 - 13)$$

Boundary condition

Assuming no friction losses at the passage between pre-combustion chamber and the power chamber, the values of pressure and density at the edge of the power chamber are taken as the same as those in the pre-combustion chamber. Therefore, the boundary conditions of pressure and density are

$$P(1,t) = P1 = 6.0E5\ Pa \qquad (5-14)$$

$$\rho(1,t) = \rho 1 = 4.6457\ kg/m^3 \qquad (5-15)$$

Considering the velocity of the rotors at the edge point ($\mathbf{N}$ = rotational speed of the rotor, $\mathbf{R_0}$ = radial distance of the point)

$$U = \omega * R_0 = \frac{2\pi N}{60} R_0$$

we have velocity vector diagram at the input port as shown in figure 5.5. In the diagram, **V** is the absolute velocity which has the same value of $\mathbf{V_2(t)}$ calculated in the last section and $\mathbf{V_r}$ is the relative velocity to the chamber, which is the boundary velocity of the flow field. The angle θ is determined by design parameters. From the diagram we have:

$$V_x = V\cos\theta = U + V_r\cos\varphi \qquad (a)$$

$$V_y = V\sin\theta = V_r\sin\varphi \qquad (b)$$

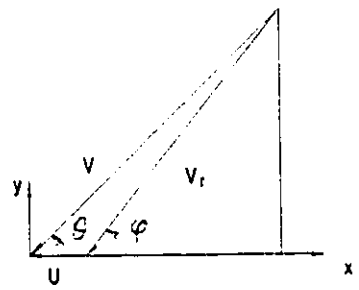

Figure 5.5 Velocity vector diagram

Applying (equ.(a))^2 + (equ.(b))^2, we have the boundary condition of velocity at x direction:

$$V_r^2 + U^2 + 2V_r U\cos\phi - V^2 = 0 \qquad (5 - 16)$$

An iterative technique is needed to solve for V_r. In the y direction, from assumption (d) we have

$$V(x, 1, t) = 0 \qquad (5 - 17)$$

$$V(x, J+1, t) = V(x, J-1, t) \qquad (5 - 18)$$

where **J** corresponds to the boundary coordinate at the gas side in the y direction. Equation (5-18) represents the assumption of zero slope of velocity profile at the boundary of the gas side.

Solving equations (5 - 8A) through (5 - 10A) simultaneously together with the initial conditions (5 -11) through (5 - 13) and boundary conditions (5 - 14) through (5 - 18) we can obtain the velocity profile **V (x,y,t)** and the variation of pressure **P (x,t)** and density ρ**(x,t)**. It is an non-linear, unsteady and compressible problem. Thus only a numerical solution is possible. A finite difference method was used in this work to solve the problem.

5.3.4 Finite Difference Solutions

Finite difference equations

In focusing attention on the values at the grid points in the domain, a finite difference method is used to replace the continuous information contained in the exact solution of the partial differential equations as shown in (5 - 8A) through (5 - 10A) with discrete values to be obtained from a set of simple algebraic equations.

Based on the fact that the flow is strongly unidirectional in the η direction, which means significant influences travel only from upstream to downstream. Therefore, the upwind scheme is used in the numerical solutions. According to the upwind method and using average values of velocity to represent the non-linear item in the momentum equation, the partial difference equations of (5 - 8A) through (5 - 10A) can be replaced by the following finite difference equations respectively:

$$\frac{V_{ij}^{k+1}-V_{ij}^{k}}{\Delta t}+\frac{V_{ij}^{k+1}+V_{i-1j}}{2h_{ij}}\frac{V_{ij}^{k+1}-V_{i-1j}^{k+1}}{\Delta x}-A_{ij}\frac{V_{i+1j}^{k+1}-2V_{ij}^{k+1}+V_{i-1j}^{k+1}}{\Delta x^2}- B_{ij}\frac{V_{ij+1}^{k+1}-2V_{ij}^{k+1}+V_{ij-1}^{k+1}}{\Delta y^2}+C_{ij}*D_{ij}*V_{ij}^{k+1}+\frac{1}{h_{ij}\rho_{ij}^{k+1}}\frac{P_{ij}^{k+1}-P_{i-1j}^{k+1}}{\Delta x} = 0 \qquad (5 - 8B)$$

$$\frac{\rho_{ij}^{k+1}-\rho_{ij}^{k}}{\Delta t}+\frac{V_{ij}^{k+1}}{h_{ij}}\frac{\rho_{ij}^{k+1}-\rho_{i-1j}^{k+1}}{\Delta x}+E_i*V_{ij}^{k+1}\rho_{ij}^{k+1}+\frac{\rho_{ij}^{k+1}}{h_{ij}}\frac{V_{ij}^{k+1}-V_{i-1j}^{k+1}}{\Delta x} = 0 \qquad (5 - 9B)$$

$$\frac{P_{ij}^{k+1}-P_{ij}^{k}}{\Delta t}+\frac{V_{ij}^{k+1}}{h_{ij}}\frac{P_{ij}^{k+1}-P_{i-1j}^{k+1}}{\Delta x}-\frac{\gamma P_{ij}^{k+1}}{\rho_{ij}^{k+1}}\left(\frac{\rho_{ij}^{k+1}-\rho_{ij}^{k}}{\Delta t}+\frac{V_{ij}^{k+1}}{h_{ij}}\frac{\rho_{ij}^{k+1}-\rho_{i-1j}^{k+1}}{\Delta x}\right) = 0 \qquad (5 - 10B)$$

where, i and j represent the elliptical coordinates η and ζ or simply x and y and k represents the time coordinate. Equation (5 - 8B) can be rearranged to be

$$V_{ij}^{k+1} = V_{ij}^{k}-\frac{\Delta t}{2h_{ij}\Delta x}[(V_{ij}^{k+1})^2-(V_{i-1j}^{k+1})^2]+\frac{A_{ij}\Delta t}{\Delta x^2}[V_{i+1j}^{k+1}-2V_{ij}^{k+1}+V_{i-1j}^{k+1}]$$
$$\frac{B_{ij}\Delta t}{\Delta y^2}[V_{ij+1}^{k+1}-2V_{ij}^{k+1}+V_{ij-1}^{k+1}]-C_{ij}*D_{ij}*\Delta t*V_{ij}^{k+1}-\frac{\Delta t}{h_{ij}\rho_{ij}^{k+1}}\frac{P_{ij}^{k+1}-P_{i-1j}^{k+1}}{\Delta x} \qquad (5 - 8C)$$

Using averaged velocity **VA** and converting factor **H** in y (ζ) direction

$$VA_i^{k} = \sum_{j-1}^{J} V_{ij}^{k} / J$$
$$H_i = \sum_{j-1}^{J} h_{ij} / J$$

and assuming pressure and density to be uniform in that direction, equations (5 - 9B) and (5 - 10B) can be written as

$$\rho_i^{k+1} = \rho_i^{k}+VA_i^{k+1}*F_i*\rho_{i-1}^{k+1}+[-VA_i^{k+1}*F_i-E_i*\Delta t*VA_i^{k+1}-$$
$$(VA_i^{k+1}-VA_{i-1}^{k+1})*F_i]\rho_i^{k+1} \qquad (5 - 9C)$$

$$P_i^{k+1} - P_i^k + VA_i^{k+1}F_iP_{i-1}^{k+1} + [-VA_i^{k+1}F_i + \frac{\gamma}{\rho_i^{k+1}}(\rho_i^{k+1} - \rho_i^k + VA_i^{k+1}F_i(\rho_i^{k+1} - \rho_{i-1}^{k+1})]P_i^{k+1} \qquad (5 - 10C)$$

Equations (5 - 8C), (5 - 9C) and (5 - 10C) are a set of algebraic equations which can be solved for $V_{i,j}^{k+1}$, P_i^{k+1} and ρ_i^{k+1} in the domain considered.

Mesh arrangement

In elliptical coordinates, the original domain along the elliptical wall has been replaced by a rectangular domain as shown in figure 6.

From appendix C we know the initial boundary coordinate $\eta_0 = 30^0$. Setting the ending coordinate $\eta_I = 350^0$ and using uniform mesh $\Delta x = 10^0$ we have

$$I = \frac{350-30}{10} = 32$$

Combining assumption (a) for the boundary of wall and the elliptical coordinate

$$\frac{X^2}{C^2\cosh^2\xi} + \frac{Y^2}{C^2\sinh^2\xi} = 1$$

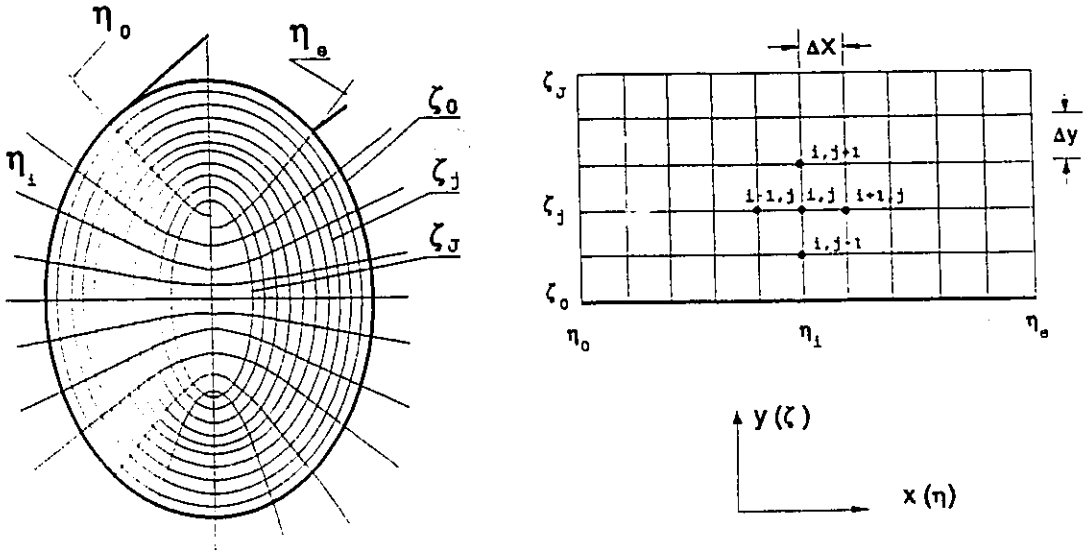

(a) original domain

(b) rectangular domain

Figure 5.6 Demonstration of the Calculation Domain

where

$$C = \sqrt{a_0^2 - b_0^2} = \sqrt{0.0131^2 - 0.0106^2} = 0.0077$$

we have

$$a_0 = 0.0131 = C * \cosh\xi_0$$

$$\xi_0 = \cosh^{-1}\frac{a_0}{C} = \cosh^{-1}\frac{0.0131}{0.0077} = 1.123$$

Assuming the width of the flowing domain is the same as that of the input port, which is 0.008 m in the particular design, we have (also refer to assumption (c))

$$a_J = a_0 - 0.008 = C * \cosh \xi_J$$

$$\xi_J = \cosh^{-1} \frac{a_J}{C} = \cosh^{-1} \frac{0.0131 - 0.008}{0.0077} = 1.044$$

Dividing the domain in the ζ direction by 10 and again using a uniform mesh, we have

$$\Delta y = \frac{\xi_0 - \xi_J}{10} = \frac{1.123 - 1.044}{10} = 7.9E\text{-}3$$

Solution scheme and flow chart of calculation

An explicit scheme was used to solve equations (5 - 8C) through (5 - 10C). The procedure can be simply described as the following:

(1) for each coordinate of x (η), set the value of pressure **P** and density ρ as the same as those of previous time step

(2) calculate the velocity along the y (ζ) axis using the above value of **P** and ρ by the iteration method for the unknown value of **V** at the point of **(i,j)** and **(i,j+1)**

(3) update the value of ρ by equation (5 - 9C) with the value of **V** obtained

(4) update the value of **P** by equation (5 - 10C) with the value of **V** obtained and the updated value of ρ

(5) repeat step (2) using the updated **P** and ρ values

(6) repeat steps (2) to (5) until velocity **V** converges

(7) for the next coordinate x, repeat steps (1) to (6) until velocity **V** = 0 or the end of the domain is reached

(8) for the next time step, repeat steps (1) to (7) until the flow to the chamber stops

The iteration procedure is converges successfully in the calculations based on the techniques to be discussed in next section. The above procedure is also shown in a flow chart of the Fortran program in figure 5.7.

Convergence and stability

If the max velocity $\mathbf{V}_{max}$ is 500 m/s, the following statements are sufficient conditions for convergence of the iteration (Chen, 1992 and Patankar, 1980):

$$\Delta t \le \frac{\Delta x * a_0}{V_{max}} = \frac{\frac{10^0 * \pi}{180} * 0.0131}{500} = 0.46E\text{-}5$$

$$\Delta t \le \frac{W_j/10}{V_{max}} = \frac{0.008/10}{500} = 0.16E\text{-}5$$

It was verified from the calculation that the above conditions are not necessary. Δt = 0.2E-5 gives a good convergent result for the calculations.

To get good stability of the results, an underrelaxation technique was used in the calculation of pressure and density. In each iterated step, the value of the variables were revised by the following method:

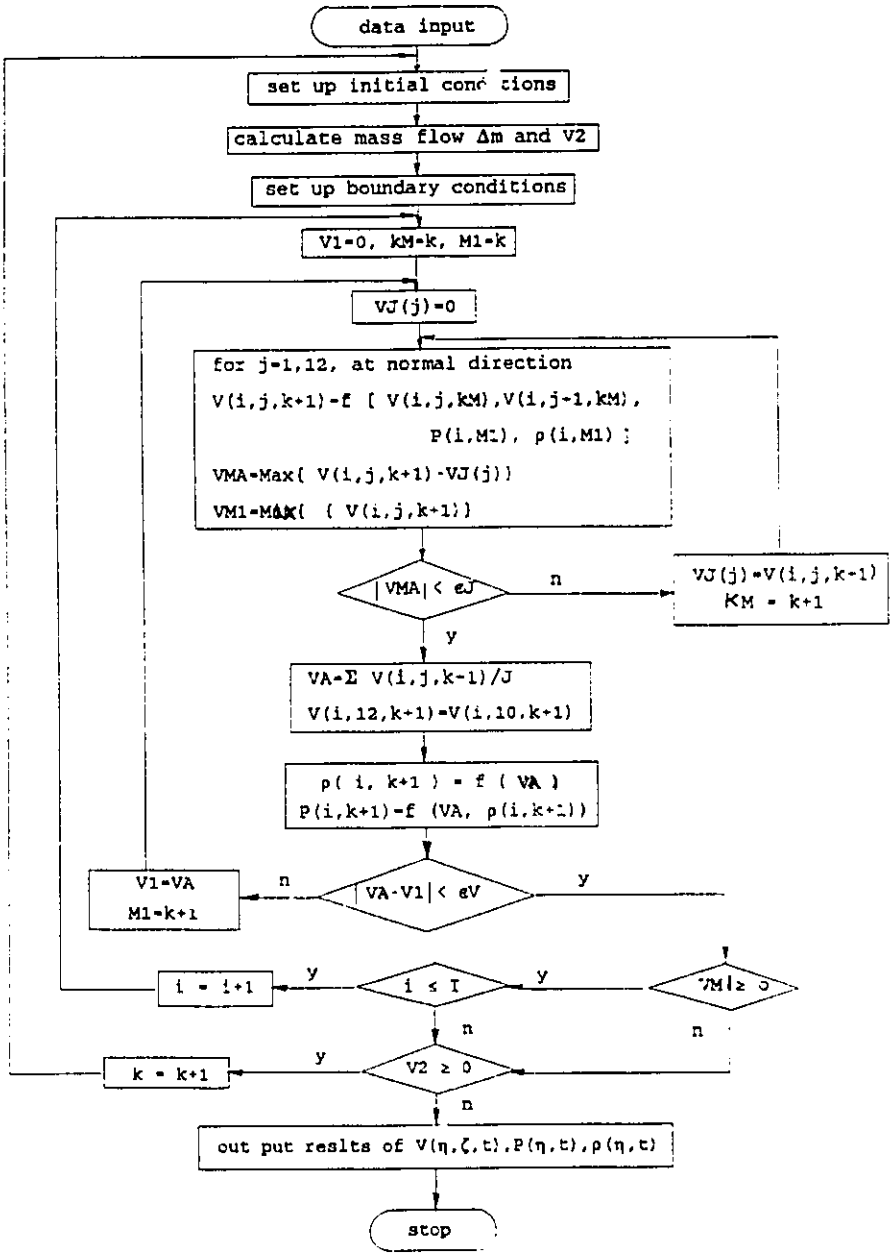

Figure 5.6 Flow Chart of Fortran Program to solve for velocity profile

$$\rho^{k+1}(x,t) = \alpha_\rho * \rho^{k}(x,t) + (1-\alpha_\rho) * \rho^{k+1}(x,t)$$

$$P^{k+1}(x,t) = \alpha_P * P^{k}(x,t) + (1-\alpha) * P^{k+1}(x,t)$$

where **k** is the iteration counter number, α_p and α_ρ are underelaxation factors for pressure and density respectively.

It was found that as long as **P** and ρ converged, the results will not be affected by the choice of α_p and α_ρ. The best value of the factors for the purpose of good convergence in this calculation were found to be:

$$\alpha_p = 0.618 , \qquad \alpha_\rho = 0.75$$

CHAPTER 6

ROTARY ENGINE -- THERMODYNAMIC MODEL

6.1 Introduction

The RVP rotary engine has a unique thermodynamic system which is a combination of external and internal combustion systems.

The mode of operation is as follows. Semi-burnt gases are injected into the power chamber, thrusting onto the lobes of the outer rotor. The kinetic energy of the gases is converted into pressure energy during the process and power is generated by the rotating rotors. This is a typical turbine working process -- an external combustion system. The difference is that instead of a continuous steady state flow process as in the case of the turbine, the gas mixture in the RVP rotary engine will accumulate in the power chamber. It is a unsteady/discontinuous flow process.

After the gases have entered the power chamber, they will undergo a typical internal combustion working process. The semi products of combustion will continuously mix with more fresh air to complete the combustion as the volume increases until the exhaust port opens to that chamber. Expansion work will be done on the rotors during the process.

No existing thermodynamic system is similar to the RVP engine combustion

system and, as a consequence, there is no corresponding theoretical work. A proper special theoretical model has to be created in this work in order to investigate this unique thermodynamic system.

The flow simulation conducted in the previous chapter provided us with a partial solution of the problem -- the thrust process. With the velocity profile and information of the gas properties, we can calculate the thrust power generated in the process. It is the objective of this chapter to develop a thermodynamic model properly describing the internal combustion process between the period of injection and exhaust. A phenomenological model - namely a multi-zone zero-dimensional thermodynamic model has been developed. In the model, an artificially created three zone sub-combustion model is adapted in order to make the theoretical research feasible.

6.2 Three zone combustion submodel

6.2.1 Three zone assumptions

The hot burning mixture from the pre-combustion chamber is injected through the injection port into the power chamber at a pre-organized timing to start the combustion in the main chamber. The burning gases thrust at high velocity along the lobe and divide the power chamber into two zones: a burning zone and an air zone. The burning zone is physically a thick gas ring along the wall of the chamber. It is initially comprised of

the semi-products of combustion injected from the pre-combustion chamber. It is an active zone with chemical reactions. The species of the gases and the properties of each species inside the burning zone are functions of time. On the other hand, the air zone which is located in the centre of the chamber area is a relatively 'quiet zone'. It consists of compressed fresh air from the intake port and some portion of the combustion residuals left in the chamber from the previous cycle. All of the species are chemically inert. These two zones are separated by a flame front. The flame front is a thin surface wrinkled by micro turbulence along which rapid chemical reactions take place. Enhanced by the chemical reactions, the flame front propagates from the burning zone to the air zone until the combustion process is completed. From a physical point of view, it is a process of mass transportation of air from the air zone to the burning zone. There is also an energy transportation between these two zones. Because of the heat release from the chemical reaction, high temperature and high pressure will be built up within the burning zone. The temperature and pressure difference causes the energy transportation from the burning zone to the air zone across the flame front by heat transfer and compression.

It is the burning zone and flame front that control the heat release within the chamber. Such characteristics as those listed below are important:

i) The fuel/air ratio is a function of time: decrease of the volume of the air zone results in a decrease of the fuel/air ratio of the burning zone.

ii) The degree of heat release is a function of time: at any time before completion of combustion, the burning zone is charged with various kinds of combustion

products, semi combustion products and fuel/air mixture; heat is released only partially from some individual species at some time interval.

This means for a chemical reaction process, both the reactants and conditions of the reaction change with time. It is clear that the combustion process is extremely complex. The details of the process depend on the characteristics of the fuel, on the design of the engine's combustion chamber, on the status of the gases inside the pre-combustion chamber and on the engine operating conditions. It is an unsteady, heterogeneous, three-dimensional combustion process. While an adequate conceptual understanding of combustion in an engine has been developed, to date an ability to describe critical processes like the above has been lacking.

A three zone combustion model is created in this work to simplify the analysis of the combustion process. It is done by dividing the burning zone into two thermodynamically equivalent zones: a burnt zone and an unburnt zone. The flame front is the boundary of the burnt zone with a negligible thickness and has no physical properties. The chemical reaction process of the burning zone and flame front are substituted by discrete heat release steps. By these steps the boundary of the burnt zone propagates into the unburnt zone. The definition of the air zone is not changed. The mass transportation rate of air depends on the boundary area of the air zone and its pressure/temperature conditions (refer to Figure 6.1 for three zone assumptions).

In order to create the three zone model, the following assumptions are necessary:

(1) Residual products left from the previous cycle are chemically inert. Air is

compressed isentropically by the boundary of the air zone.

(2) The amount of air reduced in the air zone is equal to that increased in the burning zone. Mass leakages are negligible.

(3) The degree of heat release of the burning mixture is equal to the mass fraction of an equivalently burnt fuel to the total fuel. In other words, an amount of completely burnt fuel can be artificially specified so as to contribute the same amount of heat as the whole burning fuel does in its semi combustion products status. Therefore:

(a) the burning zone can be divided into a burnt zone and an unburnt zone according to the equivalent burnt mass fraction calculations. The burnt zone contains completely burnt residuals which are nonactive and the unburnt zone is

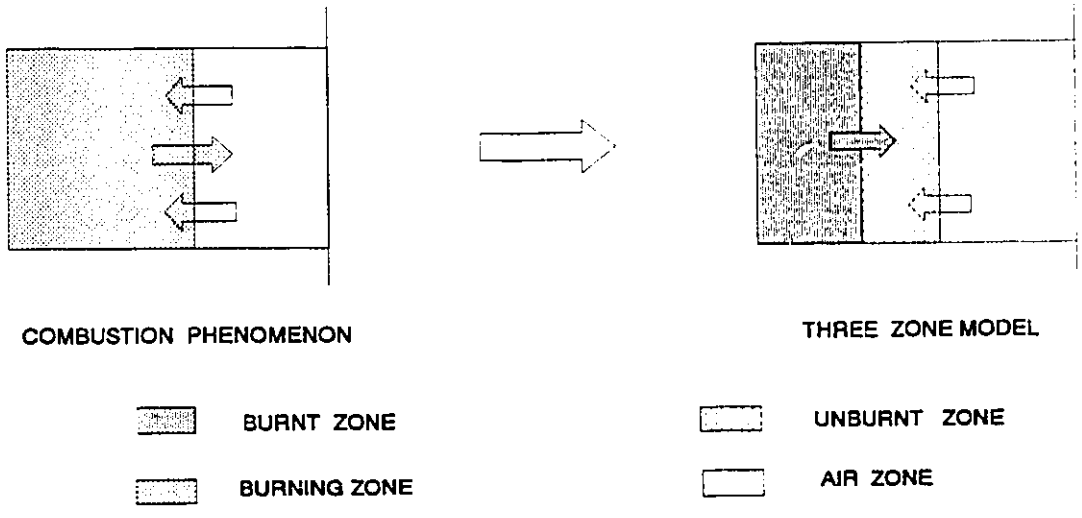

Figure 6.1 Three zone assumption

charged with premixed flammable mixture.

(b) as soon as the unburnt zone reaches zero, combustion stops.

During the following modelling analysis further assumptions are adopted:

(4) All the gases concerned satisfy the ideal gas law

(5) A spatially uniform pressure exists across the combustion chamber

(6) Each zone has a different uniform zone temperature and gas density. The air zone shares the same temperature with the unburnt zone

For most of carbon-hydrogen components under the condition of pressure less 4 MPa and temperature greater than 1000 K, the compressibility factor will be greater than 0.90 (Wark, 1988). Since biatomic molecule substances such as oxygen and nitrogen that must always be treated as ideal gases occupy the greater portion of the gases, assumption (4) is accepted here. The uniform pressure assumption is a standard assumption for the reciprocating engine and has been verified by experiments (Heywood, 1988). For the Wankel Rotary Engine, an experimental result showed that when N = 2,000 rpm, the maximum error is only of the order of 0.5% for a very short time (Danieli, 1976).

6.2.2 Combustion submodel with a turbulence eddy entrainment model

The combustion submodel is designed to calculate the flame propagation speed and heat release rate during the combustion process using the known pressure, temperature and other gas properties. The combustion submodel is set up with the foregoing three zone model and a turbulence eddy entrainment model (Blizard and Keck,

1974).

According to assumption (3) the progress of the combustion process inside the burning zone can be represented by the propagation of burning front(s) having infinitesimal by small thickness within a premixed flammable mixture. The propagation can be expressed by a turbulent speed S_T :

$$S_T = K_T(\rho, S_p) * S_l(T_u, T_b, p, \phi)^{\alpha} \qquad (6-1)$$

where, S_l is the laminar speed of the flame, which is a function of the pressure p, temperatures within the burnt zone T_b and the unburnt zone T_u and equivalent ratio of the unburnt mixture ϕ.

α is a constant depending on the design of engine.

K_T is a turbulent factor, which is the function of gas density of the unburnt zone and the characteristic speed S_p. K_T will be calculated with the Turbulence Eddy Entrainment Model

Bantiggelen and Deckere (1957) derived a formula for the laminar speed S_l for a hydrocarbon stationary flame using the theory of chain branching,

$$S_l = KC_m[Y_F{}^a Y_{O_2}{}^b \exp(\frac{-E_a}{RT_m})]^{\frac{1}{2}} \qquad (6-2)$$

where, $C_m = (8RT_m/\pi M_R)^{1/2}$ is the mean molecular speed of chain carriers whose mean molecular weight is M_R. $T_m = T_u + 0.74(T_b - T_u)$ is the mean temperature of the reaction zone. $K = 2T/(\sqrt{3\pi}Tm)*(P/Pr)^{\alpha}$, (Pr = 1 atm).

For the fuel C_8H_8 for example:

$$M_R = 68,\ \alpha = -0.22,\ a = -0.71,\ b = 1.71 \text{ and } E_a = 38.6 \quad \text{(kcal/mole)}$$

Defining a turbulent intergrade length scale of the eddies L and a characteristic burning time τ_b, we have

$$S_T = L / \tau_b \qquad (6-3)$$

According to the eddy entrainment model, two assumptions are made as the following:

(1) At spark ignition, turbulence integral scale L_i and turbulent intensity U'_i are proportional to the chamber height h_i and the piston speed S_p respectively. i.e.

$$L_i = C_L h_i \qquad U'_i = C_u S_p \qquad (6-4A)$$

(2) After the beginning of measurable heat release, taken as 1% mass fraction burned, the turbulence intensity and integral scale of the unburned gas are governed by the conservation of angular momentum of the individual eddies.

That is

$$L = L_i \left(\rho_{ui} / \rho_u \right)^{1/3} \qquad U' = U'_i \left(\rho_u / \rho_{ui} \right)^{1/3} \qquad (6\text{-}4B)$$

Thus

$$L = L_i \left(\rho_i / \rho_u \right)^{1/3} = C_L h_i \left(\rho_i / \rho_u \right)^{1/3} = C_1 \rho_u^{-1/3} \qquad (6\text{-}4)$$

From experimental results and a series derivation based on the above assumptions and assumption of an inner structure of the eddies, we also have the result (refer to appendix G for derivation):

$$\tau_b = C_2 \left(S_p S_l \right)^{-2/3} \rho_u^{-4/9} \qquad (6\text{-}5)$$

Therefore

$$S_T = C_1 \rho_u^{-1/3} C_2 \left(S_p S_l \right)^{2/3} \rho_u^{4/9} = \left(C \rho_u^{1/9} S_p^{2/3} \right) S_l^{2/3} \qquad (6\text{-}6)$$

Compared with equation (6 - 1) we know:

$$K_T(\rho, S_p) = C \rho_u^{1/9} S_p^{1/3} \qquad (6\text{-}7a)$$

and

$$\alpha = 2/3 \qquad (6\text{-}7b)$$

Where, C is a constant dependent only on the structure of the specific engine. During the computer calculations, C is used as a relaxation variable to compensate the

assumption errors. Piston speed S_p can be replaced by edge speed of the rotor for the RVP engine as has been similarly done in the Wankel engine research (Danieli, 1978).

Mass burning rate **DX/Dt** can thus be calculated as:

$$DX/Dt = A_f * S_T * \rho_u / m_f \qquad (6-8)$$

where A_f is the area of flame front which could be approximately determined by the volumes of the combustion chamber and the burnt zone:

$$A_f = \sqrt{4.0 * \pi * W * (V - V_B)}$$

where W is the depth of the combustion chamber.

The heat released in a time interval $\Delta\theta$ is:

$$Q = H_u * m_f * \Delta X \qquad (6-9)$$

6.3 Other thermodynamic submodels

6.3.1 Gas property submodel

The objective of the gas property submodel is to calculate the properties of air, burnt and unburnt gases with the known temperatures T_b, T_u, pressure P and equivalence ratio ϕ. The specific formulas derived in this section are for the combustion of Octane

(C_8H_{18}) with one mole of dry air ($O_2 + N_2$).

The following gas properties will be solved in this submodel: mole number, molecular weight, specific volume and internal energy.

The possible combustion products of the fuel C_nH_m with dry air are assumed to be N_2, O_2, H_2O, CO_2 and CO according to the following reaction equation:

$$\phi C_nH_m+\frac{79}{21}(n+\frac{m}{4})N_2+(n+\frac{m}{4})O_2 \rightarrow$$

$$\frac{79}{21}(n+\frac{m}{4})N_2+(1-\phi)(n+\frac{m}{4})O_2+\frac{m}{2}\phi H_2O+n\phi CO_2 \qquad (\phi \le 1)$$

$$\frac{79}{21}(n+\frac{m}{4})N_2+\frac{m}{2}\phi H_2O+[n\phi-(2n+\frac{m}{2})(\phi-1)]CO_2$$

$$+[(2n+\frac{m}{2})(\phi-1)]CO \qquad (\phi>1)$$

a) **Calculation of mole number of the mixture per mole of air:**

For the complete combustion of a stoichiometrically correct fuel-air mixture, the above reaction can be reduced to

$$C_nH_m + (n+m/4)\ O_2 \text{ -- } n\ CO_2 + m/2\ H_2O$$

or

$$C_nH_m + (n+m/4)/0.21\ \text{Air} \text{ -- } n\ CO_2 + m/2\ H_2O$$

Therefore, the number of moles of fuel required to completely burn one mole of air is

$$f_c = \frac{1}{\frac{1}{0.21}(n+\frac{m}{4})} = \frac{0.42}{n(2+\frac{m}{2n})} = \frac{0.42}{n(2+\mu)} \qquad (6-10)$$

where $\mu = m/2n$

The number of moles of unburnt mixture per mole of air can be calculated as

$$\begin{aligned} n_u &= n_{air} + n_{correct\ fuel} + n_{extra\ fuel} + n_{recycled\ burnt\ gas} \\ &= (1-\eta)*1 + (1-\eta)*f_c + (1-\eta)(\phi-1)*f_c + \eta*n_b^0 \\ &= 1 + f_c + \eta(n_b^0 - 1 - f_c) + (\phi-1)(1-\eta)*f_c \end{aligned}$$

For fuel C_8H_{18}, n=8, H=18 thus $\mu = 9/8$, $f_c = 0.0168$; n_b^0 is the mole number of burnt mixture from the last cycle. If we set $\phi_r = 1$ for simplification: $n_b^0 = 1.0756$.

Therefore

$$n_u = 1.0168 + 0.0588*\eta + 0.0168(\phi-1)(1-\eta) \qquad (6-11)$$

The number of moles of burnt mixture per mole of air for the fuel C_8H_{18} can also be calculated as

when $\phi <= 1$

$$\begin{aligned} n_b &= 1 + 0.21\mu/(\mu+2) + 0.21(\phi-1)\mu/(\mu+2) \\ &= 1.0756 + 0.0756\,(\phi-1) \end{aligned} \qquad (6-12a)$$

when $\phi > 1$

$$n_b = 1 + 0.21\mu/(\mu+2) + 0.42(\phi - 1)(\mu + 1)/(\mu + 2)$$

$$= 1.0756 + 0.2856\,(\phi - 1) \qquad (6 - 12\ b)$$

b) Molecular weight of the mixture

To calculate the mass of reactants we assume the percentage of recycled gases is η with the products of N_2, H_2O and CO_2. Thus the mixture of reactant can be described as

$$(1-\eta)[\phi C_n H_m + \frac{29}{21}(n+\frac{m}{4})N_2) + (n+\frac{m}{4})O_2] + \eta[\frac{79}{21}(n+\frac{m}{4})N_2 + \frac{m}{2}\phi_r H_2O + n\phi_r CO_2]$$

further assuming $n = 8$, $m = 18$ and $\phi_r = 1$ for the recycled gases we have the reaction

$$(1-\eta)[\phi C_8 H_{18} + 47.02N_2 + 12.5O_2] + \eta[47.02N_2 + 9.0H_2O + 8.0CO_2]$$

Therefore, the mass of reactants

$$M_{rac} = 1716.56 + 114\,\phi\,(1 - \eta) + 162\,\eta$$

From the law of mass conservation, we know the mass of combustion products

$$M_{pro} = M_{rac}$$

With the molecular number n we can calculate the molecular weight of the reactants (unburnt mixture) and products (burnt mixture):

$$M_u = \frac{M_{rac}}{n_u * n_{air}} = \frac{1716.56+114\phi(1-\eta)+162\eta}{1.0168+0.0168(\phi-1)(1-\eta)+0.0588\eta]*59.52} \quad (kg/kgmole) \qquad (6\text{-}13)$$

$$M_b = \frac{M_{pro}}{n_b * n_{air}} = \begin{cases} \dfrac{1716.56+114\phi(1-\eta)+162\eta}{[1.0756+0.0756(\phi-1)]*59.52} & (\phi \le 1) \\ \dfrac{1716.56+114\phi(1-\eta)+162\eta}{[1.0756+0.2856(\phi-1)]*59.52} & (\phi > 1) \end{cases} \quad (kg/kgmole) \qquad (6 - 14)$$

c) **Specific volume of the mixture**

For the mixture of perfect gases we have

$$p\,v = \frac{R_0}{M}\,T$$

where R_0 = 8314 J/K,kgmole is the universal gas constant and

M is the molecular weight in kg/kgmole

Thus

$$v_u = \frac{8314.0 * T_u}{M_u * p} = v_u(T_u, p, \phi, \eta) \quad (m^3/kg) \qquad (6 - 15)$$

$$v_b = \frac{8314.0 * T_b}{M_b * p} = v_b(T_b, p, \phi, \eta) \quad (m^3/kg) \quad (6 - 16)$$

d) Internal energy

The internal energy of the gases may be calculated using empirical results for some specific mixture. Based on the empirical data and assumptions introduced by Blizard and Keck (1974) the internal energy of the burnt, unburnt and air per mole of air for the mixture of C_8H_{18} and dry air can be calculated using the following formulas (refer Appendix H for derivations):

For unburnt mixture:

$$e_u(Tu,\phi,\eta) = [79{,}459 - 116{,}218\eta + 86{,}992(\phi - 1)(1 - \eta)]$$

$$+ (25.1 + 19.68\eta + 2.1(\phi - 1)(1 - \eta)] * T_u \quad \text{(kJ/kgmole)} \qquad (6 - 17)$$

For unburnt air:

$$e_{au}(T_b, \phi) = -7443 + 23.0 * T_u \quad \text{(kJ/kgmole)} \qquad (6 - 18)$$

For burnt lean mixture ($\phi <= 1$):

$$e_b(T_b, \phi) = -[36{,}750 + 22{,}330(\phi - 1)] + [44 + 16.3(\phi - 1)]T_b \quad \text{(kJ/kgmole)} \qquad (6 - 19a)$$

For burnt rich mixture ($\phi > 1$):

$$e_b(T_b, \phi) = -36{,}750 + 93{,}923(\phi - 1) + [44 + 16.3(\phi - 1)]T_b \quad \text{(kJ/kgmole)} \qquad (6\text{-}19b)$$

6.3.2 Heat transfer submodel

Heat transfer from the wall of the combustion chamber is assumed to take the form of forced convection without radiation:

$$Q_w(\theta) = A(\theta)\, h(\theta)\, [\, T_b(\theta) - T_w \,] \qquad (6\text{-}20)$$

G. Woschni's (1967) empirical equation is used to calculate the heat transfer coefficient $h(\theta)$:

$$h = 110 d^{-0.2} P^{0.8} T^{-0.53} \left[C_1 C_m + C_2 \frac{V_S T_1}{P_1 V_1} (P - P_0) \right]^{0.8}$$

A geometrical calculation of $A(\theta)$ will be conducted for the RVP engine. Gas temperature T_b has to be determined by a trial and error method and an empirical constant wall temperature T_w will be used.

6.4 Thermodynamic model analysis

With the three zone assumptions, an eddy entrainment combustion submodel and other submodels have been set up in the last section. A thermodynamic model may then be developed for the engine analysis.

From the first law of thermodynamics we can solve for the internal energy of the

system which is a function of temperature and gas composition according to the perfect gas assumption:

$$E\ (\ T_u,\ T_b,\ \phi,\ \eta\ ) = E_0 + Q - Q_w - p\ dV \qquad (\ 6 - 21\ )$$

where, E_0 is the initial internal energy that could be obtained by using iterative techniques. Q is the amount of heat released during the calculated step. During the compression process no heat is released, Q equals to zero; during the injection and expansion process Q is to be calculated based on the combustion submodel. Q_w is the energy loss through heat transfer. The heat transfer submodel will be used to solve for it. **pdV** is the expansion work done by the gases, which is one of the objectives of this thermodynamic model.

The internal energy described in equation (6-21) is distributed among the three zones:

$$E(T_u,T_b,\phi,\eta) = e_b(T_b,\phi)*m_b(T_b,X,\phi) + e_u(T_u,\phi,\eta)* m_u(T_u,1-X,\phi,\eta) + e_a(T_u)*m_a(T_u,1-X,\phi) \qquad (\ 6 - 22\ )$$

This internal energy for different zones can be calculated in the gas property submodels and the mass in each zone can be determined by combustion submodel.

For the mass conservation we have:

$$V = v_b(T_b,p,\phi,\eta)*m_b(T_b,X,\phi,\eta) + v_u(T_u,p,\phi,\eta)*m_u(T_u,1-X,\phi,\eta) + v_a(p)*m_a(T_u,1-X,\phi) \qquad (\ 6 - 23\ )$$

where the specific volume of gases in each zones v_b, v_u and v_a can be determined from the gas property submodel and the volume of the combustion chamber V is to be calculated numerically.

Furthermore, from the isentropic assumption of the compression process in the air zone, we have

$$T_u = T_0 (p / p_0)^{k-1/k} \qquad (6 - 24)$$

So far, we have four equations (6 - 21) through (6 - 24) to solve for four unknown variables:

$$E(\theta),\ T_b(\theta),\ T_u(\theta) \text{ and } p(\theta)$$

where, equation (6 - 15) through (6 - 20) will be employed to calculate the specific volume and internal energy for the gases in different zones and the heat transfer rate Q_w.

We have a non-linear system of coupled equations with transcendental terms, which has to be solved numerically.

From those results the performance parameters of the engine can be calculated as:

output work $$W = \sum p(\theta)\ \Delta V \qquad (6 - 25)$$

fuel consumption $$g_e = m_f / (W * t) \qquad (6 - 26)$$

CHAPTER 7

ROTARY ENGINE -- PERFORMANCE PREDICTION AND PARAMETER OPTIMIZATION

7.1 Introduction

The purpose of the flow simulation and theoretical model investigations is to predict performance of the engine and optimize some engine structure and operation parameters before a physical prototype is built. Based on this theoretical research it may be seen that the RVP rotary engine with its unique mechanical structure and thermodynamic system has many potential advantages over conventional reciprocating engines and the Wankel rotary engine. The next critical step is to built a prototype engine to verify its potential as well as the theoretical simulation and modelling.

Power is generated by the rotors through the thrusting of burning gases injected into power chamber from the pre-combustion chamber. The value of this power is calculated based on the velocity profile obtained from the flow simulation as described in chapter 5.

The combustion is completed in the power chamber after the injected gases mix with more fresh air. The overall fuel/air mixture is lean while a rich mixture burns in pre-combustion chamber in order to achieve an efficient and clean combustion. The

expansion work is calculated through the thermodynamic model analysis. Then the specific fuel consumption rate is calculated based on the total fuel consumed divided by the total power obtained within a working cycle.

In this chapter, the calculated results are presented and compared with some typical commercial engines from power and economic points of view. Furthermore, through the theoretical model analysis, some essential construction parameters of the engine are optimized to obtain a better performance.

7.2 Engine performance prediction and comparison with other commercial engines

7.2.1 Calculation of power generated by thrust gases

If we take the injection port of the power chamber as a jet and the moving lobe as a vane, the flow that starts at the port and then goes along the boundary (wall) of the lobe is similar to the flow that takes place in a turbine. A part of the kinetic energy of the gases will be transferred to the work acting on the lobe through the thrust. The calculation of the work or power generated in that process is straightforward after we have obtained detailed information about velocity profile and mass transformation.

Referring to the engine shown in Figures 3.2 and 5.1, if we define the first 180^0 range of wall to be in the positive direction the other side will be in the negative direction. Therefore, the net power output to the shaft will be the algebraic summation

of these two parts.

For any section of wall, there is a force acting on it by the flowing fluid (refer to Figure 7.1)

$$F_{xi} = (\frac{dm}{dt})_i(V_{\eta i-1}\cos\phi_{i-1} - V_{\eta i}\cos\phi_i) \qquad (7-1)$$

Integrating equation (7-1) according to the definition of the positive force (for the considered grid, $3 < i < 21$) and the negative force ($22 < i < 35$) we have:

The positive force:

$$F_{x+} = \sum_{i=3}^{21} F_{xi}$$

and the negative force:

$$F_{x-} = \sum_{22}^{35} F_{xi}$$

The net power is

$$Power(t) = U*(F_{x+} - F_{x-}) \qquad (7-2)$$

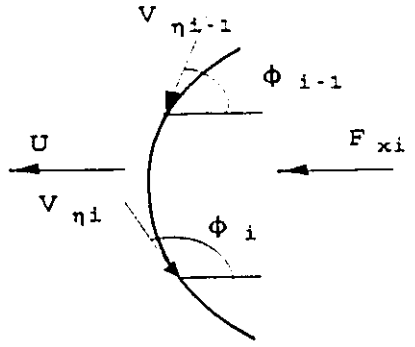

Figure 7.1 Forces Acted on the Moving Vane

In equation (7-1)

$$\frac{dm}{dt} = \frac{d(\rho V)}{dt} = V\frac{\partial \rho}{\partial t} + \rho\frac{\partial V}{\partial t}$$

For a fixed control volume **V** we have in **X** direction:

$$\left(\frac{dm}{dt}\right)_i = \left(V\frac{\partial \rho}{\partial t}\right)_i = \frac{\Delta x \Delta y}{\Delta t}\left[\rho(x,t) - \rho(x,t-1)\right] \qquad (7-3)$$

In chapter 5 we calculated

$$V_{\eta i} = VA(x,\ t) \qquad (7-4)$$

The angle ϕ_i has a relationship with η_i, which can be derived as follows (Figure 7.2):

For an ellipse

$$\frac{X^2}{a^2} + \frac{Y^2}{b^2} = 1$$

or

$$Y^2 = \frac{b^2}{a^2}(a^2 - X^2) \qquad (7-5)$$

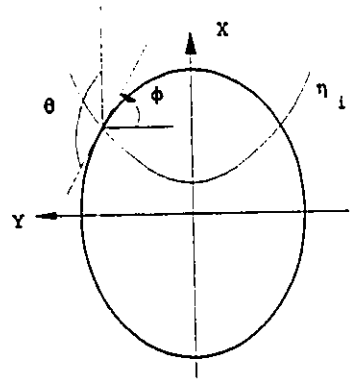

Figure 7.2 Relationship of the Angles

and

$$tg\theta = \frac{dY}{dX} = -\frac{b}{a}\frac{X}{\sqrt{a^2-X^2}} \qquad (7-6)$$

Substituting (7-5) in the equation of the hyperbolic line crossing that point

$$\frac{X^2}{C^2\cos^2\eta_i} - \frac{Y^2}{C^2\sin^2\eta_i} = 1$$

we can solve for X

$$X^2 = (b^2+c^2\sin^2\eta)\frac{a^2\cos^2\eta}{a^2\sin^2\eta+b^2\cos^2\eta}$$

Substituting the above result to equation (7-6) we have

$$tg\theta = \frac{b^2}{a^2}\,ctg^2\eta \qquad (7-7)$$

From

$$\cos\theta = \pm\frac{1}{\sqrt{1+tg^2\theta}}$$

thus

$$\cos\theta = \pm\frac{a}{\sqrt{a^2+b^2ctg^2\eta}} \qquad (7-8)$$

From Figure 7.2 we see that

$$\cos\phi = \cos(\theta-\frac{\pi}{2}) = \sin\theta = \pm\sqrt{1-\cos^2\theta}$$

Therefore

$$\cos\phi = \pm\frac{bctg\eta}{\sqrt{a^2+b^2ctg^2\eta}} = \pm\frac{1}{\sqrt{1+1.527tg^2\eta}} \qquad (7-9)$$

where the values of **a** = 0.0131 and **b** = 0.0106 are used.

Substituting equations (7-3), (7-4) and (7-9) into equations (7-1) and (7-2) we can calculate the power generated by the thrust gas.

Figure 7.3 shows the results of the input mass flow on the power chamber. The velocity reaches local sonic velocity for a length of time. Then it decreases because of the decrease of the pressure difference between the two chambers. The mass flow rate increases along with the increase of the opening area while velocity stays constant. Afterwards, it decreases along with the velocity.

Figure 7.4 through Figure 7.6 show the calculated results of velocity profile.

Figure 7.4 (a) shows that the velocity develops from zero at the wall sharply to a approximately constant value. It is a typical velocity profile for a viscous flow along a solid boundary. It is interest to note from Figure 7.4 (b) that the velocity profile along the wall seems not change too much in the normal direction except for the range $\eta = 150^0$ -- 250^0. This is caused by the sharp curvature change of the ellipse at that range. The influence of the curvature change on the flow is bigger at a position close to the wall ($\mathbf{Y} = 2$, for example) than that away from the wall ($\mathbf{Y} = 10$). From Figure 7.5 and Figure 7.6 we will see that along the wall direction the velocity profile becomes flatter as time goes on, which means the flow field has a tendency to become a uniform field with time.

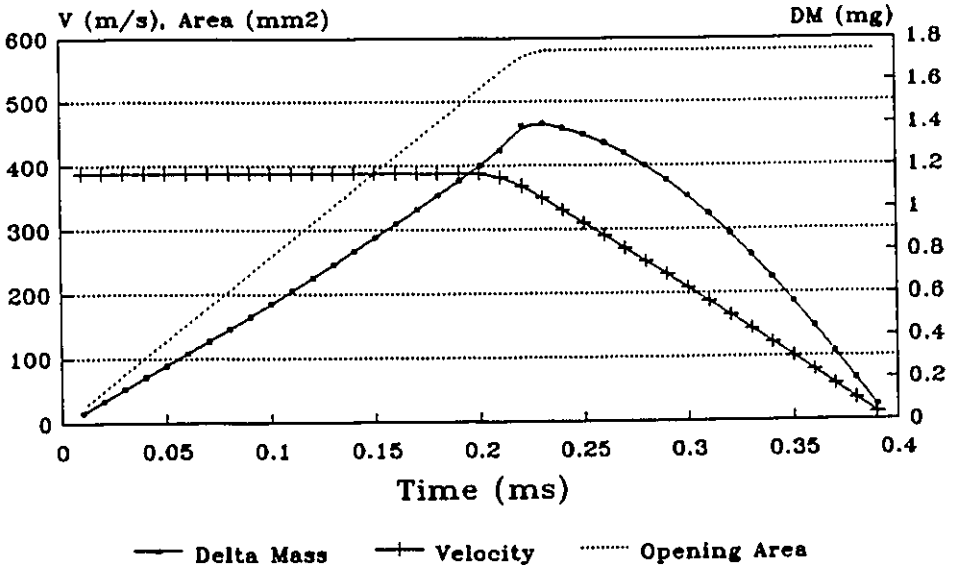

Figure 7.3 Input Mass Flow

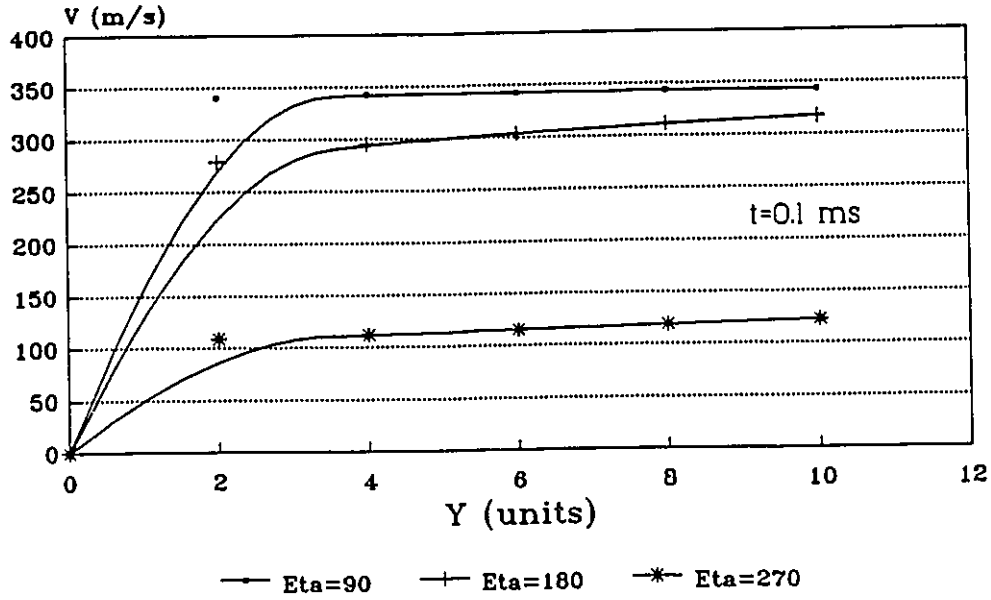

Figure 7.4 (a) Velocity Profile Along ζ Axis (normal to the wall) at t=0.1 ms

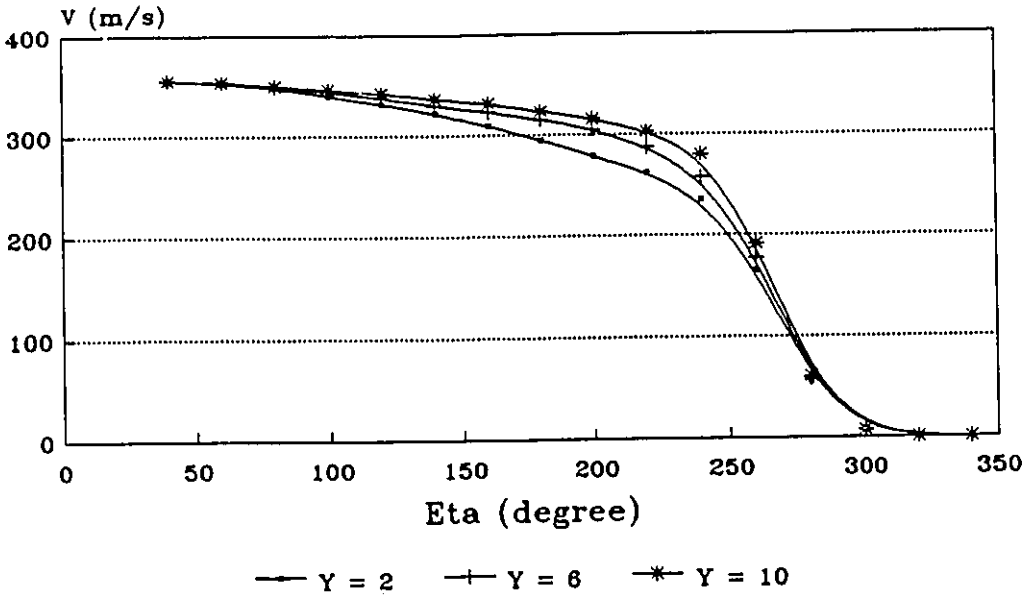

Figure 7.4 (b) Velocity Profile Along η Axis (tangential direction) at t=0.1ms

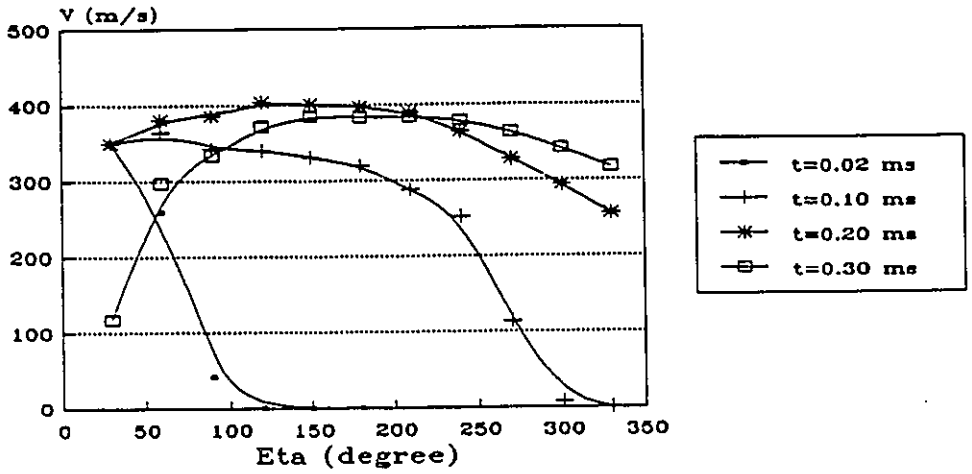

Figure 7.5 Velocity Profile History

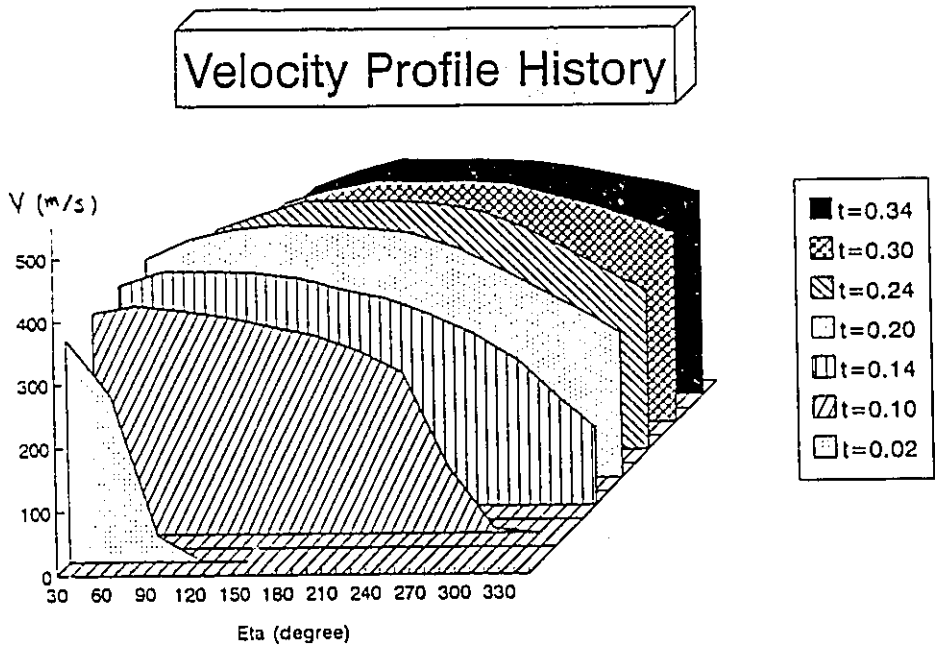

Figure 7.6 Demonstration of the Velocity Profile

The calculated results of the power generated by the thrust gas are shown in Figure 7.7. Positive power comes from the force acting on the positive side of the wall and negative power on the negative side. Both of the curves have a peak midway, which is determined by the velocity and the rate of mass change. At the beginning, velocity has not fully developed, while at the end the mass tends to be uniform. The distance on the negative side to the centre is smaller than that on the positive side. Because that, the positive power is always bigger than the negative one which makes the net power always greater than zero. An average value of 4.84 KW of power is generated by the thrust gas in the period of 0 to 0.36 ms.

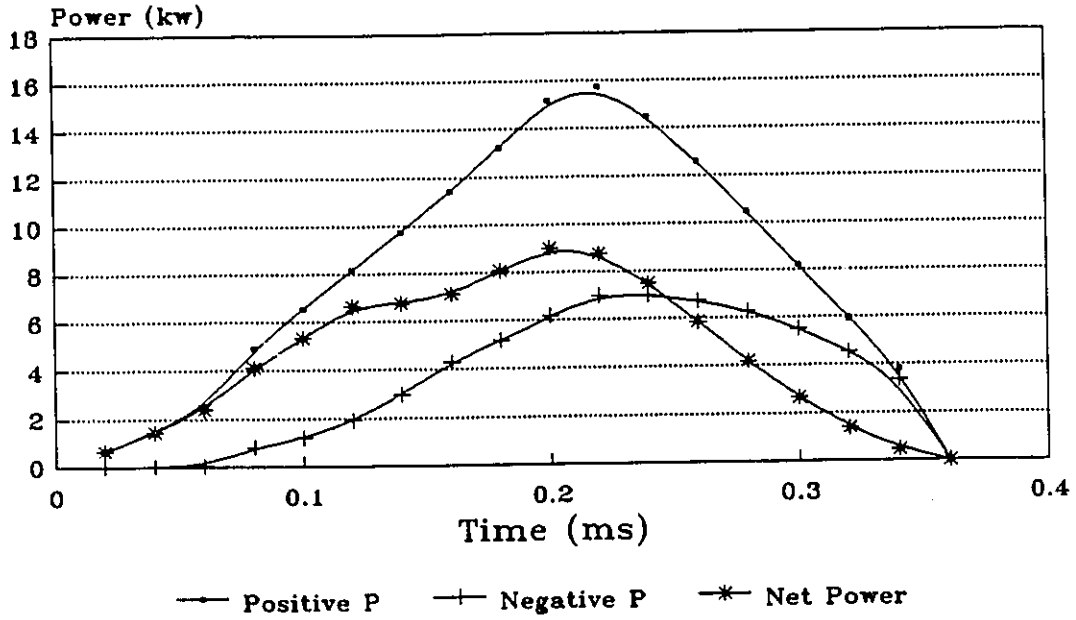

Figure 7.7 Power generated by the thrust gases

7.2.2 Predicted performance of RVP rotary engine

A three zone thermodynamic model has been developed in Chapter 6 to predict the performance of the RVP rotary engine. This is to calculate the output power and fuel consumption rate based on information from flame propagation and heat release rate. The calculated results are dependent on the engine structural parameters such as the shape and volume of the power chamber, compression ratio and number of power strokes per revolution and operating parameters such as rotational speed, fuel/air ratio, injection advance angle and wall temperature control. To get better performance we could optimize these parameters through the model analysis.

As an example, a specific working condition has been selected for theoretical analysis by means of the model. Table 7.1 shows the selected engine conditions.

Table 7.1 Working conditions of RVP engine for model analysis

Item	symbol	unit	value
engine speed	N	rpm	5000
injection advance	θ	degree	-17.5
pressure in pre-combustion chamber	p	KPa	600
wall temperature	Tw	K	470
equivalent ratio	ϕ		2.0
gas recycle rate	Eta	%	10
rotors displacement	V	cc/rev.	830
fuel consumed			gasoline

A Fortran program was written according to the model developed in Chapter 6 to calculate the brake horse power and fuel consumption rate as well as the pressure and temperature history during the injection and expansion process. A brief flow chart of the program shown in Figure 7.8 presents the outline of the program. The total power that could be obtained from the engine which will be indicated in Figure 7.12 is the sum of the value from equation (7-2) and equation (6-25) plus the consideration of mechanical efficiency loss.

The combustion process is continuous while injection takes place. The amount of total fuel injected into the power chamber depends both on the injection, which is assumed to be isentropic one dimensional flow, and the heat release of the combustion which builds up pressure quickly to decrease the flow rate. This process has to be calculated iteratively. Newton's iterative method has been used to solve equations (6-21) through (6-24), which are non-linear system of coupled equations with transcendental terms, in order to calculate pressure and temperatures with the assumed heat release rate **DX** and equivalent ratio **FI**. **DX** is then updated with the obtained values of pressure and temperature based on the three zone eddy entrance combustion submodel. The computer program worked successfully and all the iterative routines converged well.

Figures 7.9 through 7.12 show the calculated results of the model. A value of mechanical efficiency (80%) of the engine has been selected to calculate the brake power and fuel consumption.

Figure 7.9 shows the diagrams of the results of heat release rate, temperature and

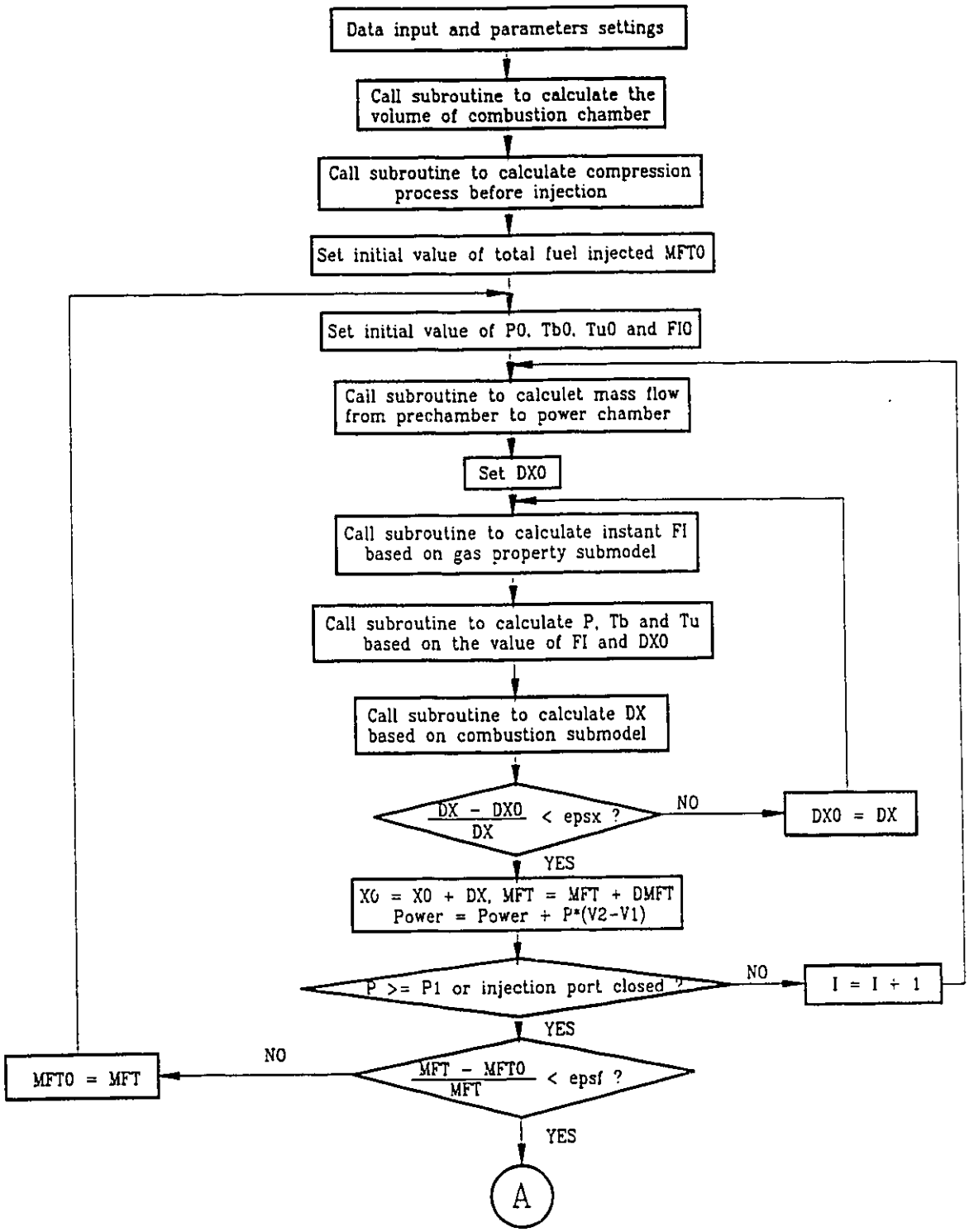
Data input and parameters settings
Call subroutine to calculate the volume of combustion chamber
Call subroutine to calculate compression process before injection
Set initial value of total fuel injected MFT0
Set initial value of P0, Tb0, Tu0 and FI0
Call subroutine to calculet mass flow from prechamber to power chamber
Set DX0
Call subroutine to calculate instant FI based on gas property submodel
Call subroutine to calculate P, Tb and Tu based on the value of FI and DX0
Call subroutine to calculate DX based on combustion submodel
(DX - DX0) / DX < epsx ?
NO
DX0 = DX
YES
X0 = X0 + DX, MFT = MFT + DMFT
Power = Power + P*(V2-V1)
P >= P1 or injection port closed ?
NO
I = I + 1
YES
(MFT - MFT0) / MFT < epsf ?
NO
MFT0 = MFT
YES
A

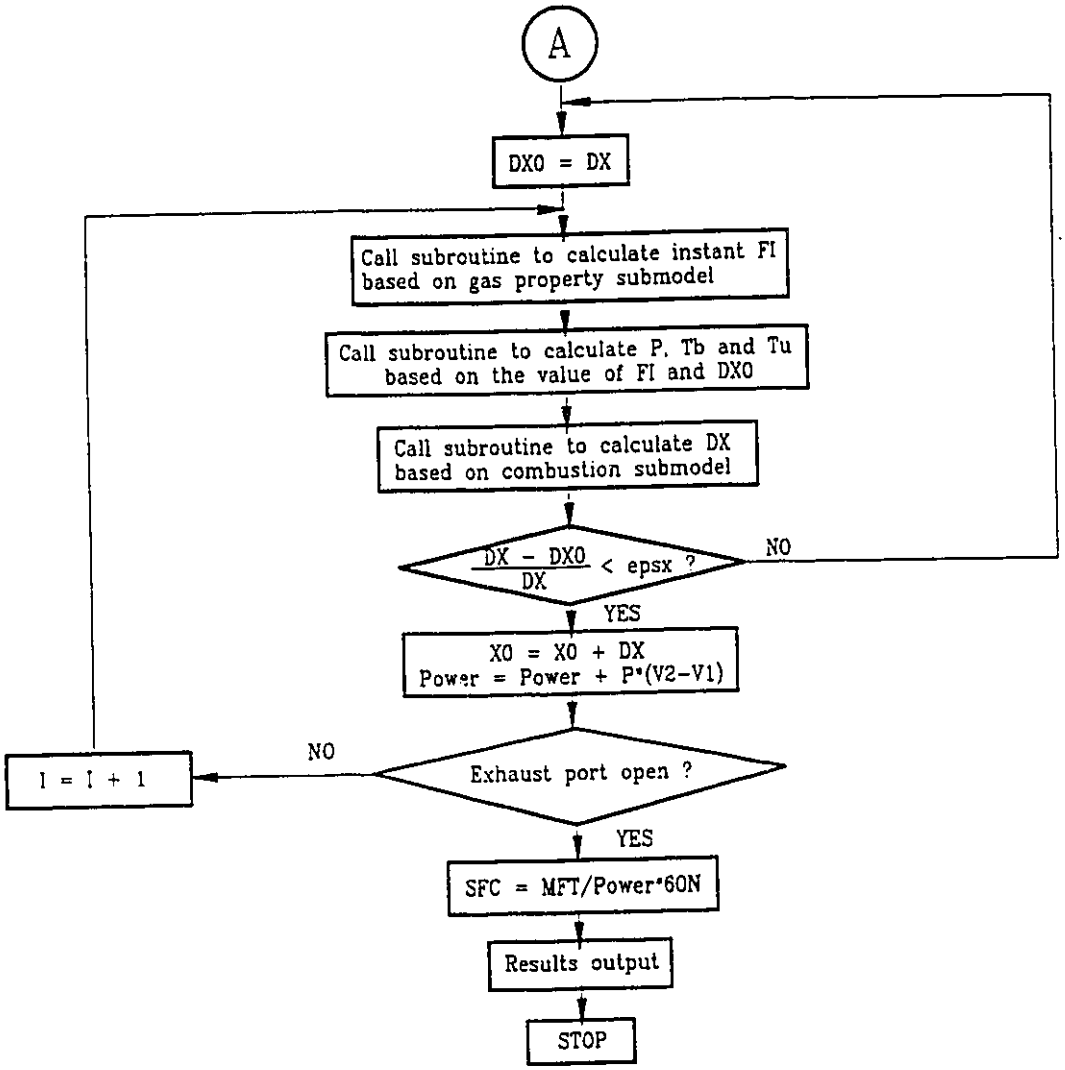

Figure 7.8 Flow Chart of the Fortran Program of the Thermodynamic Model

pressure history. **TM** is defined as the average temperature based on the burnt and unburnt masses. Examining the burning rate **DX** vs time (crank angle) in Figure 7.9 (a) we can see that there is a sharp pulse at the beginning of injection. This reflects the combustion of the first part of the burning mixture injected into the chamber. Within a short period of time it mixes with oxygen and releases its energy rapidly. When the mixture following the first part is injected into the chamber, the flame propagates at a limited speed and heat release rate falls to normal. This sharp pulse in heat release also results in a pressure jump in the chamber in a corresponding fashion (refer to Figure 7.9 (b)). There is a retardation of the temperature pulse compared with those of the pressure and heat release pulses. The combustion stops at 60 degree after upper dead centre when the burning rate **DX** reaches zero and burnt mass fraction **X** reaches about 100%. At this point all the injected fuel has completely burnt. Because of the low compression ratio, the major combustion time (about 80 degree of crank angle in Figure 7.9) is longer than that of a normal engine and the peak pressure is also lower. The temperature of burning gases reaches its maximum value around the upper dead centre. This is a result of the double action of the heat release and volume contraction. It decreases smoothly as volume increases afterwards. The average temperature of the three zones (this is a simple algebraic average) increases rapidly around upper dead centre and then stays almost constant. At the time that the exhaust port opens to the power chamber, the burnt gases still have a high value of energy with high pressure and temperature. Thus another assembly of rotors is proposed to be stacked on the same shaft as an expander to use this

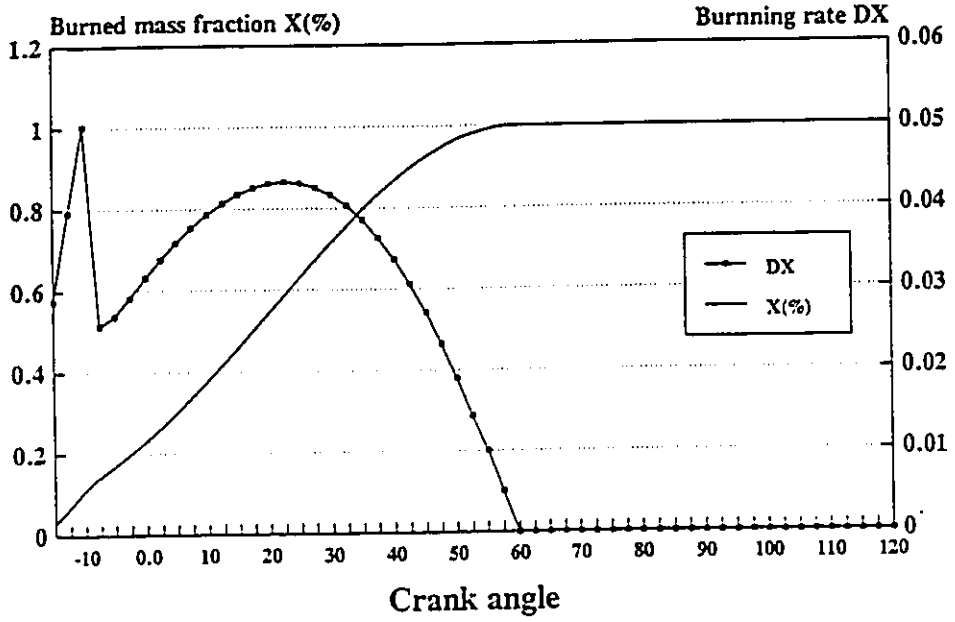

N=5000 rpm, Theta=-17.5

(a)

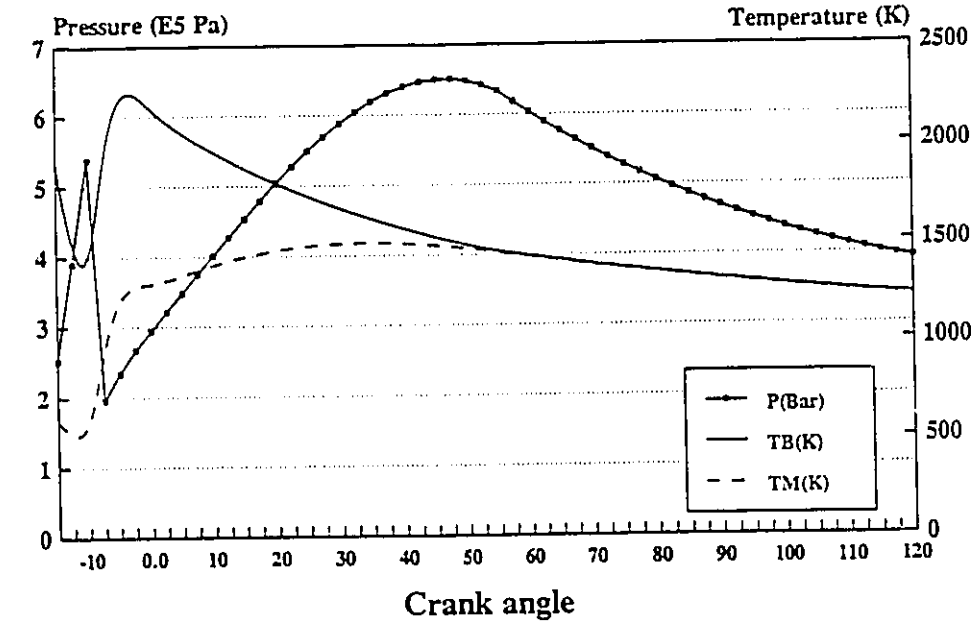

N=5000 rpm, Theta=-17.5

(b)

Figure 7.9 Calculated results of thermodynamic model

exhaust energy in order to obtain a higher efficiency and cleaner emission.

The engine's performance is largely dependent on the working conditions. Figure 7.10 shows the performance changes as the engine speed decreases from 5,000 rpm to 2,500 rpm. From the diagrams we can see that when the engine speed decreases, the combustion rate slows down so that the heat release rate becomes lower and the combustion period lasts longer (compare Figure 7.10 (a) and (c)). On the other hand, with lower speeds there will be a retardation of the pressure increase resulting from the lower heat release (because of less turbulence). More fuel will be injected to the chamber each cycle and hence both pressure and temperatures will increase with decreasing engine speed. It appears that the output torque will also increase (refer to Figure 7.12). This is a unique feature of the RVP rotary engine that regular engines do not have, which is a result of the unique semi-internal/external combustion system. An increased torque performance at decreased speeds gives a better driveability for such an engine in a vehicle.

Figure 7.11 shows the engine performance variations as the injection advance is decreased from -17.5 to -5.0 degree. At -5.0 degree advance both the heat release pulse and pressure pulse are shifted beyond the upper dead centre. Combustion then is largely weakened because of the expansion effect. The combustion rate is lower and the combustion period is longer than those with -17.5 degree advance. As a result the gases are not fully expanded and the pressure and temperature are much higher at exhaust time.

As a performance prediction of the engine, Figure 7.12 is plotted from the

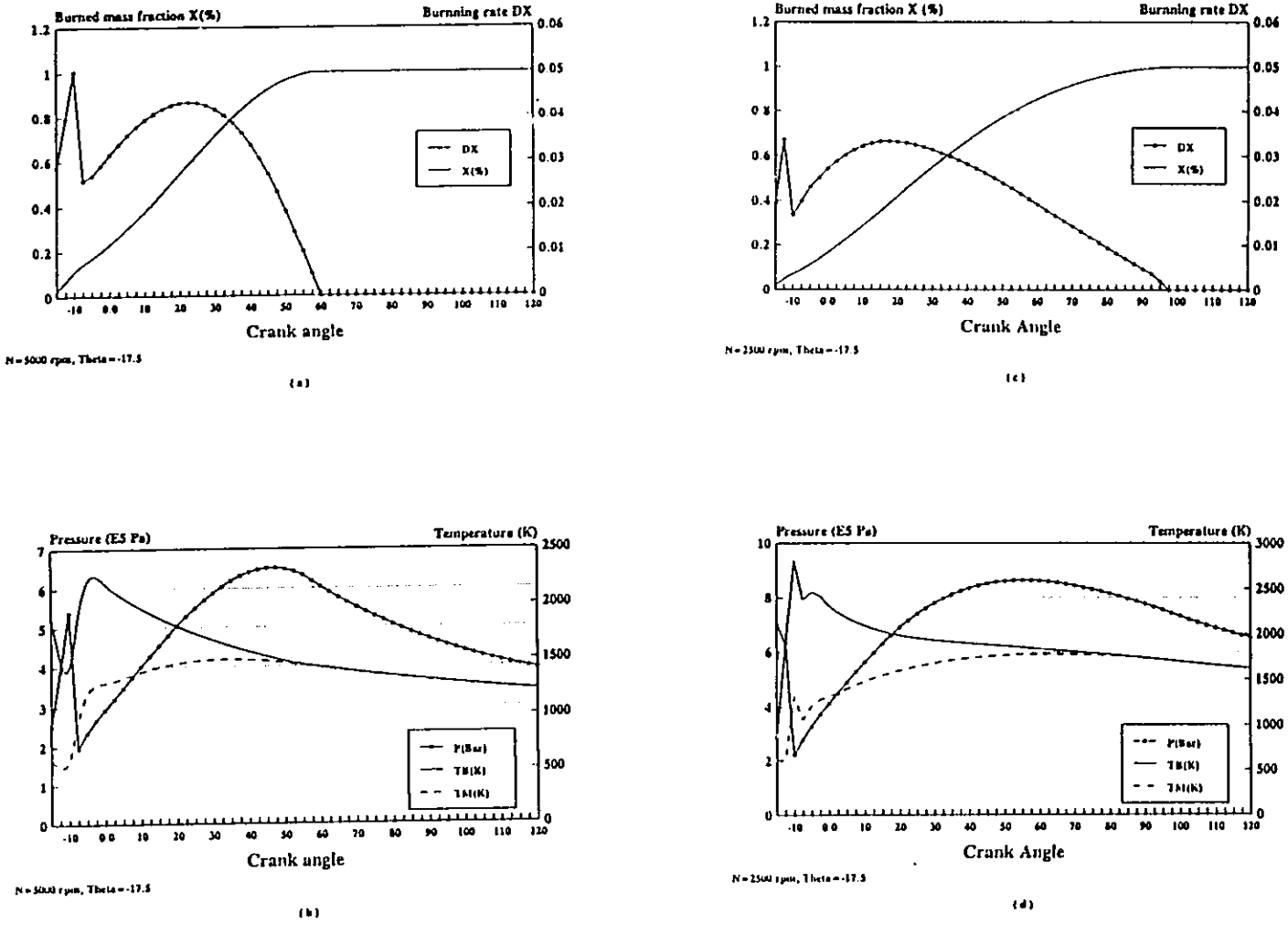

Figure 7.10 Performance Changes as the Engine Speed Changes

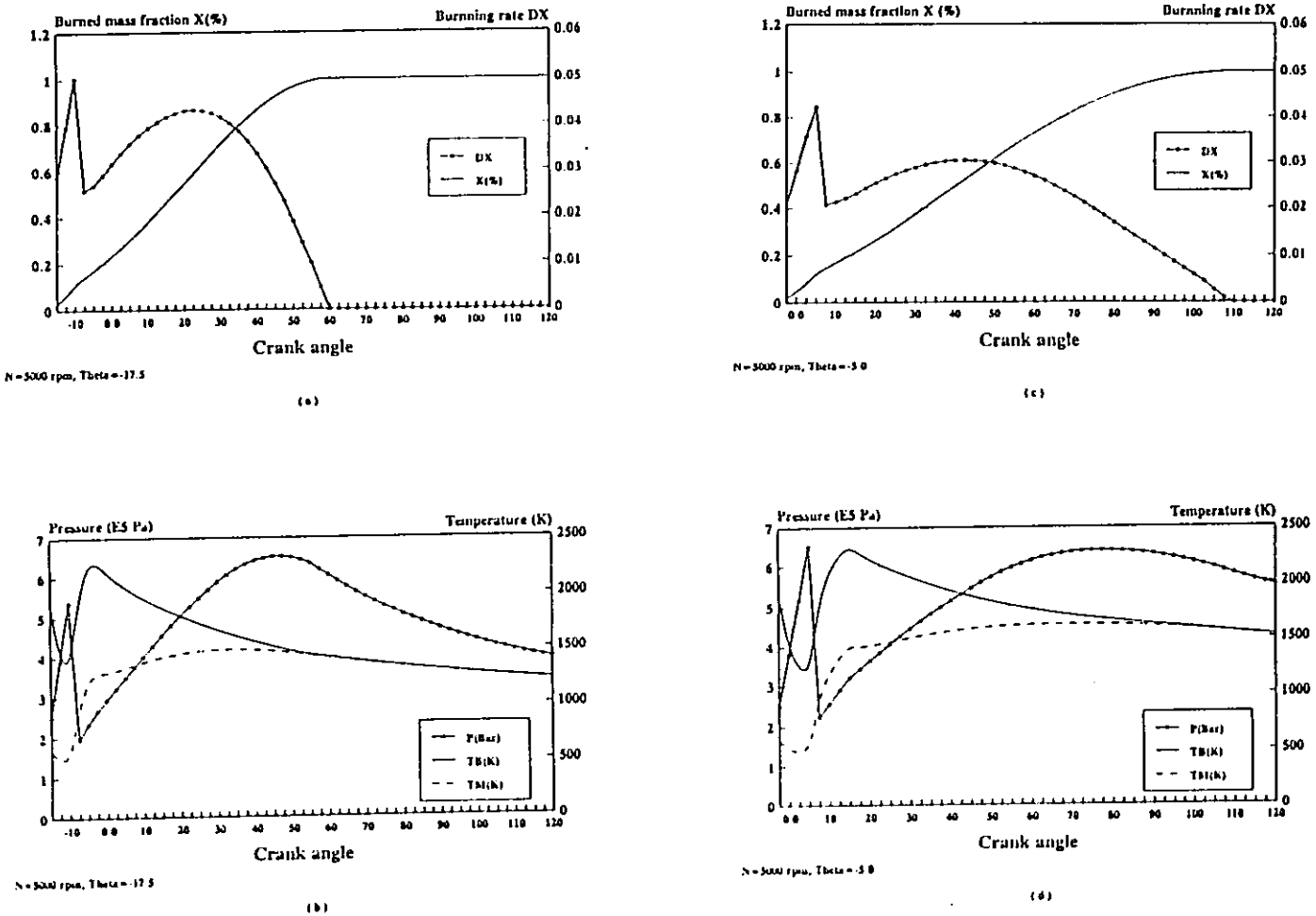

Figure 7.11 Engine Performance Varies as the Injection Advance Changes

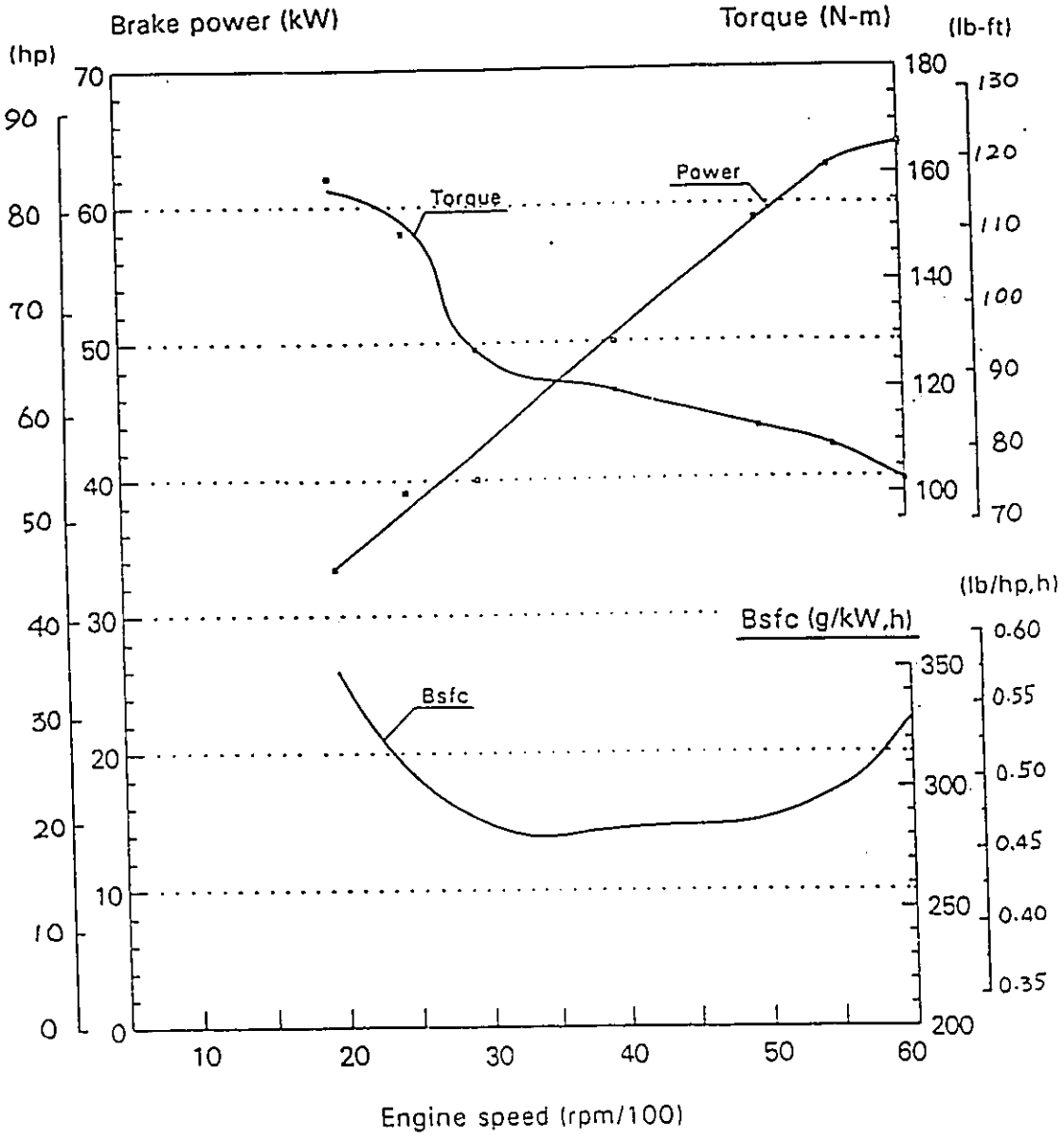

Theta = -17.5, P1 = 600 kPa, Fl = 2.0, Eta = 10%, Tw = 470 k
Mechanical efficiency set to be 0.8

Figure 7.12 Predicted performance of RVP engine at full load

calculated results of the theoretical model. It is the full load performance characteristics of the engine, which is done by setting the maximum fuel delivery rate or the maximum fuel/air ratio (equivalent ratio) at the pre-combustion chamber which corresponds to a wide-open throttle condition in a SI engine. From Figure 7.12 we can see that the RVP engine has a typical power-speed diagram which has linear increase vs speed, tending to be flatten at high speed. However, the torque curve is quite different from that of a typical SI engine without auxiliary adjustment devices. It was mentioned earlier in this section that the amount of injected fuel increases while speed decreases. This provides very good stability of the engine and driveability of the vehicle. The fuel consumption curve is fairly flat over a wide range of speed. Since engine torque is varied by varying the amount of fuel delivered to the pre-combustion chamber with the air flow essentially unchanged (a gas quality control mechanism), the engine is operated unthrotted. Thus, pumping work requirements are low, improving part-load mechanical efficiency relative to the SI engines. Therefore, there will be a better economic performance when the engine is partially loaded.

7.2.3 Engine parameter optimization through theoretical model analysis

In order to examine the effects of design and operating parameters on the engine's performance and consequently to optimize them, some of the critical parameters are varied and analyzed through the theoretical model. The results are shown in Figure 7.13 through Figure 7.16.

Figure 7.13 shows the effect of injection advance on engine power and efficiency at various speeds when the engine is fully loaded. The horizontal axis displays the advanced angle theta referenced to upper dead centre. The minus values mean that injection takes place after upper dead centre so that the advance is negative. Since the injected amount increases with increasing advance (because of the larger chamber at injection), the engine power increases at each speed. There is, however an optimum advance angle from the view point of fuel consumption rate (around 35^0 in the figure). Injection advance gives sufficient time for initial mixing and combustion before it is affected by expansion. As a result, the pressure peak will be closer to the upper dead

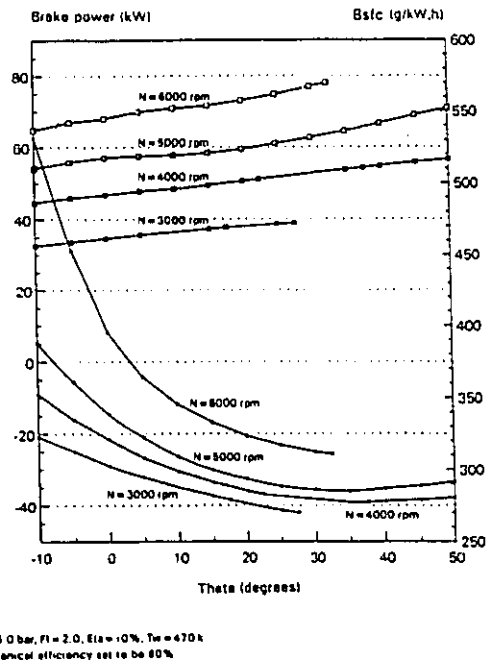

Figure 7.13 Performance vs injection advance

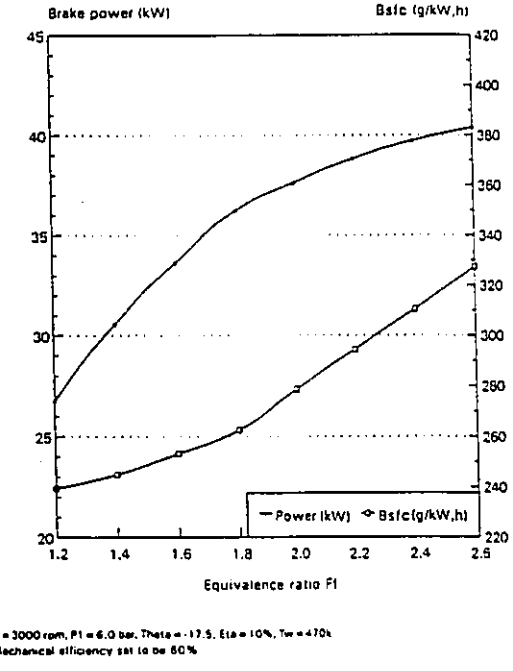

Figure 7.14 Performance vs equivalence ratio

centre and full expansion will be obtained. However, an advance that is longer than necessary will cause a larger power loss to overcome the pressure needed against compression.

Figure 7.14 shows the effects of equivalence ratio at pre-combustion chamber FI on engine performance. The amount of air entering the engine is essentially constant, the change in equivalence ratio which is defined as the ratio of the real fuel/air ratio to the stoichiometrical ratio indicating the amount of fuel injected to the power chamber per cycle. It is therefore a parameter measuring engine load condition at some speed. It is clear that as **FI** increases the engine output will increase. Meanwhile, the richer the mixture the worse the economy. When **FI** increases to some point (around 1.8 - 2.0 in the case of Figure 7.14) the combustion progress will be not as good as before. After that point the tangent of both the power and fuel consumption curves will change: power slow down and fuel consumption will increase. Obviously, this optimal point will change at different engine speeds.

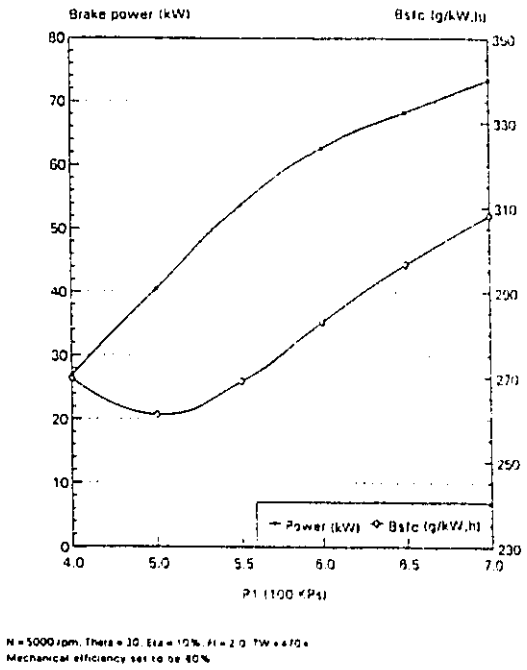

Figure 7.15 Performance vs injection pressure

There will be an equilibrium balance of both the mass and energy

inside the pre-combustion chamber at some engine working condition. This balance will determine the value of pressure achieved in the chamber. Figure 7.15 shows the effect of this pressure. Power will continuously increase as pressure increases because of the increase of the amount of energy delivered to the power chamber. For the fuel consumption rate, the effect of pressure is double sided. The higher pressure indicates more fuel charge thus a worse combustion environment. On the other hand, higher injection pressure could help to recover more kinetic energy through the thrust process. Therefore an optimal pressure exists in the view point of economy (about 500 - 550 kPa in the case of Figure 7.15).

The effect of temperature of the combustion chamber wall on the fuel consumption is not in doubt. The higher the temperature, the better the economy. Figure 7.16 shows that when wall temperature increases from 500 K to 1100 K the fuel consumption ratio will decrease about 20%. Ceramic materials could be used to work properly at that temperature level. One of the advantages of the RVP rotary engine working at high temperatures is that the stacked rotor set

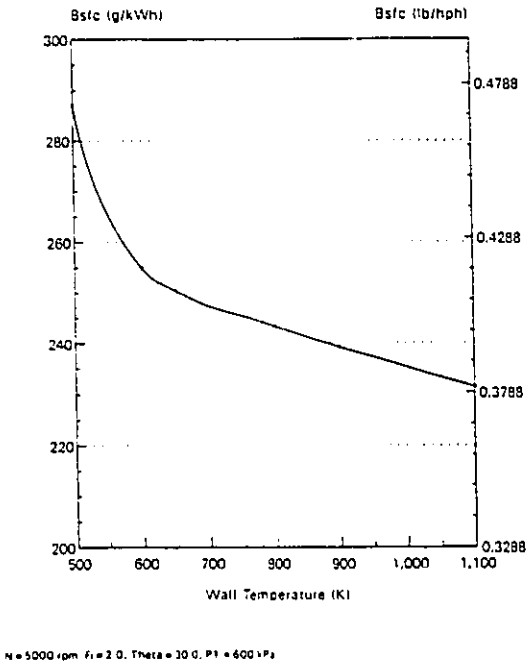

Figure 7.16 Fuel consumption rate vs wall temperature

will use the higher exhaust energy from the first stage because of less heat transfer losses.

The performance predicted theoretically in this section is then compared with that of some typical commercial engines for its evaluation.

7.3 Performance comparison with other commercial engines

Table 7.2 is generated to compare the predicted performance of the RVP rotary engine with those of other typical commercial engines. The comparison is based on the full load working conditions of the engines. The power/volume ratio is calculated by dividing the maximum power rated by the engine outline volume. From the table it would appear that the following is apparent:

i) The RVP rotary engine has the greatest power/volume ratio compared to other typical commercial engines. That means for same size engines, an RVP rotary engine could develop more power.

ii) The RVP rotary engine is in the same economy level as a gasoline engine which, in turn, is better than a Wankel rotary engine at full power. When it is partially loaded, because of its quality adjustment character instead of quantity adjustment, economy will be better than that of gasoline engines.

iii) Compared with diesel engines, the RVP rotary engine has a greater power density either with regard to volume or weight (its power/volume ratio is about 3 times

larger than that of diesels). The fuel consumption rate of the RVP engine is higher than that of diesel engines at normal working conditions. When ceramic material is employed for the rotors and pre-combustion chamber the economy will be even further improved (refer to 'Fuel Consumption Rate vs Wall Temperature').

iv) Only the Wankel rotary engine is comparable with the RVP rotary engine as far as the power density is concerned. However, the RVP rotary engine is much better than the Wankel engine both from the viewpoints of power and economy.

v) One of the unique features of the RVP engine that other commercial engines do not have is that the RVP rotary engine can run on many kinds of fuels including natural gas, propane and hydrogen. Thanks to the continuous pre-combustion system, the combustion of those alternative fuels can easily be accommodated.

TABLE 7.2

PERFORMANCE COMPARISON OF RVP ENGINE WITH OTHER TYPICAL COMMERCIAL ENGINES

	Power rating P, kW/(hp)	Peak torque T_b,Nm/(lb-ft)	Min bsfc at WOT g/kW,h/(lb/hp,h)	Displacement V_d, L/(in^3)	Power/Volume PVN, kPa/(psi)	Fuel Capability	Reference
RVP	64 / (86) @ 5,000 rpm	156 / (115) @2000 rpm	278 / (0.457) 231 / (0.38)*	0.83 / (50)	925 / (134)	Gasoline, Diesel, Natural Gas, Propane, Hydrogen	
WANKEL	61 / (82) @ 7,000 rpm	84 / (62) @6000 rpm	310 / (0.51)	0.59 / (36)	886 / (128)	Gasoline	NR 612 Norton Motors
GASOLINE	99 / (133) @ 3,500 rpm	NA	271 / (0.445)	4.7 / (287)	361 / (52)	Gasoline	Oldsmobile V8 General Motors
DIESEL	57 / (76) @ 2,500 rpm	250 / (184) @1250 rpm	234 / (0.385)	3.9 / (239)	350 / (50)	Diesel	4B3.9 Cummins Engine
TURBO DIESEL	86 / (116) @ 2,500 rpm	407 / (300) @1600 rpm	210 / (0.345)	3.9 / (239)	529 / (77)	Diesel	4BTA3.9 Cummins Engine

* This is under the condition that wall temperature reaches 1100 K when ceramic material is used

CHAPTER 8

SUMMARY AND FUTURE WORK

8.1 Summary of the work

Rotary machines with their features of high speed capacity, high mechanical efficiency, simple structure and smooth performance have a great potential to replace the reciprocating machines. While the constant speed rotary electric motor superseded the reciprocating motor long long time ago, the reciprocating engine still dominates internal combustion engines. The Wankel rotary engine is the only successful rotary engine in the market so far. However, with its weakness of low thermal efficiency and high exhaust emission rate it is not the best machine to demonstrate the great features of the rotary engine.

The RVP rotary machine developed in this work is a unique rotary machine. It is a simple rotation machine with an internal parallel axis arrangement. In developing this unique rotary machine, following fundamental research has been performed:

1) A curve fitting method has been created in order to generate the curve to have the inner rotor mesh with the outer rotor all around 360^0 degree range. While these two rotors rotate in the same direction around their own stationary centres of gravity the chambers defined by the arms of the inner rotor and lobes of the outer rotor contract on

one side and expand on the other. Therefore, energy conversion either from fluid/chemical energy to mechanical energy or from mechanical/electrical energy to fluid energy may occur.

2) A physical model of the RVP rotary machine has been built to verify the principles. It runs as an air motor. Compressed air thrusts through the inlet port to the expansion chamber and drives the rotors. Pressure energy of the air is converted to mechanical energy by both thrusting and expansion. The successful operation of the model demonstrated the success of the mechanism of the rotary machine. CAD/CAM techniques were intensively employed during the process of design and manufacture of the model which in turn will be useful for the manufacture of the practical work of the RVP rotary machine.

3) A hydraulic pump has been built and tested. Operated in the opposite way of the air motor, the pump sucks the fluid into its expansion chambers and compresses it out from contraction chambers. Mechanical energy has been consumed to obtain fluid pressure energy. The prototype pump performed excellently. Compared with other commercial rotary pumps such as internal/external gear pumps and vane pumps, the RVP pump has much bigger capacity per unit bulk volume and greater suction lift ability without cavitation. It is a unique hydraulic pump.

4) A series of engineering design and theoretical investigations of a unique rotary engine have been conducted. By substituting the compressed air supply of the air motor with a pre-combustion chamber external to the rotary machine, a unique rotary

engine has been designed. The following features demonstrate its uniqueness:

a) It has a pure rotational mechanical structure. Two rotors rotate around their own stationary centres of gravity to form contraction and expansion chambers.

b) It has an semi-external/internal combustion system. Burning gases that burnt externally in the pre-combustion chamber thrust into the power chamber to perform a typical Otto internal combustion processes. It combines features of both an internal combustion engine and an external combustion engine - combining the benefits accruing from both.

c) It has a multi fuel ability. Because of the external combustion feature, any liquid or gas fuel can be easily adapted to the engine. Furthermore by sealing a proper medium inside the engine and substituting the pre-combustion chamber with a heat exchanger, solar energy may be used for the engine.

5) Intensive theoretical research has been performed for the RVP rotary engine in order to predicted the performance and optimize the parameters of the design before a hardware prototype engine can be manufactured. The three zone combustion model created based on the complex combustion phenomena makes further theoretical research feasible. Because of the unique combustion system, both the flow simulation and thermodynamic model developed in this work are unique. It is an advance of the current state of the art in the field of internal combustion engine in the sense that a combination of the internal and external combustion system is investigated.

Comparing the performances of some typical internal combustion engines with

those of predicted RVP rotary engine it is evident that the RVP rotary engine has the greatest power/volume ratio with the same economic level. Considering its fuel flexible feature and smooth operation, the RVP rotary engine may have greater market potential.

8.2 Recommendation for future work

Fundamental research on the RVP rotary machine has been completed in this work. The principles has been verified by the physical model, the RVP hydraulic pump has been built and tested and the RVP rotary engine has been developed to the stage that an initial prototype is ready to be built.

However, as far as the engine is concerned it is far away from the development stage. Such a huge project to develop a unique engine for the market requires a large capital and labour investment. In this work, the problems such as cooling, sealing and lubrication have been left to concentrate on more fundamental problems. As soon as the initial prototype engine has been built and tested, information about thermal load distributions, leakage and friction can be obtained. With this information, modifications could be made to the engine and a more practical prototype could be redesigned and manufactured.

At the same time, as the engine is improved step by step, the theoretical model could be improved through the verification of the results of the test. The engine in turn, can be improved much faster in the light of model analysis.

REFERENCES

Adam, A. "Syvaro's SP-440 Air Cooled Rotary - Trochoidal Engine", SAE Paper 800974, 1980

Annand, J.D. "Heat Transfer in the Cylinders of Reciprocating Internal Combustion Engines",Proc. Inst. Mech. Eng., Vol. 177, No. 36, 1963

Austen, A.E.W. and Lyn, W.-T. "Relation Between Fuel Injection and Heat Release in a Direct-Injection Engine and the Nature of the Combustion Precess", Proc. Instn. Mech. Engrs (A.D.) (1960/65)

Bantiggelen, A. and Deckers, J. Sixth Symposium (international) on Combustion, Reinhold New York, 1957 PP 61

Bartok, W. and Sarofim, A.F. Fossil Fuel Combustion, a Source Book, John Wiley & Sons, Inc, 1991

Bedard, P. "Speeding Beauties", Car and Driver, February, 1992, PP 34-41

Blizard, N.C. and Keck, J.C. "Experimental and Theoretical Investigation of Turbulent Burning Modelling for Internal Combustion Engines", SAE Paper 740191, 1974

Blumberg, P. and Kummer, J.T. "Prediction of NO Formation in Spark-Ignited Engines -- An Analysis of Methods of Control", Combustion Sci. and Tech., 1971, Vol.4 PP 73-95

Blumverg, P.N., Lavoie, G.A. and Tabaczynski, R.J. "Phenomenological Models For Reciprocating Internal Combustion Engines", Prog. Energy Combust Sci. 1979, Vol. 5, PP 123-167

Borman, G. and Nishiwaki, K. "Internal Combustion Engine Heat Transfer", Prog. Energy and Combust. Sci. 1987, Vol. 13, PP 1-46

Bracco, F.V. and Sirgnano, W.A. "Theoretical Analysis of Wankel Engine Combustion", Combustion Science and Technology, Vol.7, 1973, PP 109-123

Chouinard, E., Hamady, F. and Schoci, H. "Airflow Visualization and LDV

Measurements in a Motored Rotary Engine Assembly. Part 2. LDV Measurements", SAE Paper 900031, 1990

Chan, R. Computational Fluid Mechanics and Heat Transfer, Lecture notes, in McMaster University, 1992

Earl L.Jr, Turbomachinary, Basic theory and Applications, John Wiley & Sons. INC, 1981

Craig, E.J., Umstatter, L.H. and Lee, Y.D. "Visualization of Flows in a Motored Rotary Combustion Engine Using Holographic Interferometry", NASA Tech. Memo 88804 PP 16

Damkohler, G. "The Effect of Turbulence on the Flame Velocity in Gas Mixture", NACA TM 1112, 1940

Danieli, G.A., Keck, J.C. and Heywood, J.B. "Experimental and Theoretical Analysis of Wankel Engine Performance", SAE Paper 780416

Danieli, G.A., Ferguson, C.R.R., Heywood, J.B. and Keck, J.C. "Predicting the Emissions and Performance Characteristics of a Wankel Engine", SAE Paper 740186, 1974

Danieli, G.A. "A Performance Model of a Wankel Engine, Including the Effects of Burning Rates, Heat Transfer, Leakage and Quenching Compared With Measured Pressure Time Histories" Ph.D thesis in MIT, 1976

Dent, J.C. and Salama, N.S. "The Measurement of the Turbulence Characteristics in an Internal Combustion Engine Cylinder", SAE Paper 750886, 1975

Dimpefled, P. and Humke, A. "Heat Release Characteristics of Stratified-Charge Rotary Engines", SAE Paper 870443, 1987

Dow Chemical Co. "JANAF Thermochemical Tables", distributed by Clean house

Eichelberg, G. "Some New Investigations on Old Combustion Engine Problems", Engineering (1939)

Ganic, E.N. and Hicks, T.G. The McGraw-Hill Handbook of Essential Engineering Information and Data, McGraw-Hill, Inc., 1991

Garside, D.W. "Development of the Norton Rotary Motorcycle Engine", SAE Paper 821068, 1982

Gatowski, J.A., Balles, E.N., Chun, K.M., Nelson, F.E., Ekchian, J.A. and Heywood, J.B. "Heat Release Analysis of Engine Pressure Data", SAE Paper 841359, 1984

Grasso, F., Wey, M.-J., Bracco, F.V. and Abuaham, J. "Three-Dimensional Computations of Flows in a Stratified-Charge Rotary Engine", SAE Paper 870409, 1987

Groff, E.G. "An Experimental Evaluation of an Entrainment Flame-Propagation Model", Combustion and Flame 67, 1987, PP 153-162

Gudzenko, L.I. etc. "Rotary - Piston Laser Engine", Journal of Soviet Laser Research, V3 n3 July - September, 1965

Heywood, J.B. Internal Combustion Engine Fundamentals, McGraw-Hill, Inc, 1988

Heywood, J.B., Higgins, J.M. Watts, R.A. and Tabaczynski, R.J. "Development and Use of a Cycle Simulation to Predict SI Engine Efficiency and NOx Emissions", SAE Paper 790291, 1979

Hires, S.D., Tabaczynski, R.J. and Novak, J.M. "The Prediction of Ignition and Combustion Internals for a Homogeneous Charge, Spark Ignition Engine", SAE Paper 780232, 1978

Hires, S.D., Ekchian, A., Heywood, J.B., Tabaczynski, R.J., Wall, J.C. "Performance and NOx Emissions Modelling of a Jet Ignition Prechamber Stratified Charge Engine", SAE Paper 760161, 1976

Iinuma, K. "Recent Advances in Spark-ignition Engine Combustion Research", JSME International Journal, Vol.30, No.262, 1987

Jones, C., Mack, J.R. and Griffith, M.J. "Advanced Rotary Engine Developments for Naval Applications", SAE Paper 851243, 1985

Lachapelle, M. "Mazda Readies Hydrogen Car for Street", The Toronto Star, August 8, 1992

Mount, R.E. and Bartel, J. "Advanced Liquid Cooled, Turbocharged and Intercooled Stratified charge Rotary Engine for Aircraft", SAE Paper 871093, 1987

Lakshminarayanan, P.A., Nagpurkar, U.P. and Chandorker, S.B. "A Heat Release Model for Divided Chamber Diesel Engines", SAE Paper 860084, 1986

Lancaster, D.R. "Effects of Engine Variable on Turbulence in a Spark-Ignition Engine", SAE Paper 760159, 1976

Lavoie, G.A., Heywood, J.B. and Keck, J.C. "Experimental and Theoretical Study of Nitric Oxide Formation in Internal Combustion Engine", Combustion Sci. and Tech. 1970, Vol. 1, PP 313-326

Lucas, G.G. and James, E.H., "A Computer Simulation of a Spark Ignition Engine", SAE Paper 730053, 1973

Martin, N.K. and Heywood, J.B. "Approximate Relationship for the Thermodynamic Properties of Hydrocarbon-Air Combustion Products", Combustion Science and Technology Vol. 15, 1977, PP 1-10

MeCuiston, F.D., Lavoie, G.A. and Kauffman, C.W. "Validation of a Turbulent Flame Propagation Model for a Spark Ignition Engine", SAE Paper 770045, 1977

Miller, G.H., Uyehara, O.A. and Myers, P.S. "Practical Application of Engine Flame Temperature Measurements", SAE Trans. 62,514, 1954

Nishida, K., Hiroyasu, H., Matsuoka, j.T. and Yamauchi, H. "Characterization of Combustion Processes in the Prechamber and Main Chamber of an Indirect Injection Diesel Engine by High-Speed Photography", SAE Paper 861181, 1986

Norbye, J.P. The Wankel Engine, design development applications, Kingprint Ltd. Printed in Great Britiain

Nusselt, W. "Der Wämeübergang in der Verbrennungs-kraftmaschine", V.D.I. - Forschungsheft, 264 (1923)

Patankar, S.V. Numerical Heat Transfer and Fluid Flow, Hemisphere publishing Corporation 1989

Peng, L.X., Round, G.F. and Valavaara, V.K "A Unique Rotary Machine", Proceeding of The First Rotating Machinery Conference and Exposition, November, 1993, PP 387 - 391

Pinchon, Ph., Guillot, B. "Thermodynamic and Flow Analysis of an Indirect Injection

diesel Combustion Chamber by Modelling", SAE Paper 851686, 1985

Qing Hua, Fundamental of Fluid Mechanics, Mechanical Industry Publishing House, 1983

Rao, K.S., Ganesan, V., Gopalakrishnan, K.V. and Hurthy, B.S. "Modelling of Combustion Process in a Spark Ignited Hydrogen Engine", Int. J. Hydrogen Energy, Vol. 8, No.11/12, 1983, PP 931-933

Rask, R.B. "Laser Doppler Anemometer Measurements in a Internal Combustion Engine", SAE Paper 790094, 1979

Roberts, J.A., Norman, T.J., Ekchian, J.A. and Heywood, J.B. "Computer Models for Evaluating Premixed and Disc Wankel Engine Performance", SAE Paper 860613, 1986

Round, G.F. and Garg, V.K. Applications of Fluid Dynamics, Edward Arnold Ltd, 1986

Samaga, B.S. and Murthy, B.S. "On the Problem of Predicting Burning Rates in a SparkIgnition Engine", SAE Paper 750688, 1975

Shchelkin, K.I. "On Combustion in a Turbulent Flow", NACA TM 1110, 1943

Shih, T.I.-P., Yany, S.L. and Schock, H.J. "A Two-Dimensional Numerical Study of the Flow Inside the Combustion Chamber of a Motored Rotary Engine", SAE Paper 860615, 1986

Sirgnano, W.A. "One-Dimensional Analysis of Combustion in a Spark Ignition Engine", Combustion Science and Technology, Vol. 7, 1973, PP 99-108

Steinthorsson, E., Shih, T.I.-P. Schock, H.J. and Stegiman, J. "Calculations of the Unsteady, Three-Dimensional Flows Field Inside a Motored Wankel Engine", SAE Paper 880625, 1988

Streeter, V. L. and Wylie, E.B. Fluid Mechanics, McGraw-Hill Ryerson, 1981

Tabaczynski, R.J., Trinker, F.H. and Shannon, B.A.S. "Further Refinement and Validation of a Turbulence Flame Propagation Model for Spark-Ignition Engines", Combustion and Flame Vol. 39, 1980, PP 111-121

Tabaczynski, R.J. and Ferguson, C.R. "A Turbulence Entrainment Model for Spark-Ignition Engine Combustion", SAE Paper 770647, 1977

Tashima, S., Taqdokoro, T., etc. "Development of Sequential Twin Turbo System for Rotary Engine", SAE Paper 910624, 1991

Wankel, F. Rotary Piston Machines, London Iliffe Books Ltd, 1963, English edition, 1965

Yamamoto, K. Rotary Engine, Sankaido Co. Ltd. 5-5-18, Hongo, Bunkyo-ku, Tokyo, Japan, 1981

Taylor, C.F. and Taylor, E.S. The Internal Combustion Engine, Scranton Pa. International Textbook Co. 1966

Tennekes, H. and Lumley, J.L. A First Course in Turbulence, the M.I.T. Press, Cambridge, Mass, 1972

Wark, J.K. Thermodynamics Fifth edition, McGraw-Hill, Inc. 1988

Woschni, G. "Beitrag zum Problem des Wämeüber-ganges im Verbrennungsmotor", MTZ 26 (1965)

Zellat, M., Rolland, Th. and Poplow, F. "Three Dimensional Modelling of Combustion and Soot Formation in a Indirect Injection Diesel Engine", SAE Paper 900254, 1990

Zimmerman, D.R. "Laser Anemometer Measurements of the Air Motion in the Prechamber of an Automotive Diesel Engine", SAE Paper 830452, 1983

APPENDIX A

OPENING AREA OF THE PASSAGE BETWEEN TWO CHAMBERS A(T)

Assume included angles for the openings of the housing and the rotor are θ_1 and θ_2 respectively. When the rotor sweeps along the opening on the housing, the 'common' area shared by these two openings is the area of the flow, which may be calculated as:

$$A(\alpha) = \begin{cases} \dfrac{A_0}{\theta_1} * \alpha & 0 \le \alpha < \theta_1 \\ A_0 & \theta_1 \le \alpha \le \theta_2 \\ \dfrac{\theta_1+\theta_2}{\theta_1} A_0 - \dfrac{A_0}{\theta_1} * \alpha & \alpha > \theta_2 \end{cases}$$

where A_0 is the opening area of the housing, and $\theta_1 \le \theta_2$

As far as time is concerned, when the rotational speed is N we have

$$\Delta t_1 = \frac{\theta_1}{2\pi N/60} = \frac{30\theta_1}{\pi N}, \qquad \Delta t_2 = 30\frac{\theta_2}{\pi N}, \qquad \alpha = \frac{\pi N}{30} * t$$

therefore:

$$A'(t) = \begin{cases} \dfrac{2\pi NA_0}{60\theta_1} * t & 0 \le t < \Delta t_1 \\ A_0 & \Delta t_1 \le t \le \Delta t_2 \\ \dfrac{\theta_1+\theta_2}{\theta_1} * A_0 - \dfrac{2\pi NA_0}{60\theta_1} * t & t > \Delta t_2 \end{cases}$$

If the opening area of the prechamber is A_p we have (refer to figure A-2)

$$A(t) = \min (A'(t), A_p)$$

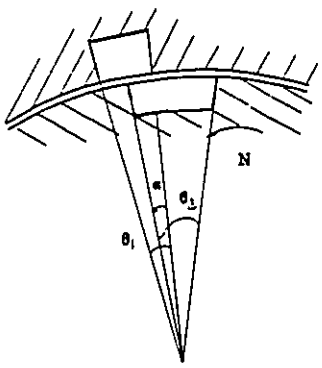

Figure A-1 Relative Position of the Openings

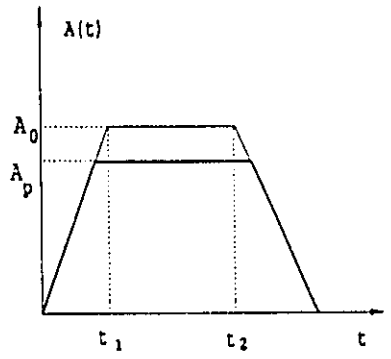

Figure A-2 Area Pattern vs Time

APPENDIX B

ELLIPTICAL COORDINATE TRANSFORMATIONS

Setting

$$X = c*\cosh\xi*\cos\eta \qquad (B-1)$$

$$Y = c*\sinh\xi*\sin\eta$$

with

$$c^2 = a^2 - b^2$$

we have elliptical coordinates (ξ, η).

If η is eliminated from equation (B - 4), we have

$$\frac{X^2}{c^2\cosh^2\xi} + \frac{Y^2}{c^2\sinh^2\xi} = 1$$

so that any $\xi = \xi_i$ corresponds to an ellipse, with semimajor axis **c cosh** ξ_i and semiminor axis **c sinh** ξ_i. If ξ is eliminated from the equation, it results in:

$$\frac{X^2}{c^2\cos^2\eta} - \frac{Y^2}{c^2\sin^2\eta} = 0$$

so that any $\eta = \eta_i$ correspond to hyperbolas.

The curves ξ = constant and η = constant are therefore confocal ellipses and hyperbolas as shown in figure B-1.

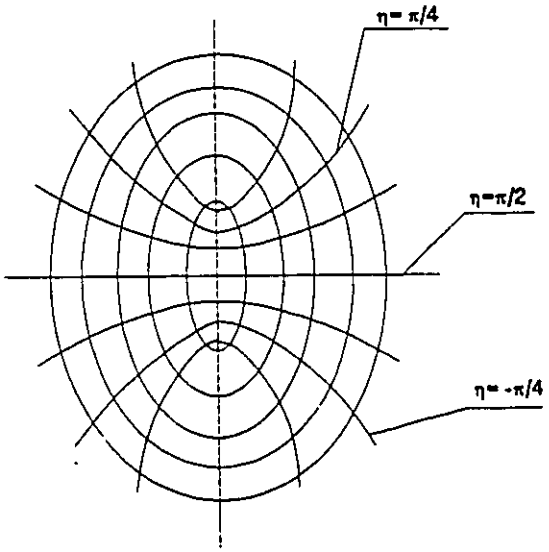

Figure B-1 Elliptical Coordinate

APPENDIX C

BOUNDARY COORDINATE OF THE FLOWING DOMAIN

The purpose of this calculation is to find the point (x_1,y_1) and (x_2,y_2) at which the flow for the power chamber starts and ends respectively - that is, the boundary coordinate η_0 and η_e of the flowing domain. In Figure C-1a the data are recorded from the particular design. For the ellipse in Figure C-1b

$$\frac{X^2}{0.0131^2} + \frac{Y^2}{0.0106^2} = 1 \qquad (C-1)$$

The equation of tangent line for that ellipse is

$$Y_1 = kX_1 \pm \sqrt{a^2k^2+b^2} = tg128^0 X_1 \pm \sqrt{0.0131^2 tg^2 128^0 + 0.0106^2} \qquad (C-2)$$

$$= -1.2799X_1 + 0.01984$$

Combining (C-1) and (C-2) we can solve for point (X_1,Y_1)

$$X_1 = 0.011073 \qquad Y_1 = 0.00566$$

Through point (X_1,Y_1), there is a hyperbolas:

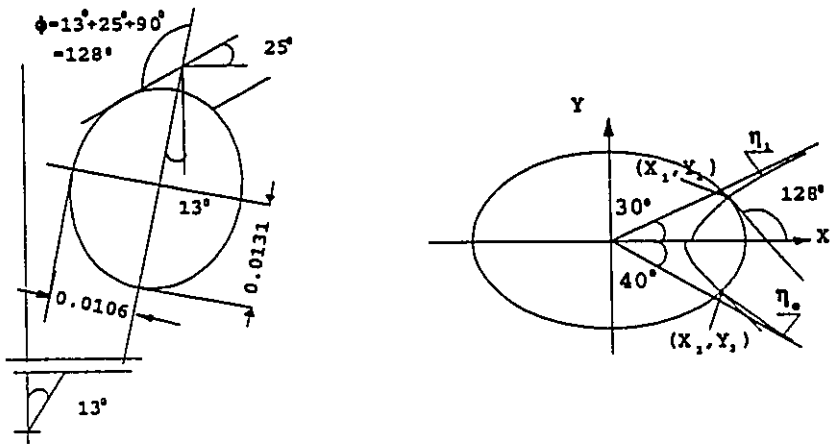

Figure C-1 Boundary Coordinate Calculation

$$\frac{X_1^2}{C^2\cos^2\eta_1} - \frac{Y_1^2}{C^2\sin^2\eta_1} = 1 \qquad (C-3)$$

Thus

$$\sin^2\eta_1 * 0.011073^2 - \cos^2\eta_1 * 0.00566^2 = 0.0077^2\cos^2\eta_1\sin^2\eta_1$$

Solving the equation for η_1 we have

$$\eta_1 = 32.3^0$$

For convenience, $\eta_0=30^0$ was used in the calculations.

The straight line parallel to that expressed in equation (C-2) can be defined as

$$Y_2 = KX_2+C_2 = -1.2799X_2+C_2 \qquad (C-4)$$

The distance between these two lines is 0.008 m for the particular design:

$$0.008 = \frac{|C_2-0.01984|}{\sqrt{1.2799^2+1^2}}$$

Therefor C_2 and then equation (C-4) and be solved as

$$Y_2 = -1.2799X_2+0.00685 \qquad (C-5)$$

Solving equations (C-1) and (C-5) simultaneously for point (X_2, Y_2) we have

$$X_2 = 0.0104, \qquad Y_2 = -0.00645$$

Using the same techniques as for η_1 we can solve for the end coordinate in η direction

$$\eta_e = 37.445^0$$

For convenience, $\eta_e = 40^0$ was used in the calculations.

APPENDIX D

CALCULATED RESULTS OF MASS FLOW

TIME (ms)	P2 (KPa)	MS (mg)	DM (mg)	V2 (m/s)	AREA (mm^2)
0.01	150.33	70.08	0.048	388.17	22.87
0.02	151.31	70.41	0.103	388.17	49.01
0.03	152.96	70.96	0.157	388.17	75.15
0.04	155.28	71.73	0.213	388.17	101.29
0.05	158.29	72.72	0.268	388.17	127.43
0.06	162.00	73.93	0.324	388.17	153.57
0.07	166.43	75.37	0.381	388.17	179.71
0.08	171.61	77.03	0.438	388.17	205.85
0.09	177.55	78.93	0.496	388.17	231.99
0.10	184.30	81.06	0.555	388.17	258.13
0.11	191.89	83.43	0.615	388.17	284.27
0.12	200.35	86.04	0.675	388.17	310.41
0.13	209.72	88.90	0.737	388.17	336.55
0.14	220.04	92.00	0.800	388.17	362.69
0.15	231.37	95.36	0.864	388.17	388.83
0.16	243.74	98.98	0.928	388.17	414.97
0.17	257.22	102.86	0.995	388.17	441.11
0.18	271.85	107.00	1.062	388.17	467.25
0.19	287.69	111.42	1.130	388.17	493.39
0.20	304.80	116.12	1.200	388.17	519.53
0.21	323.25	121.09	1.271	372.18	545.67
0.22	343.45	126.45	1.388	368.34	571.81
0.23	364.95	132.06	1.398	349.40	581.00
0.24	386.56	137.60	1.376	330.07	581.00
0.25	408.09	143.03	1.346	310.42	581.00
0.26	429.37	148.31	1.306	290.48	581.00
0.27	450.20	153.42	1.257	270.24	581.00
0.28	470.40	158.31	1.199	249.74	581.00
0.29	489.79	162.94	1.132	228.99	581.00
0.30	508.16	167.28	1.056	208.00	581.00
0.31	525.32	171.30	0.972	186.80	581.00
0.32	549.08	174.95	0.879	165.40	581.00
0.33	565.29	178.22	0.779	133.82	581.00
0.34	577.76	181.07	0.672	119.10	581.00
0.35	585.35	183.48	0.559	88.24	581.00
0.36	590.95	185.42	0.441	58.28	581.00
0.37	596.44	186.89	0.270	36.23	581.00
0.38	599.75	187.85	0.095	14.12	581.00

APPENDIX E

CALCULATED RESULTS OF VELOCITY PROFILE

The calculated results of the velocity profile (in m/s) along the wall of combustion chamber are shown as following. The calculation is based on the speed of N=5000 rpm. Therefore the interval crank angle in degree is 30*TIME (ms). X is in the tangential direction and Y in normal direction of the chamber.

Time = 0.04 ms

X\Y	0	2	4	6	8	10
30	0.00	349.76	349.76	349.76	349.76	349.76
40	0.00	353.36	353.53	353.58	353.63	353.67
50	0.00	351.81	352.52	352.91	353.26	353.55
60	0.00	343.74	345.74	347.11	348.39	349.49
70	0.00	323.68	327.73	330.85	333.80	336.41
80	0.00	295.67	301.82	306.91	311.83	316.28
90	0.00	269.52	276.82	283.26	289.66	295.60
100	0.00	242.71	249.94	256.67	263.55	270.13
110	0.00	200.50	206.59	212.52	218.71	224.82
120	0.00	138.68	142.79	146.94	151.32	155.75
130	0.00	75.38	77.43	79.52	81.75	84.02
140	0.00	32.17	32.92	33.69	34.50	35.32
150	0.00	11.43	11.66	11.90	12.15	12.40
160	0.00	3.19	3.26	3.32	3.39	3.46
170	0.00	0.62	0.64	0.65	0.66	0.68
180	0.00	0.10	0.10	0.10	0.10	0.11
190	0.00	0.01	0.01	0.01	0.01	0.01

Time = 0.08 ms

X\Y	0	2	4	6	8	10
30	0.00	349.76	349.76	349.76	349.76	349.76
40	0.00	359.65	359.77	359.78	359.79	359.80

50	0.00	362.09	362.42	362.46	362.49	362.52
60	0.00	357.57	358.25	358.33	358.40	358.47
70	0.00	347.17	348.33	348.50	348.66	348.80
80	0.00	334.89	336.72	337.05	337.34	337.59
90	0.00	327.17	329.88	330.53	331.10	331.54
100	0.00	325.62	329.52	330.79	331.91	332.76
110	0.00	325.83	331.32	333.59	335.61	337.18
120	0.00	322.48	329.84	333.45	336.73	339.32
130	0.00	313.46	322.71	327.83	332.57	336.38
140	0.00	300.20	311.03	317.62	323.83	328.91
150	0.00	285.58	297.48	305.32	312.88	319.17
160	0.00	272.05	284.53	293.38	302.11	309.51
170	0.00	261.78	274.41	284.04	293.74	302.17
180	0.00	255.45	267.86	278.01	288.48	297.84
190	0.00	249.59	261.42	271.80	282.75	292.88
200	0.00	236.57	247.41	257.56	268.51	279.03
210	0.00	207.37	216.44	225.42	235.29	245.14
220	0.00	156.51	162.76	169.20	176.37	183.78
230	0.00	94.30	97.41	100.67	104.29	108.11
240	0.00	42.40	43.43	44.50	45.66	46.88
250	0.00	14.80	15.06	15.32	15.59	15.86
260	0.00	3.79	3.84	3.90	3.95	4.01
270	0.00	0.68	0.69	0.70	0.70	0.71
280	0.00	0.07	0.07	0.07	0.08	0.08
290	0.00	0.01	0.01	0.01	0.01	0.01

Time = 0.12 ms

X\Y	0	2	4	6	8	10
30	0.00	349.76	349.76	349.76	349.76	349.76
40	0.00	362.44	362.55	362.55	362.56	362.56
50	0.00	368.51	368.82	368.83	368.85	368.87
60	0.00	368.20	368.80	368.84	368.88	368.91
70	0.00	362.81	363.81	363.88	363.94	364.01
80	0.00	355.83	357.33	357.44	357.55	357.66
90	0.00	351.42	353.52	353.70	353.86	354.01
100	0.00	350.44	353.23	353.49	353.73	353.94
110	0.00	351.12	354.73	355.11	355.46	355.76
120	0.00	351.38	355.93	356.48	356.98	357.40
130	0.00	349.26	354.91	355.71	356.42	356.97
140	0.00	343.20	350.19	351.33	352.31	353.06
150	0.00	332.63	341.28	342.90	344.28	345.28
160	0.00	318.96	329.64	331.95	333.88	335.24
170	0.00	307.24	320.19	323.40	326.10	327.95
180	0.00	301.94	317.05	321.39	325.05	327.55
190	0.00	300.40	317.40	323.01	327.82	331.13
200	0.00	297.45	315.96	322.97	329.10	333.38
210	0.00	290.58	310.08	318.47	326.02	331.39

220	0.00	280.29	300.09	309.75	318.70	325.24
230	0.00	269.02	288.37	299.08	309.32	317.06
240	0.00	258.77	277.08	288.54	299.90	308.83
250	0.00	249.69	266.46	278.28	290.44	300.47
260	0.00	241.16	255.94	267.54	279.91	290.69
270	0.00	233.22	245.66	256.33	268.10	278.91
280	0.00	223.21	233.24	242.48	252.88	262.92
290	0.00	204.01	211.83	219.40	227.98	236.56
300	0.00	169.08	174.81	180.54	186.97	193.56
310	0.00	120.51	124.19	127.94	132.07	136.35
320	0.00	70.80	72.74	74.73	76.87	79.09
330	0.00	34.57	35.41	36.26	37.16	38.08
340	0.00	13.91	14.22	14.54	14.86	15.19
350	0.00	4.38	4.47	4.57	4.67	4.77

Time = 0.16 ms

X\Y	0	2	4	6	8	10
30	0.00	349.76	349.76	349.76	349.76	349.76
40	0.00	364.09	364.20	364.20	364.20	364.21
50	0.00	372.64	372.94	372.95	372.96	372.97
60	0.00	375.74	376.32	376.34	376.37	376.39
70	0.00	374.49	375.42	375.47	375.51	375.56
80	0.00	371.73	373.12	373.19	373.27	373.34
90	0.00	370.91	372.81	372.93	373.04	373.14
100	0.00	372.83	375.32	375.48	375.64	375.78
110	0.00	376.27	379.41	379.63	379.84	380.03
120	0.00	379.71	383.58	383.87	384.13	384.37
130	0.00	381.47	386.19	386.55	386.88	387.18
140	0.00	379.82	385.55	386.01	386.43	386.81
150	0.00	373.49	380.48	381.07	381.61	382.08
160	0.00	362.59	371.18	371.95	372.63	373.22
170	0.00	350.74	361.23	362.22	363.10	363.83
180	0.00	342.55	355.06	356.34	357.43	358.31
190	0.00	337.79	352.34	353.94	355.29	356.34
200	0.00	333.15	349.73	351.74	353.40	354.63
210	0.00	325.70	344.38	346.91	348.95	350.41
220	0.00	313.75	334.61	337.84	340.39	342.13
230	0.00	298.08	321.17	325.32	328.59	330.70
240	0.00	281.73	306.96	312.35	316.63	319.33
250	0.00	267.22	294.27	301.25	306.91	310.47
260	0.00	256.26	284.27	293.02	300.33	305.02
270	0.00	250.61	278.11	288.38	297.33	303.24
280	0.00	249.37	275.06	286.38	296.67	303.73
290	0.00	249.68	273.02	284.88	296.17	304.26
300	0.00	249.22	270.17	282.21	294.17	303.13
310	0.00	246.18	264.99	276.93	289.28	298.95
320	0.00	238.14	255.15	266.87	279.39	289.59

330	0.00	220.61	236.31	247.83	260.46	271.13
340	0.00	197.71	212.41	223.80	236.50	247.59
350	0.00	178.62	192.58	203.98	216.79	228.33

Time = 0.2 ms

X\Y	0	2	4	6	8	10
30	0.00	349.69	349.69	349.69	349.69	349.69
40	0.00	365.11	365.21	365.21	365.22	365.22
50	0.00	375.23	375.53	375.54	375.54	375.55
60	0.00	380.59	381.15	381.16	381.18	381.19
70	0.00	382.20	383.09	383.12	383.14	383.17
80	0.00	382.54	383.84	383.88	383.93	383.97
90	0.00	384.62	386.39	386.46	386.53	386.60
100	0.00	389.14	391.43	391.53	391.63	391.72
110	0.00	394.83	397.69	397.83	397.96	398.08
120	0.00	400.00	403.48	403.66	403.82	403.97
130	0.00	403.58	404.08	404.08	404.08	404.08
140	0.00	401.65	401.65	401.65	401.65	401.65
150	0.00	401.01	401.01	401.01	401.01	401.01
160	0.00	399.54	401.73	401.78	401.83	401.87
170	0.00	394.09	399.10	399.32	399.49	399.63
180	0.00	389.16	397.07	397.51	397.87	398.17
190	0.00	385.07	395.73	396.42	397.00	397.69
200	0.00	380.56	393.67	394.87	395.95	395.95
210	0.00	373.32	388.85	390.14	391.26	391.92
220	0.00	360.33	378.50	380.04	381.32	382.31
230	0.00	341.16	362.42	364.29	365.81	367.02
240	0.00	317.61	342.51	344.82	346.66	348.08
250	0.00	293.13	322.08	325.02	327.30	328.97
260	0.00	272.40	305.05	308.81	311.66	313.63
270	0.00	260.05	294.81	299.50	302.99	305.27
280	0.00	256.28	291.27	296.88	301.06	303.66
290	0.00	256.79	291.01	297.56	302.50	305.48
300	0.00	256.24	289.64	297.22	303.06	306.53
310	0.00	249.57	282.72	291.53	298.51	302.66
320	0.00	234.59	268.23	278.56	287.00	292.08
330	0.00	214.69	249.22	261.32	271.54	277.81
340	0.00	196.54	231.47	245.32	257.46	265.09
350	0.00	186.32	219.90	234.90	248.62	257.52

Time = 0.24 ms

X\Y	0	2	4	6	8	10
30	0.00	271.64	271.64	271.64	271.64	271.64
40	0.00	313.13	313.10	312.95	312.81	312.67
50	0.00	338.08	338.15	337.92	337.69	337.46

60	0.00	353.40	353.67	353.38	353.09	352.82
70	0.00	362.51	363.05	362.74	362.43	362.14
80	0.00	368.93	369.85	369.54	369.24	368.94
90	0.00	375.87	377.23	376.95	376.67	376.40
100	0.00	383.77	385.63	385.39	385.15	384.92
110	0.00	390.71	393.13	392.94	392.74	392.54
120	0.00	394.94	397.93	397.78	397.62	397.46
130	0.00	398.23	399.88	399.88	399.87	399.82
140	0.00	399.00	399.00	399.00	399.00	399.00
150	0.00	398.00	398.00	398.00	398.00	398.00
160	0.00	397.23	397.23	397.23	397.23	397.23
170	0.00	397.48	398.32	398.32	398.31	398.30
180	0.00	397.20	397.20	397.20	397.20	397.20
190	0.00	395.58	395.58	395.58	395.58	395.58
200	0.00	394.87	394.87	394.87	394.87	394.87
210	0.00	393.04	393.04	393.04	393.04	393.04
220	0.00	393.90	394.27	394.27	394.27	394.27
230	0.00	386.99	390.65	390.71	390.74	390.76
240	0.00	370.40	378.61	378.83	378.98	379.09
250	0.00	346.63	360.97	361.53	361.93	362.21
260	0.00	321.58	343.28	344.37	345.14	345.68
270	0.00	301.60	330.49	332.24	333.47	334.35
280	0.00	288.49	323.06	325.52	327.25	328.45
290	0.00	279.67	318.17	321.34	323.55	325.07
300	0.00	270.89	312.16	316.10	318.81	320.62
310	0.00	258.49	302.19	307.00	310.30	312.42
320	0.00	241.33	287.69	293.57	297.58	300.07
330	0.00	221.12	270.39	277.58	282.50	285.43
340	0.00	204.35	255.50	264.13	270.04	273.44
350	0.00	195.78	246.79	256.77	263.70	267.55

Time = 0.28 ms

X\Y	0	2	4	6	8	10
30	0.00	185.74	185.74	185.74	185.74	185.74
40	0.00	259.76	259.76	259.62	259.49	259.36
50	0.00	293.29	293.39	293.16	292.93	292.72
60	0.00	313.21	313.49	313.18	312.88	312.59
70	0.00	326.17	326.70	326.32	325.95	325.60
80	0.00	336.21	337.03	336.60	336.17	335.77
90	0.00	346.77	347.95	347.47	347.00	346.56
100	0.00	358.34	359.92	359.41	358.91	358.45
110	0.00	369.57	371.60	371.09	370.57	370.10
120	0.00	378.76	381.32	380.81	380.29	379.81
130	0.00	384.21	387.41	386.91	386.40	385.93
140	0.00	386.31	389.85	389.73	389.27	388.82
150	0.00	386.72	390.70	390.70	390.48	390.09
160	0.00	386.05	390.64	390.64	390.56	390.29

170	0.00	384.16	389.47	389.45	389.39	389.18
180	0.00	382.75	388.36	388.36	388.36	388.36
190	0.00	382.45	388.33	388.33	388.33	388.33
200	0.00	382.25	387.81	387.81	387.81	387.80
210	0.00	383.34	387.05	387.05	387.05	387.05
220	0.00	384.40	384.94	384.94	384.94	384.94
230	0.00	385.13	385.58	385.58	385.58	385.58
240	0.00	380.76	382.36	382.36	382.36	382.36
250	0.00	369.69	372.96	372.98	373.00	373.02
260	0.00	354.84	360.60	360.69	360.75	360.81
270	0.00	340.63	350.03	350.23	350.37	350.48
280	0.00	328.45	342.72	343.10	343.36	343.55
290	0.00	317.32	337.43	338.08	338.49	338.79
300	0.00	305.80	332.28	333.30	333.93	334.37
310	0.00	292.26	325.44	326.96	327.87	328.48
320	0.00	275.21	315.52	317.69	318.97	319.81
330	0.00	254.54	302.51	305.53	307.29	308.43
340	0.00	235.53	290.78	294.84	297.20	298.68
350	0.00	221.71	282.52	287.75	290.77	292.62

Time = 0.32 ms

X\Y	0	2	4	6	8	10
30	0.00	95.38	95.38	95.38	95.38	95.38
40	0.00	235.50	235.61	235.57	235.53	235.49
50	0.00	269.13	269.40	269.30	269.21	269.12
60	0.00	287.09	287.56	287.39	287.23	287.08
70	0.00	298.45	299.17	298.92	298.68	298.46
80	0.00	308.44	309.45	309.13	308.81	308.52
90	0.00	320.17	321.50	321.11	320.73	320.38
100	0.00	333.82	335.51	335.06	334.62	334.23
110	0.00	347.72	349.80	349.31	348.83	348.40
120	0.00	360.36	362.89	362.37	361.85	361.40
130	0.00	370.16	373.22	372.69	372.15	371.67
140	0.00	375.88	379.60	379.05	378.50	378.02
150	0.00	377.40	381.80	381.37	380.80	380.31
160	0.00	376.29	381.08	381.08	380.60	380.10
170	0.00	374.16	379.96	379.90	379.47	378.95
180	0.00	372.17	378.92	378.86	378.55	378.05
190	0.00	371.40	379.02	379.01	378.85	378.42
200	0.00	370.95	379.29	379.29	379.22	379.12
210	0.00	370.15	378.92	378.92	378.92	378.87
220	0.00	370.81	379.42	379.42	379.42	379.42
230	0.00	370.48	379.69	379.69	379.69	379.69
240	0.00	366.25	376.39	376.38	376.37	376.36
250	0.00	358.64	369.37	369.36	369.34	369.32
260	0.00	349.92	360.89	360.89	360.87	360.85
270	0.00	342.80	353.87	353.87	353.86	353.84

280	0.00	337.93	349.31	349.34	349.34	349.33
290	0.00	334.20	346.55	346.62	346.64	346.66
300	0.00	329.99	344.31	344.45	344.51	344.56
310	0.00	323.39	340.93	341.19	341.32	341.42
320	0.00	312.94	335.16	335.60	335.84	336.02
330	0.00	297.87	326.43	327.17	327.56	327.84
340	0.00	280.80	317.08	318.21	318.80	319.23
350	0.00	265.86	310.21	311.86	312.69	313.27

APPENDIX F

CALCULATED RESULTS OF POWER GENERATED BY THRUST GAS

T(ms)	P1 (kW)	P2 (kW)	NET POWER
0.020	0.67456	0.00000	0.67456
0.040	1.44624	0.00000	1.44624
0.060	2.42395	-0.03940	2.38454
0.080	4.91424	-0.80272	4.11151
0.100	6.53482	-1.20076	5.33405
0.120	8.16850	-1.52280	6.64570
0.140	9.71311	-2.96653	6.74659
0.160	11.43226	-4.29594	7.13632
0.180	13.23683	-5.16886	8.06797
0.200	15.17305	-6.16885	9.00420
0.220	15.73340	-6.98176	8.75164
0.240	14.47661	-6.98781	7.48880
0.260	12.57991	-6.72742	5.85248
0.280	10.45593	-6.27283	4.18310
0.300	8.18782	-5.52902	2.65880
0.320	5.93807	-4.54486	1.39321
0.340	3.81999	-3.36318	0.45680
0.360	0.00000	0.00000	0.00000

APPENDIX G

TURBULENCE EDDY STRUCTURE AND DERIVATION OF THE FORMULA TO CALCULATE CHARACTERISTIC TIME τ_b

Tabaczynski and Ferguson (1977) extended Blizard and Keck's "eddy entrainment concept (1974) by postulating a detailed turbulent eddy structure (figure G-1) and eddy burning model.

A schematic of a typical coherent structure is shown in figure G-1. This figure shows the internal structure of a single turbulence eddy of integral scale L. The integral length scale L defines the characteristic size of the large scale structure. The Kolmogorov scale η defines the dissipation length scale. It is assumed to be the scale of the vortex tubes. In the model developed in this work, chemical reactions on the Kolmogorov scale are assumed instantaneous and the ignition sites are assumed to propagate along the vortex tubes at a rate governed by the turbulent intensity and laminar flame speed. The Taylor microscale λ is given

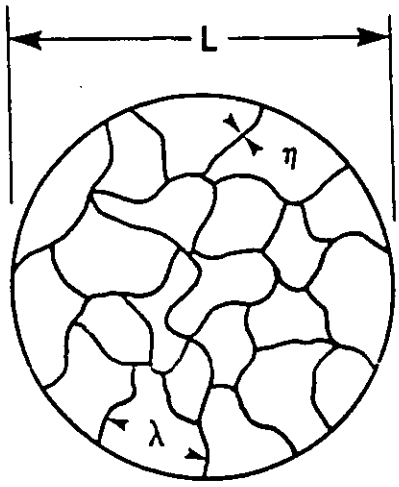

Figure G-1 Definition of turbulence structure and turbulence length scales

a physical meaning in this model. It is defined as the spaces of the spaghetti-like structure of the vortex tubes. λ is defined as a characteristic length over which diffusion occurs in a laminar fashion.

The characteristic reaction time for a large eddy τ_b which is defined as $\tau_b = L/S_T$ is essentially important to calculate the turbulence speed S_T.

Based on Tabaczynski and Ferguson's research results, we have

$$\tau_b = 1.8\tau_e(\tau_c/\tau_e)^{2/3} = 1.8\tau_c^{2/3}\tau_e^{1/3} = 1.8(\lambda/S_l)^{2/3}(L/u')^{1/3} \qquad (G-1)$$

where, u' -- turbulence intensity which is assumed to be proportional to the eddy entrainment speed u_e.

$\tau_e = L/u'$ turbulence reaction time at an integral scale.

$\tau_c = \lambda/S_l$ chemical reaction time in the Taylor microscale λ.

The Taylor microscale is calculated via the relationship for isotropic turbulence (Tennekes and Lumley, 1972):

$$\lambda = (15/A)^{1/2} Re_t^{-1/2} L$$

where A is a constant of order one and Re_t represents the turbulent Reynold's Number defined for a fluid with kinematic viscosity ν as

$$Re_t = u' L / \nu$$

Therefore

$$\begin{aligned}
\lambda &= (15/A)^{1/2} u^{-1/2} L^{1/2} \nu^{1/2} \\
&= (15/A)^{1/2} [u_i' (\rho_u / \rho_i)^{1/3}]^{-1/2} [L_i (\rho_i / \rho_u)^{1/3}]^{1/2} \nu^{1/2} \\
&= (15/A)^{1/2} u_i^{-1/2} L_i^{1/2} (\rho_i / \rho_u)^{1/3} \nu^{1/2} \\
&= (15/A)^{1/2} (C_u S_p)^{-1/2} (C_L h_i)^{1/2} (\rho_i / \rho_u)^{1/3} \nu^{1/2}
\end{aligned}$$

where assumptions (6-4) and (6-46) have been used for u_i' and L_i. Combining the constants and taking the same form as in equation (G-1) we have

$$(\lambda / S_l)^{2/3} = C' [S_p^{-1/2} \rho_u^{-1/3} \nu^{1/2} S_l^{-1}]^{2/3} = C' \rho_u^{-2/9} \nu^{1/3} S_p^{-1/3} S_l^{-2/3} \qquad (G - 2)$$

Taking account

$$\begin{aligned}
(\lambda / u')^{1/3} &= [(L_i (\rho_i / \rho_u)^{1/3} / (u_i' (\rho_u / \rho_i)^{1/3})]^{1/3} \\
&= \left(\frac{L_i}{u_i'}\right)^{\frac{1}{3}} \left(\frac{\rho_i}{\rho_u}\right)^{\frac{2}{3}*\frac{1}{3}} = \left(\frac{C_2 h_i}{C_3 S_p}\right)^{\frac{1}{3}} \left(\frac{\rho_i}{\rho_u}\right)^{\frac{2}{9}} = C'' S_p^{-1/3} \rho_u^{-2/9}
\end{aligned}$$

into equation (G-1) we finally have the characteristic reaction time of a large scale turbulence eddy

$$\begin{aligned}\tau_b &= 1.8*[C'\rho_u^{-\frac{2}{9}}\nu^{\frac{1}{3}}S_p^{-\frac{1}{3}}S_l^{-\frac{2}{3}}]*[C''S_p^{-\frac{1}{3}}\rho_u^{-\frac{2}{9}}] \\ &= C'''\rho_u^{-4/9}\nu^{1/3}S_p^{-2/3}S_l^{-2/3} \\ &= C_2(S_pS_l)^{-2/3}\rho_u^{-4/9}\nu^{1/3}\end{aligned} \qquad (G-3)$$

During the above derivations, the structure parameters A, C_u, C_L and h_i are assumed to be constant for a given engine design. Constant C_2 is the combination of these parameters.

APPENDIX H

DERIVATION OF THE FORMULA TO CALCULATE INTERNAL ENERGIES

Internal energies of the gases in unburnt, burnt and air zones are simply named as the internal energies of unburnt and burnt mixture and air respectively in the following derivations. The concerned gases are assumed to be the mixture of Octane and dry air and the results are based on one pound of air.

1) Unburnt mixture

The internal energy of unburnt mixture is the summation of that of the chemically correct (stoichiometrical) mixture, combustion residuals from last cycle and the extra air in the view point of theoretically complete combustion. That is

$$e_u = e_{uc} + \eta(e_b - e_{uc}) + (\phi - 1)(1 - \eta)(e_{uc} - e_{au}) \qquad \text{(H - 1)}$$

where, e_u -- internal energy of unburnt mixture

e_{uc}-- internal energy of chemically correct unburnt mixture

e_b -- internal energy of burnt mixture

e_{au}-- internal energy of air in unburnt environment

η -- mass percentage of the combustion residual from last cycle

ϕ -- equivalence ratio of fuel/air

Blizard and Keck (1974) gave following approximate expressions for the chemically correct unburnt and burnt mixture and air in unburnt mixture respectively:

$$e_{uc} = 34{,}200+6.0T_u \ (Btu/lbmole,R) = 79{,}549+25.1T_u \ (kJ/kgmole,K) \qquad (H-2)$$

$$e_{bc} = -15{,}800+10.7T_b \ (Btu/lbmole,R) = -36{,}750+44.8T_b \ (kJ/kgmole,K) \qquad (H-3)$$

$$e_{au} = 0.79e_{N_2}+0.21e_{O_2} = -3{,}200+5.5T_u \ (Btu/lbmole,R)$$
$$= -7{,}443+23T_u \ (kJ/kgmole,K) \qquad (H-4)$$

For the burnt gases from last cycle in unburnt environment, assuming it was the correct mixture at last cycle we have

$$e_b|_{recycled} = e_{bc} = -36{,}750+44.8T_{b_2} \ (kJ/kgmole,K) \qquad (H-5)$$

Substituting equation (I - 2), (I - 3) and (I - 5) into (I - 1) we have

$$e_u = [79{,}549-116{,}218\eta+86{,}992(\phi-1)(1-\eta)] +$$
$$[25.12+19.68\eta+2.09(\phi-1)(1-\eta)]*T_u \quad (kJ/kgmole,K) \qquad (H-6)$$

2) Burnt mixture

The internal energy of burnt mixture is the sum of that of the chemically correct burnt mixture and extra air for lean fuel/air mixture ($\phi <= 1$)

$$e_b = e_{bc} + (\phi - 1)(e_{bc} - e_{ab}) \qquad (H - 7)$$

With equation (H - 3) and following equation for the air in burnt mixture

$$e_{ab} = 6{,}200+6.8T_b \ (Btu/lbmole,R) = -14{,}421+28.5T_b \ (kJ/kgmole,K) \qquad (H - 8)$$

we have the formula to calculate the internal energy of unburnt mixture:

$$e_b = -[36{,}750+2{,}330(\phi-1)]+[44.8+16.33(\phi-1)]*T_b \ (kJ/kgmole,K) \qquad (H - 9)$$

For the rich fuel/air mixture ($\phi > 1$) with the assumption of the combustion products of C_nH_m, N_2, H_2O, CO_2 and CO we have

$$e_b = e_{bc}+(\phi-1)(e_{bc}-e_{ab}+0.21\Delta e_1)$$

where the heat of reaction of oxygen

$$\Delta e_1 = 238{,}000 \ Btu/lbmoleO_2 = 553{,}588 \ \ kJ/kgmoleO_2$$

Therefore we have the formula to calculate the internal energy of burnt mixture:

$$e_b = [-36{,}750+93{,}923(\phi-1)]+[44.8+16.33(\phi-1)]*T_b \ \ (kJ/kg\,mole,K) \qquad (H-10)$$